Heavy flavour production at the LHC: Theoretical Aspects

Z. J. Ajaltouni[a], *A. Banfi*[b], *S. Baranov*[c], *I. Bierenbaum*[d], *J. Blümlein*[e], *G. Corcella*[f], *M. Czakon*[g], *G. Ferrera*[h], *S. Klein*[e], *B.A. Kniehl*[i], *G. Kramer*[i], *A. Likhoded*[j], *D.A. Milstead*[k], *O.I. Piskounova*[l], *V.A. Saleev*[m], *I. Schienbein*[n], *H. Spiesberger*[o], *R.S. Thorne*[p], *W.K. Tung*[q], *G. Zanderighi*[r], *N. Zotov*[s]

[a] LPC, Université Blaise Pascal, F-63177 Aubière Cedex, France
[b] INFN, Sezione di Milano-Bicocca, Italy
[c] P.N. Lebedev Institute of Physics, Lenin avenue 53, Moscow 119991, Russia
[d] Deutsches Elektronen-Synchrotron, Platanenallee 6, D-15738 Zeuthen, Germany (now at IFIC, Universitat de València, Spain)
[e] Deutsches Elektronen-Synchrotron, Platanenallee 6, D-15738 Zeuthen, Germany
[f] Museo Storico della Fisica e Centro Studi e Ricerche 'E. Fermi', Roma, and Scuola Normale Superiore and INFN Sezione di Pisa, Italy
[g] University Würzburg, Germany
[h] University and INFN, Firenze, Italy
[i] II. Inst. für Theoretische Physik, Universität Hamburg, Germany
[j] Theoretical Department, Institute for High Energy Physics (IHEP), Protvino, Moscow reg., Russia
[k] Stockholm University, Sweden
[l] Lebedev Institute, Moscow, Russia
[m] Samara State University, Samara, Russia
[n] LPSC, Grenoble, France
[o] University Mainz, Germany
[p] University College London
[q] Michigan State U. and U. Washington, Seattle
[r] The Rudolf Peierls Centre for Theoretical Physics, 1 Keble Road, University of Oxford, UK
[s] Institute of Nuclear Physics, Moscow State University, Lenin Hills, Moscow 119991, Russia

Abstract

A proper inclusion of heavy quark mass effects in Parton Distribution Function fits has proved crucial. We present a review these effects in DIS and their impact on global analyses and lay out all elements of a properly defined general mass variable flavor number scheme (GM VFNS) that are shared by all modern formulations of the problem. We also report about progress in a number of theoretical problems related to exclusive measurements of heavy flavors. These topics include fragmentation functions for charmed mesons including finite mass effects, fragmentation functions including non-perturbative corrections based on an effective QCD coupling, a discussion of the status of higher-order calculations for top quark production and for polarized structure functions, heavy quark and quarkonium production in the Regge limit, double heavy baryon production, tests of time reversal and CP symmetry in Λ_b decays, as well as a study of the general properties of massive

exotic hadrons that will be relevant for an understanding of their detection at the LHC.

Coordinators: M. Cacciari and H. Spiesberger

1 PQCD Formulations with Heavy Quark Masses and Global Analysis

Authors: R.S. Thorne and W.K. Tung

1.1 Introduction

The proper treatment of heavy flavours in global QCD analysis of parton distribution functions (PDFs) is essential for precision measurements at hadron colliders. Recent studies [1–5] show that the standard-candle cross sections for W/Z production at the LHC are sensitive to detailed features of PDFs that depend on heavy quark mass effects; and certain standard model as well as beyond standard model processes depend crucially on better knowledge of the c-quark parton density, in addition to the light parton flavors. These studies also make it clear that the consistent treatment of heavy flavours in perturbative QCD (PQCD) require theoretical considerations that go beyond the familiar textbook parton picture based on massless quarks and gluons. There are various choices, explicit and implicit, which need to be made in various stages of a proper calculation in generalised PQCD including heavy quark mass effects. In the global analysis of PDFs, these choices can affect the resulting parton distributions. Consistent choices are imperative; mistakes may result in differences that are similar to, or even greater than, the quoted uncertainties due to other sources (such as the propagation of input experimental errors). In this report, we will provide a brief, but full, review of issues related to the treatment of heavy quark masses in PQCD, embodied in the general mass variable flavor scheme (GM VFNS).

In Sec. 1.2, we describe the basic features of the modern PQCD formalism incorporating heavy quark masses. In Sec. 1.3, we first delineate the common features of GM VFNS, then identify the different (but self-consistent) choices that have been made in recent global analysis work, and compare their results. For readers interested in practical issues relating to the use (or choice) of PDFs in various physics applications, we present a series of comments in Sec. 1.4 intended as guidelines. In Sec. 1.5, we discuss the possibility of intrinsic heavy flavors.

We note that, this review on GM VFNS and global analysis is not intended to address the specific issues pertinent to heavy flavor production (especially the final state distributions). For this particular process, somewhat different considerations may favor the adoption of appropriate fixed flavor number schemes (FFNS). We shall not go into details of these considerations; but will mention the FFNS along the way, since the GM VFNS is built on a series of FFNS's. We will comment on this intimate relationship whenever appropriate.

1.2 General Considerations on PQCD with Heavy Flavor Quarks

The quark-parton picture is based on the factorization theorem of PQCD. The conventional proof of the factorization theorem proceeds from the zero-mass limit for all the partons—a good approximation at energy scales (generically designated by Q) far above all quark mass thresholds

(designated by m_i). This clearly does not hold when Q/m_i is of order 1.[1] It has been recognised since the mid-1980's that a consistent treatment of heavy quarks in PQCD over the full energy range from $Q \lesssim m_i$ to $Q \gg m_i$ can be formulated [6]. In 1998, Collins gave a general proof of the factorization theorem (order-by-order to all orders of perturbation theory) that is valid for non-zero quark masses [7]. The resulting general theoretical framework is conceptually simple: it represents a straightforward generalisation of the conventional zero-mass (ZM) modified minimal subtraction ($\overline{\rm MS}$) formalism and it contains the conventional approaches as special cases in their respective regions of applicability; thus, it provides a good basis for our discussions.

The implementation of any PQCD calculation on physical cross sections requires attention to a number of details, both kinematical and dynamical, that can affect both the reliability of the predictions. Physical considerations are important to ensure that the right choices are made between perturbatively equivalent alternatives that may produce noticeable differences in practical applications. It is important to make these considerations explicit, in order to make sense of the comparison between different calculations in the literature. This is what we shall do in this section. In subsequent sections, we shall point out the different choices that have been made in recent global analysis efforts.

Heavy quark physics at HERA involve mostly charm (c) and bottom (b) production; at LHC, top (t) production, in addition, is of interest. For simplicity, we often focus the discussion of the theoretical issues on the production of a single heavy quark flavor, which we shall denote generically as H, with mass m_H. The considerations apply to all three cases, $H = c,\ b,\ \&\ t$. For global analysis, the most important process that requires precision calculation is DIS; hence, for physical predictions, we will explicitly discuss the total inclusive and semi-inclusive structure functions, generically referred to as $F^\lambda(x, Q)$, where λ represents either the conventional label $(1, 2, 3)$ or the alternative $(T, L, 3)$ where T/L stands for transverse/longitudinal respectively.

1.2.1 The Factorization Formula

The PQCD factorization theorem for the DIS structure functions has the general form

$$F_\lambda(x, Q^2) = \sum_k f_k \otimes C_k^\lambda = \sum_k \int_\chi^1 \frac{d\xi}{\xi}\, f_k(\xi, \mu)\, C_k^\lambda \left(\frac{\chi}{\xi}, \frac{Q}{\mu}, \frac{m_i}{\mu}, \alpha_s(\mu)\right). \qquad (1)$$

Here, the summation is over the active parton flavor label k, $f^k(x, \mu)$ are the parton distributions at the factorization scale μ, C_k^λ are the Wilson coefficients (or hard-scattering amplitudes) that can be calculated order-by-order in perturbation theory. The lower limit of the convolution integral χ is determined by final-state phase-space constraints: in the conventional ZM parton formalism it is simply $x = Q^2/2q \cdot p$—the Bjorken x—but this is no longer true when heavy flavor particles are produced in the final state, cf. Sec. 1.2.4 below. The renormalization and factorization scales are jointly represented by μ: in most applications, it is convenient to choose $\mu = Q$; but there are circumstances in which a different choice becomes useful.

[1] Heavy quarks, by definition, have $m_i \gg \Lambda_{QCD}$. Hence we always assume $Q, m_i \gg \Lambda_{QCD}$. In practice, $i = c, b, t$.

1.2.2 Partons and Schemes for General Mass PQCD

In PQCD, the summation $\sum_k$ over "parton flavor" label k in the factorization formula, Eq. (1), is determined by the *factorization scheme* chosen to *define* the Parton Distributions $f_k(x,\mu)$.

If mass effects of a heavy quark H are to be taken into account, the simplest scheme to adopt is the *fixed flavor number scheme* (FFNS) in which all quark flavors below H are treated as zero-mass and one sums over $k = g, u, \bar{u}, d, \bar{d}, ...$ up to n_f flavors of *light* (massless) quarks. The mass of H, m_H, appears explicitly in the Wilson coefficients $\{C_k^\lambda\}$, as indicated in Eq. 1. For $H = \{c, b, t\}$, $n_f = \{3, 4, 5\}$ respectively. Historically, higher-order ($\mathcal{O}(\alpha_S^2)$) calculations of the heavy quark production [8] were all done first in the FFNS. These calculations provide much improved results when μ (Q) is of the order of m_H (both above and below), over those of the conventional ZM ones (corresponding to setting $m_H = 0$).

Unfortunately, at any finite order in perturbative calculation, the n_f-FFNS results become increasingly unreliable as Q becomes large compared to m_H: the Wilson coefficients contain logarithmic terms of the form $\alpha_s^n \ln^m(Q/m_H)$, where $m = 1 \ldots n$, at order n of the perturbative expansion, implying they are not infrared safe—higher order terms do not diminish in size compared to lower order ones—the perturbative expansion eventually breaks down. Thus, even if all n_f-flavor FFNS are mathematically equivalent, in practice, the 3-flavor scheme yields the most reliable results in the region $Q \lesssim m_c$, the 4-flavor scheme in $m_c \lesssim Q \lesssim m_b$, the 5-flavor scheme in $m_b \lesssim Q \lesssim m_t$, and, if needed, the 6-flavor scheme in $m_t \lesssim Q$. (Cf. related discussions later in this section.)

This leads naturally to the definition of the more general *variable flavor number scheme* (VFNS): it is a *composite scheme* consisting of the sequence of n_f-flavor FFNS, each in its region of validity, for $n_f = 3, 4, ..$ as described above; and the various n_f-flavor schemes are related to each other by perturbatively calculable transformation (finite-renormalization) matrices among the (running) coupling α_s, the running masses $\{m_H\}$, the parton distribution functions $\{f_k\}$, and the Wilson coefficients $\{C_k^\lambda\}$. These relations ensure that there are only one set of independent renormalization constants, hence make the definition of the composite scheme precise for all energy scale μ (Q); and they ensure that physical predictions are well-defined and continuous as the energy scale traverses each of the overlapping regions $Q \sim m_H$ where both the n_f-flavor and the (n_f+1)-flavor schemes are applicable. The theoretical foundation for this intuitively obvious scheme can be found in [6, 7], and it was first applied in detail for structure functions in [9]. Most recent work on heavy quark physics adopt this general picture, in one form or another. We shall mention some common features of this general-mass (GM) VFNS in the next few paragraphs; and defer the specifics on the implementation of this scheme, as well as the variations in the implementation allowed by the general framework until Sec. 1.3.

As mentioned above, the n_f-flavor and the $(n_f + 1)$-flavor schemes within the GM VFNS should be matched at some *match point* μ_M that is of the order of m_H. In practice, the matching is commonly chosen to be exactly $\mu_M = m_H$, since it has been known that, in the calculational scheme appropriate for GM VFNS[2], the transformation matrices vanish at this particular scale

[2]Technically, this means employing the CWZ subtraction scheme [10] in calculating the higher-order Feynman diagrams. CWZ subtraction is an elegant extension of the $\overline{\rm MS}$ subtraction scheme that ensures the decoupling of heavy quarks at high energy scales order-by-order. This is essential for factorization to be valid at each order of perturbation theory. (In the original $\overline{\rm MS}$ subtraction scheme, decoupling is satisfied only for the full perturbation

at NLO in the perturbative expansion [6]; thus discontinuities of the renormalized quantities are always of higher order, making practical calculations simpler in general.

Strictly speaking, once the component n_f-flavor schemes are unambiguously matched, one can still choose an independent *transition scale*, μ_T, at which to switch from the n_f-flavor scheme to the $(n_f + 1)$-flavor scheme in the calculation of physical quantities in defining the GM VFNS. This scale must again be within the overlapping region, but can be different from μ_M [1,7]. In fact, it is commonly known that, from the physics point of view, in the region above the m_H threshold, up to $\eta\, m_H$ with a reasonable-sized constant factor η, the most natural parton picture is that of n_f-flavor, rather than $(n_f + 1)$-flavor one.[3] For instance, the 3-flavor scheme calculation has been favored by most HERA work on charm and bottom quark production, even if the HERA DIS kinematic region mostly involves $Q > m_c$; and it is also used in the dynamically generated parton approach to global analysis [11].

In practice, almost all implementations of the GM VFNS simply choose $\mu_T = \mu_M = m_H$ (often not explicitly mentioning the conceptual distinction between μ_T and $\mu_M = m_H$). The self-consistency of the GM VFNS guarantees that physical predictions are rather insensitive to the choice of the transition point as long as it is within the overlapping region of validity of the n_f- and $(n_f + 1)$-flavor ones. The simple choice of $\mu_T = m_H$ corresponds to opting for the lower end of this region for the convenience in implementation. In the following, we shall use the terms matching point and transition point interchangeably. As with all definition ambiguities in perturbative theory, the sensitivity to the choice of matching and transition points diminishes at higher orders.

1.2.3 Treatment of Final-state Flavors

For total inclusive structure functions, the factorization formula, Eq. (1), contains an implicit summation over all possible quark flavors in the final state. One can write,

$$C_k = \sum_j C_k^j \tag{2}$$

where "j" denotes final state flavors, and $\{C_k^j\}$ represent the Wilson coefficients (hard cross sections) for an incoming parton "k" to produce a final state containing flavor "j" calculable perturbatively from the relevant Feynman diagrams. It is important to emphasize that "j" labels quark flavors that can be produced *physically* in the final state; it is *not* a *parton* label in the sense of initial-state parton flavors described in the previous subsection. The latter (labeled k) is a theoretical construct and scheme-dependent (e.g. it is fixed at three for the 3-flavor scheme); whereas the final-state sum (over j) is over *all flavors* that can be physically produced. Furthermore, the initial state parton "k" does not have to be on the mass-shell, and is commonly treated as massless; whereas the final state particles "j" should certainly be *on-mass-shell* in order to satisfy the correct kinematic constraints for the final state phase space and yield physically meaningful

series—to infinite orders.)

[3] Specifically, the n_f-flavor scheme should fail when $\alpha_s(\mu)\ln(\mu/m_H) = \alpha_s(\mu)\ln(\eta)$ ceases to be a small parameter for the effective perturbation expansion. However, no theory can tell us precisely how small is acceptably "small"—hence how large η is permitted. Ardent FFNS advocates believe even the range of the 3-flavor scheme extends to all currently available energies, including HERA [11]. For GM VFNS, see the next paragraph.

results.[4] Thus, in implementing the summation over final states, the most relevant physical scale is W—the CM energy of the virtual Compton process—in contrast to the scale Q that controls the initial state summation over parton flavors.

The distinction between the two summations is absent in the simplest implementation of the conventional (i.e., textbook) zero-mass parton formalism: if all quark masses are set to zero to begin with, then all flavors can be produced in the final state. This distinction becomes blurred in the commonly used zero-mass (ZM) VFNS, where the heavy quark masses $\{m_H\}$ implicitly enter because the number of effective parton flavors is incremented as the scale parameter μ crosses each heavy quark threshold. This creates apparent paradoxes in the implementation of the ZM VFNS, such as: for $\mu = Q < m_b$, b is not counted as a parton, the partonic process $\gamma + g \to b\bar{b}$ would not be included in DIS calculations, yet physically this can be significant if $W \gg 2m_b$ (small x); whereas for $\mu = Q > m_b$, b is counted as a massless parton, the contribution of $\gamma + g \to b\bar{b}$ to DIS would be the same as that of $\gamma + g \to d\bar{d}$, but physically this is wrong for moderate values of W, and furthermore, it should be zero if $W < 2m_b$ (corresponding to large x). (We shall return to this topic in Sec. 1.3.1.)

These problems were certainly overlooked in conventional global analyses from its inception until the time when issues on mass-effects in PQCD were brought to the fore after the mid 1990's [9, 12–15]. Since then, despite its shortcomings the standard ZM VFNS continues to be used widely because of its simplicity and because NLO Wilson coefficients for most physical processes are still only available in the ZM VFNS. Most groups produce the standard ZM VFNS as either their default set or as one of the options, and they form the most common basis for comparison between groups, e.g. the "benchmark study" in [16].

It is obvious that, in a proper implementation of PQCD with mass (in any scheme), the distinction between the initial-state and final-state summation must be unambiguously, and correctly, observed. For instance, even in the 3-flavor regime (when c and b quarks are *not counted as partons*), the charm and bottom flavors still need to be counted in the final state—at tree-level via $W^+ + d/s \to c$, and at 1-loop level via the gluon-fusion processes such as $W^+ + g \to \bar{s} + c$ or $\gamma + g \to c\bar{c}\,(b\bar{b})$, provided there is enough CM energy to produce these particles.

1.2.4 Phase-space Constraints and Rescaling

The above discussion points to the importance of the proper treatment of final state phase space in heavy quark calculations. Once mass effects are taken into account, kinematic constraints have a significant impact on the numerical results of the calculation; in fact, they represent the dominant factor in the threshold regions of the phase space. In DIS, with heavy flavor produced in the final state, the simplest kinematic constraint that comes to mind is

$$W - M_N > \sum_f M_f \tag{3}$$

where W is the CM energy of the vector-boson–nucleon scattering process, M_N is the nucleon mass, and the right-hand side is the sum of *all* masses in the final state. W is related to the famil-

[4] Strict kinematics would require putting the produced heavy flavor mesons or baryons on the mass shell. In the PQCD formalism, we adopt the approximation of using on-shell final state heavy quarks in the underlying partonic process.

iar kinematic variables (x, Q) by $W^2 - M_N^2 = Q^2(1-x)/x$, and this constraint should ideally be imposed on the right-hand side of Eq. (1). Any approach achieving this represents an improvement over the conventional ZM scheme calculations, that ignores the kinematic constraint Eq. (3) (resulting in a gross over-estimate of the corresponding cross sections). The implementation of the constraint in the most usual case of NC processes, say $\gamma/Z + c \to c$ (or any other heavy quark) is not automatic (and is absent in some earlier definitions of a GM VFNS) because in this partonic process one must account for the existence of a *hidden heavy particle*—the $\bar{c}$—in the target fragment. The key observation is, heavy objects buried in the target fragment are still a part of the final state, and should be included in the phase space constraint, Eq. (3).

Early attempts to address this issue were either approximate or rather cumbersome, and could not be naturally extended to high orders.[5] A much better physically motivated approach is based on the idea of rescaling. The simplest example is given by charm production in the LO CC process $W + s \to c$. It is well-known that, when the final state charm quark is put on the mass shell, kinematics requires the momentum fraction variable for the incoming strange parton, χ in Eq. (1) to be $\chi = x(1 + m_c^2/Q^2)$ [17], rather than the Bjorken x. This is commonly called the *rescaling variable*. The generalization of this idea to the more prevalent case of NC processes took a long time to emerge [18, 19] which extended the simple rescaling to the more general case of $\gamma/Z + c \to c + X$, where X contains only light particles, it was proposed that the convolution integral in Eq. (1) should be over the momentum fraction range $\chi_c < \xi < 1$, where

$$\chi_c = x\left(1 + \frac{4m_c^2}{Q^2}\right) \quad . \tag{4}$$

In the most general case where there are any number of heavy particles in the final state, the corresponding variable is (cf. Eq. (3))

$$\chi = x\left(1 + \frac{(\Sigma_f\, M_f)^2}{Q^2}\right) \quad . \tag{5}$$

This rescaling prescription has been referred to as ACOTχ in the recent literature [18–20].

Rescaling shifts the momentum variable in the parton distribution function $f^k(\xi, \mu)$ in Eq. (1) to a higher value than in the zero-mass case. For instance, at LO, the structure functions $F_\lambda(x, Q)$ are given by some linear combination of $f^k(x, Q)$ in the ZM formalism; but, with ACOTχ rescaling, this becomes $f^k(\chi_c, Q)$. In the region where $(\Sigma_f\, M_f)^2 / Q^2$ is not too small, especially when $f(\xi, \mu)$ is a steep function of ξ, this rescaling can substantially change the numerical result of the calculation. It is straightforward to show that, when one approaches a given threshold ($M_N + \Sigma_f\, M_f$) from above, the corresponding rescaling variable $\chi \to 1$. Since generally $f^k(\xi, \mu) \longrightarrow 0$ as $\xi \to 1$, rescaling ensures a smoothly vanishing threshold behavior for the contribution of the heavy quark production term to all structure functions. This results in a universal[6], and intuitively physical, realization of the threshold kinematic constraint for all heavy flavor production processes that is applicable to all orders of perturbation theory. For this reason, most recent global analysis efforts choose this method.

[5] In [9], the threshold violation was minimized by an artificial choice of the factorization scale $\mu(m_H, Q)$. In [14, 15] the kinematic limit was enforced exactly by requiring continuity of the slope of structure functions across the matching point, resulting in a rather complicated expression for the coefficient functions in Eq.(1).

[6] Since it is imposed on the (universal) parton distribution function part of the factorization formula.

1.2.5 *Difference between $\{F_\lambda^{\rm tot}\}$ and $\{F_\lambda^{\rm H}\}$ Structure Functions*

In PQCD, the most reliable calculations are those involving infra-red safe quantities—these are free from logarithmic factors that can become large (thereby spoiling the perturbative expansion). The total inclusive structure functions $\{F_\lambda^{\rm tot}\}$ defined in the GM VFNS are infrared safe, as suggested by the discussion of Sec. 1.2.2 and proven in Ref. [7].

Experimentally, the semi-inclusive DIS structure functions for producing a heavy flavor particle in the final state is also of interest. Theoretically, it is useful to note that the structure functions $\{F_\lambda^{\rm H}\}$ for producing heavy flavor H are not as well defined as $F_\lambda^{\rm tot}$.[7] To see this, consider the relation between the two,

$$F_\lambda^{\rm tot} = F_\lambda^{\rm light} + F_\lambda^{\rm H} \,, \tag{6}$$

where $F_\lambda^{\rm light}$ denotes the sum of terms with only light quarks in the final state, and $F_\lambda^{\rm H}$ consist of terms with at least one heavy quark H in the final state. Unfortunately, $F_\lambda^{\rm H}(x,Q,m_H)$ is, strictly speaking, *not infrared safe* beyond order α_s (1-loop): they contain residual $\ln^n(Q/m_H)$ terms at higher orders (2-loop and up). The same terms occur in $F_\lambda^{\rm light}$ due to contributions from virtual H loops, with the opposite sign. Only the sum of the two, i.e. the total inclusive quantities $F_\lambda^{\rm tot}$ are infra-red safe. This problem could be addressed properly by adopting a physically motivated, infrared-safe cut-off on the invariant mass of the heavy quark pair, corresponding to some experimental threshold [21] in the definition of $F_\lambda^{\rm H}$ (drawing on similar practises in jet physics). In practice, up to order α_s^2, the result is numerically rather insensitive to this, and different groups adopt a variety of less sophisticated procedures, e.g. including contributions with virtual H loops within the definition of $F_\lambda^{\rm H}$. Nonetheless, it is prudent to be aware that the theoretical predictions on $F_\lambda^{\rm H}$ are intrinsically less robust than those for $F_\lambda^{\rm tot}$ when comparing experimental results with theory calculations.

1.2.6 *Conventions for "LO" , "NLO" , ... calculations*

It is also useful to point out that, in PQCD, the use of familiar terms such as LO, NLO, ... is often ambiguous, depending on which type of physical quantities are under consideration, and on the convention used by the authors. This can be a source of considerable confusion when one compares the calculations of $F_\lambda^{\rm tot}$ and $F_\lambda^{\rm H}$ by different groups (cf. next section).

One common convention is to refer LO results as those derived from tree diagrams; NLO those from 1-loop calculations, ... and so on. This convention is widely used; and it is also the one used in the CTEQ papers. Another possible convention is to refer to LO results as the ***first non-zero term*** in the perturbative expansion; NLO as one order higher in α_s, ... and so on. This convention originated in FFNS calculations of heavy quark production; and it is also used by the MRST/MSTW authors. It is a process-dependent convention, and it depends ***a priori*** on the knowledge of results of the calculation to the first couple of orders in α_s.

[7] In the following discussion, we shall overlook logarithmic factors normally associated with fragmentation functions for simplicity. These are similar to those associated with parton distributions, but are less understood from the theoretical point of view—e.g. the general proof of factorization theorem (with mass) [7] has not yet been extended to cover fragmentation.

Whereas the two conventions coincide for quantities such as $F_2^{\rm tot}$, they lead to different designations for the longitudinal structure function $F_L^{\rm tot}$ and the n_f-flavor $F_2^{\rm H,n_f}$, since the tree-level results are zero for these quantities. These designations, by themselves, are only a matter of terminology. However, mixing the two distinct terminologies in comparing results of different groups can be truly confusing. This will become obvious later.

1.3 Implementations of VFNS: Common Features and Differences

In this section, we provide some details of the PQCD basis for the GM VFNS, and comment on the different choices that have been made in the various versions of this general framework, implemented by two of the major groups performing global QCD analysis.

1.3.1 Alternative Formulations of the ZM VFNS

As pointed out in Sec. 1.2.3, the ZM VFNS, as commonly implemented, represents an unreliable approximation to the correct PQCD in some kinematic regions because of inappropriate handling of the final-state counting and phase-space treatment, in addition to the neglect of heavy-quark mass terms in the Wilson coefficients. Whereas the latter is unavoidable to some extent, because the massive Wilson coefficients have not yet been calculated even at 1-loop level for most physical processes (except for DIS), the former (which can be more significant numerically in certain parts of phase space) can potentially be remedied by properly counting the final states and using the rescaling variables, as discussed in Secs. 1.2.3 and 1.2.4 under general considerations. Thus, alternative formulations of the ZM VFNS are possible that only involve the zero-mass approximation in the Wilson coefficient. This possibility has not yet been explicitly explored.

1.3.2 Parton Distribution Functions in VFNS (ZM and GM)

In PQCD, the factorization scheme is determined by the choices made in defining the parton distribution functions (as renormalized Green functions). In a GM VFNS based on the generalized $\overline{\rm MS}$ subtraction (cf. footnote 2) the evolution kernel of the DGLAP equation is *mass-independent*; thus the PDFs, so defined, apply to GM VFNS calculations as they do for the ZM VFNS.

In the VFNS, the PDFs switch from the n_f-flavor FFNS ones to the (n_f+1)-flavor FFNS ones at the matching point $\mu = m_H$ (cf. Sec. 1.2.2); the PDFs above/below the matching point are related, order-by-order in α_s, by:

$$f_j^{VF}(\mu \to m_H^+) \equiv f_j^{(n_f+1)FF} = A_{jk} \otimes f_k^{n_f FF} \equiv A_{jk} \otimes f_j^{VF}(\mu \to m_H^-), \tag{7}$$

where $m_H^{+/-}$ indicate that the $\mu \to m_H$ limit is taken from above/below, and we have used the shorthand VF/FF for VFNS/FFNS in the superscripts. The transition matrix elements $A_{jk}(\mu/m_H)$, representing a finite-renormalization between the two overlapping FFNS schemes, can be calculated order by order in α_s; they are known to NNLO, i.e. $\mathcal{O}(\alpha_S^2)$ [12, 13]. (Note that A_{jk} is not a square matrix.) It turns out, at NLO, $A_{jk}(\mu = m_H) = 0$ [7]; thus f_k^{VF} are continuous with this choice of matching point. There is a rather significant discontinuity in heavy quark distributions and the gluon distribution at NNLO.

With the matching conditions, Eq. 7, $\{f_j^{VF}(\mu)\}$ are uniquely defined for all values of μ. We shall omit the superscript VF in the following. Moreover, when there is a need to focus on $f_j(\mu)$ in the vicinity of $\mu = m_H$, where there may be a discontinuity, we use $f_j^{+/-}(\mu)$ to distinguish the above/below branch of the function. As indicated in Eq. 7, f_j^- correspond to the n_f-flavor PDFs, and f_j^+ to the (n_f+1)-flavor ones.

1.3.3 The Structure of a GM VFNS, Minimal Prescription and Additional Freedom

Physical quantities should be independent of the choice of scheme; hence, in a GM VFNS, we must require the theoretical expressions for the structure functions to be continuous across the matching point $\mu = Q = m_H$ to each order of perturbative theory:

$$F(x,Q) = C_k^-(m_H/Q) \otimes f_k^-(Q) = C_j^+(m_H/Q) \otimes f_j^+(Q) \quad (8)$$

$$\equiv C_j^+(m_H/Q) \otimes A_{jk}(m_H/Q) \otimes f_k^-(Q). \quad (9)$$

where we have suppressed the structure function label (λ) on F's and C's, and used the notation $C_k^{+/-}$ to denote the Wilson coefficient function $C_k(m_H/Q)$ above/below the matching point respectively. Hence, the GM VFNS coefficient functions are also, in general, discontinuous, and must satisfy the transformation formula:

$$C_k^-(m_H/Q) = C_j^+(m_H/Q) \otimes A_{jk}(m_H/Q). \quad (10)$$

order-by-order in α_s. For example, at $\mathcal{O}(\alpha_S)$, $A_{Hg} = \alpha_s P_{qg}^0 \ln(Q/m_H)$, this constraint implies,

$$C_{H,g}^{-,1}(m_H/Q) = \alpha_s C_{H,H}^{+,0}(m_H/Q) \otimes P_{qg}^0 \ln(Q/m_H) + C_{H,g}^{+,1}(m_H/Q). \quad (11)$$

where the numeral superscript (0,1) refers to the order of calculation in α_s (for P_{jk}, the order is by standard convention one higher then indicated), and the suppressed second parton index on the Wilson coefficients (cf. Eq. 2) has been restored to make the content of this equation explicit. Eq. (11) was implicitly used in defining the original ACOT scheme [9]. The first term on the RHS of Eq. 11, when moved to the LHS, becomes the *subtraction term* of Ref. [9] that serves to define the Wilson coefficient $C_{H,g}^{+,1}(m_H/Q)$ (hence the scheme) at order α_s, as well as to eliminate the potentially infra-red unsafe logarithm in the gluon fusion term ($C_{H,g}^{-,1}(m_H/Q)$) at high energies.

The GM VFNS as described above, consisting of the general framework of [6, 7], along with transformation matrices $\{A_{jk}\}$ calculated to order α_s^2 by [12,13], is accepted in principle by all recent work on PQCD with mass. Together, they can be regarded as the *minimal GM VFNS*.

The definition in Eq. 10 was applied to find the asymptotic limits ($Q^2/M_H^2 \to \infty$) of coefficient functions in [12, 13], but it is important to observe that it does not completely define all Wilson coefficients across the matching point, hence, there are additional flexibilities in defining a specific scheme [7, 14, 15, 22]. This is because, as mentioned earlier, the transition matrix $\{A_{jk}\}$ is not a square matrix—it is $n_f \times (n_f+1)$. It is possible to swap $\mathcal{O}(m_H/Q)$ terms between Wilson coefficients on the right-hand-side of Eq. 10 (hence redefining the scheme) without violating the general principles of a GM VFNS. For instance, one can swap $\mathcal{O}(m_H/Q)$ terms between $C_H^{+,0}(m_H/Q)$ and $C_g^{+,1}(m_H/Q)$ while keeping intact the relation (11) that guarantees the

continuity of $F(x,Q)$ according to Eq. 8. This general feature, applies to (10) to all orders. It means, in particular, that there is no need to calculate the coefficient function $C_H^{+,i}(m_H/Q)$, for any i – it can be chosen as a part of the definition of the scheme. Also, it is perfectly possible to define coefficient functions which do not individually satisfy the constraint in Eq. 3, since Eq. 10 guarantees ultimate cancellation of any violations between terms. However, this will not occur perfectly at any finite order so modern definitions do include the constraint explicitly, as outlined in Sec. 1.2.4.

The additional flexibility discussed above has been exploited to simplify the calculation, as well as to achieve some desirable features of the prediction of the theory by different groups. Of particular interest and usefulness is the general observation that, given a GM VFNS calculation of $\{C_j^+\}$, one can always switch to a simpler scheme with constant $\{\tilde{C}_j^+\}$

$$\tilde{C}_H^+(m_H/Q) = C_H^+(0) \tag{12}$$

This is because the shift $(C_H^+(m_H/Q) - C_H^+(0))$ vanishes in the $m_H/Q \to 0$ limit, and can be absorbed into a redefinition of the GM scheme as mentioned above. The detailed proof are given in [7, 22]. By choosing the heavy-quark-initiated contributions to coincide with the ZM formulae, the GM VFNS calculation becomes much simplified: given the better known ZM results, we only need to know the full m_H-dependent contributions from the light-parton-initiated subprocesses; and these are exactly what is provided by the n_f-flavor FFNS calculations available in the literature. This scheme is known as the *Simplified ACOT scheme*, or SACOT [7, 22].

Further uses of the freedom to reshuffle $\mathcal{O}(m_H/Q)$ terms between Wilson coefficients, as well as adding terms of higher order in the matching condition (without upsetting the accuracy at the given order) have been employed extensively by the MRST/MSTW group, as will be discussed in Sec. 1.3.5.

1.3.4 CTEQ Implementation of the GM VFNS

The CTEQ group has always followed the general PQCD framework as formulated in [6, 7]. Up to CTEQ6.1, the default CTEQ PDF sets were obtained using the more familiar ZM Wilson coefficients, because, the vast majority of HEP applications carried out by both theorists and experimentalists use this calculational scheme. For those applications that emphasized heavy quarks, special GM VFNS PDF sets were also provided; these were named as CTEQnHQ, where $n = 4, 5, 6$.

The earlier CTEQ PDFs are now superseded by CTEQ6.5 [1] and CTEQ6.6 [3] PDFs; these are based on a new implementation of the general framework described in previous sections, plus using the simplifying SACOT choice of heavy quark Wilson coefficients [9, 23] specified by Eq. 12 above. There are no additional modifications of the formulae of the minimal GM VFNS, as described in previous sections. CTEQ uses the convention of designating tree-level, 1-loop, 2-loop calculations as LO, NLO, and NNLO, for all physical quantities, $F_\lambda^{\rm tot}$, $F_\lambda^{\rm H}$, ... etc., cf. Sec. 1.2.6.

With these minimal choices, this implementation is extremely simple. Continuity of physical predictions across matching points in the scale variable $\mu = Q$ is guaranteed by Eqs. 8 and 10; and continuity across physical thresholds in the physical variable W, for producing heavy

flavor final states, are guaranteed by the use of ACOT-χ rescaling variables 5, as described in Sec. 1.2.4.

For example, to examine the continuity of physical predictions to NLO in this approach, we have, for the below/above matching point calculations:

$$\begin{aligned} F_2^{-H}(x,Q^2) &= \alpha_s C_{2,Hg}^{-,1} \otimes g^{n_f} \\ F_2^{+H}(x,Q^2) &= \alpha_s C_{2,Hg}^{+,1} \otimes g^{n_f+1} + (C_{2,HH}^{+,0} + \alpha_s C_{2,HH}^{+,1}) \otimes (h+\bar{h}) \end{aligned} \tag{13}$$

where non-essential numerical factors have been absorbed into the convolution $\otimes$. The continuity of $F_2^H(x,Q^2)$ in the scaling variable $\mu = Q$ is satisfied by construction (Eq. 9) because the relation between the PDFs given by Eq. 7 and that between the Wilson coefficients given by Eq. 8 involve the same transformation matrix $\{A_{jk}\}$ (calculated in [12, 13, 21]). In fact, to this order, $A_{Hg} = \alpha_s P_{qg}^0 \ln(Q/m_H)$, hence

$$\begin{aligned} h(\bar{h}) &= 0 \\ g^{n_f+1} &= g^{n_f} \\ C_{2,Hg}^{+,1} &= C_{2,Hg}^{-,1}\,, \end{aligned}$$

at the matching point $\mu = Q = m_H$. Thus, the two lines in Eq. 13 give the same result, and $F_2^H(x,Q^2)$ is continuous. The separate issue of continuity of $F_2^H(x,Q^2)$ in the physical variable W across the production threshold of $W = 2m_H$ is satisfied automatically by each individual term (using the ACOT-χ prescription for the quark terms and straightforward kinematics for the gluon term).

In the CTEQ approach, all processes are treated in a uniform way; there is no need to distinguish between neutral current (NC) and charged current (CC) processes in DIS, (among others, as in MRST/MSTW). All CTEQ global analyses so far are carried out up to NLO. This is quite adequate for current phenomenology, given existing experimental and other theoretical uncertainties. Because NNLO results has been known to show signs of unstable behavior of the perturbative expansion, particularly at small-x, they are being studied along with resummation effects that can stabilize the predictions. This study is still underway.

1.3.5 MRST/MSTW Implementation of the GM VFNS

Prescription. In the Thorne-Roberts (TR) heavy flavour prescriptions, described in [14, 15] the ambiguity in the definition of $C_{2,HH}^{\mathrm{VF},0}(Q^2/m_H^2)$ was exploited by applying the constraint that $(d\,F_2^{\mathrm{H}}/d\,\ln Q^2)$ was continuous at the transition point (in the gluon sector). However, this becomes technically difficult at higher orders. Hence, in [20] the choice of heavy-flavour coefficient functions for F_2^H was altered to be the same as the SACOT(χ) scheme described above. This choice of heavy-flavour coefficient functions has been used in the most recent MRST/MSTW analysis, in the first instance in [2]. To be precise the choice is

$$C_{2,HH}^{\mathrm{VF},n}(Q^2/m_H^2, z) = C_{2,HH}^{\mathrm{ZM},n}(z/x_{max}). \tag{14}$$

This is applied up to NNLO in [20] and in subsequent analyses. For the first time at this order satisfying the requirements in Eq.(10) leads to discontinuities in coefficient functions, which up

to NNLO cancel those in the parton distributions. This particular choice of coefficient functions removes one of the sources of ambiguity in defining a GM VFNS. However, there are additional ambiguities in the MRST/MSTW convention for counting LO, NLO, ... calculations (cf. Sec.1.2.6), coming about because the ordering in α_S for $F_2^H(x,Q^2)$ is different above and below matching points in Eqs. 9-11. (These complications do not arise in the minimal GM VFNS adopted by CTEQ, as already mentioned in the previous subsection.)

For the neutral current DIS F_2 structure function, the above-mentioned ambiguities can be see as follows:

$$\begin{array}{lcc} & \text{below} & \text{above} \\ \text{LO} & \frac{\alpha_S}{4\pi} C_{2,Hg}^{-,1} \otimes g^{n_f} & C_{2,HH}^{+,0} \otimes (h+\bar{h}) \\ \text{NLO} & \left(\frac{\alpha_S}{4\pi}\right)^2 (C_{2,Hg}^{-,2} \otimes g^{n_f} + C_{2,Hq}^{-,2} \otimes \Sigma^{n_f}) & \frac{\alpha_S}{4\pi}(C_{2,HH}^{+,1} \otimes (h+\bar{h}) + C_{2,Hg}^{+,1} \otimes g^{n_f+1}) \\ \text{NNLO} & \left(\frac{\alpha_S}{4\pi}\right)^3 & \sum_i C_{2,Hi}^{+,2} \otimes f_i^{n_f} \left(\frac{\alpha_S}{4\pi}\right)^2 \sum_j C_{2,Hj}^{+,2} \otimes f_j^{n_f+1}, \end{array} \tag{15}$$

with obvious generalization to even higher orders. This means that switching directly from a fixed order with n_f active quarks to fixed order with n_f+1 active quarks leads to a discontinuity in $F_2^H(x,Q^2)$. As with the discontinuities in the ZM-VFNS already discussed this is not just a problem in principle – the discontinuity is comparable to the errors on data, particularly at small x. The TR scheme, defined in [14, 15], and all subsequent variations, try to maintain the particular ordering in each region as closely as possible. For example at LO the definition is

$$\begin{aligned} F_2^H(x,Q^2) &= \frac{\alpha_S(Q^2)}{4\pi} C_{2,Hg}^{-,1}(Q^2/m_H^2) \otimes g^{n_f}(Q^2) \\ &\to \frac{\alpha_S(m_H^2)}{4\pi} C_{2,Hg}^{-,1}(1) \otimes g^{n_f}(m_H^2) + C_{2,HH}^{+,0}(Q^2/m_H^2) \otimes (h+\bar{h})(Q^2). \end{aligned} \tag{16}$$

The $\mathcal{O}(\alpha_S)$ term is frozen when going upwards through $Q^2 = m_H^2$. This generalizes to higher orders by freezing the term with the highest power of α_S in the definition for $Q^2 < m_H^2$ when moving upwards above m_H^2. Hence, the definition of the ordering is consistent within each region, except for the addition of a constant term (which does not affect evolution) above $Q^2 = m_H^2$ which becomes progressively less important at higher Q^2, and whose power of α_S increases as the order of the perturbative expansion increases.

This definition of the ordering means that in order to define a GM VFNS at NNLO [20] one needs to use the $\mathcal{O}(\alpha_S^3)$ heavy-flavour coefficient functions for $Q^2 \leq m_H^2$ (and that the contribution will be frozen for $Q^2 > m_H^2$). This would not be needed in a ACOT-type scheme. As mentioned above, these coefficient functions are not yet calculated. However, as explained in [20], one can model this contribution using the known leading threshold logarithms [24] and leading $\ln(1/x)$ terms derived from the k_T-dependent impact factors [25]. This results in a significant contribution at small Q^2 and x with some model dependence. However, variation in the free parameters does not lead to a large change.[8]

[8] It should be stressed that this model is only valid for the region $Q^2 \leq m_H^2$, and would not be useful for a NNLO

The above discussions focused on F_2^H; but they mostly apply to F_L as well. We only need to mention that, with the adoption of the SACOT prescription for heavy-quark initiated contributions (i.e. using the ZM version of the Wilson coefficient), F_L^H vanishes at order α_s^0 as it does in the TR prescriptions.(This zeroth order coefficient function does appear in some older GM VFNS definitions.) According to the MRST/MSTW convention, the order α_s^1 term of F_L (both light and heavy flavour) counts as LO, and so on, whereas in the CTEQ convention each relative order is a power of α_S lower.

The general procedure for the GM VFNS for charged-current deep inelastic scattering can work on the same principles as for neutral currents, but one can produce a *single* charm quark from a strange quark so $\chi = x(1 + m_c^2/Q^2)$. However, there is a complication compared to the neutral current case because the massive FFNS coefficient functions are not known at $\mathcal{O}(\alpha_S^2)$ (only asymptotic limits [27] have been calculated). These coefficient functions are needed in a TR-type scheme at low Q^2 at NLO, and for any GM VFNS at all Q^2 at NNLO. This implies that we can only define the TR scheme to LO and the ACOT scheme to NLO. However, known information can be used to model the higher order coefficient functions similarly to the TR scheme definition to NNLO for neutral currents. A full explanation of the subtleties can be found in [28].

Scheme variations. The inclusion of the complete GM VFNS in a global fit at NNLO first appeared in [2], and led to some important changes compared a previous NNLO analysis, which had a much more approximate inclusion of heavy flavours (which was explained clearly in the Appendix of [29]). There is a general result that $F_2^c(x, Q^2)$ is flatter in Q^2 at NNLO than at NLO, as shown in Fig. 4 of [2], and also flatter than in earlier (approximate) NNLO analyses. This had an important effect on the gluon distribution. As seen in Fig. 5 of [2], it led to a larger gluon for $x \sim 0.0001 - 0.01$, as well as a larger value of $\alpha_S(M_Z^2)$, both compensating for the naturally flatter evolution, and consequently leading to more evolution of the light quark sea. Both the gluon and the light quark sea were $6 - 7\%$ greater than in the MRST2004 set [30] for $Q^2 = 10,000\mathrm{GeV}^2$, the increase maximising at $x = 0.0001 - 0.001$. As a result there was a 6% increase in the predictions for σ_W and σ_Z at the LHC. This would hold for all LHC processes sensitive to PDFs in this x range, but would be rather less for processes such as $t\bar{t}$ pair production sensitive to $x \geq 0.01$. This surprisingly large change is a correction rather than a reflection of the uncertainty due to the freedom in choosing heavy flavour schemes and demonstrates that the MRST2004 NNLO distributions should now be considered to be obsolete.

To accompany the MRST 2006 NNLO parton update there is an unofficial "MRST2006 NLO" set, which is fit to exactly the same data as the MRST2006 NNLO set. By comparing to the 2004 MRST set one can check the effect on the distributions due to the change in the prescription for the GM VFNS at NLO without complicating the issue by also changing many other things in the analysis. The comparison of the up quark and gluon distributions for the "MRST2006 NLO" set and the MRST2004 NLO set, i.e. the comparable plot to Fig. 5 of [2] for NNLO, is shown in Fig. 1. As can be seen it leads to the same trend for the partons as at NNLO, i.e. an increase in the small-x gluon and light quarks, but the effect is much smaller –

FFNS at all Q^2 since it contains no information on the large Q^2/m_H^2 limits of the coefficient functions. A more general approximation to the $\mathcal{O}(\alpha_S^3)$ coefficient functions could be attempted, but full details would require first the calculation of the $\mathcal{O}(\alpha_S^3)$ matrix element A_{Hg}. This more tractable project is being investigated at present [26].

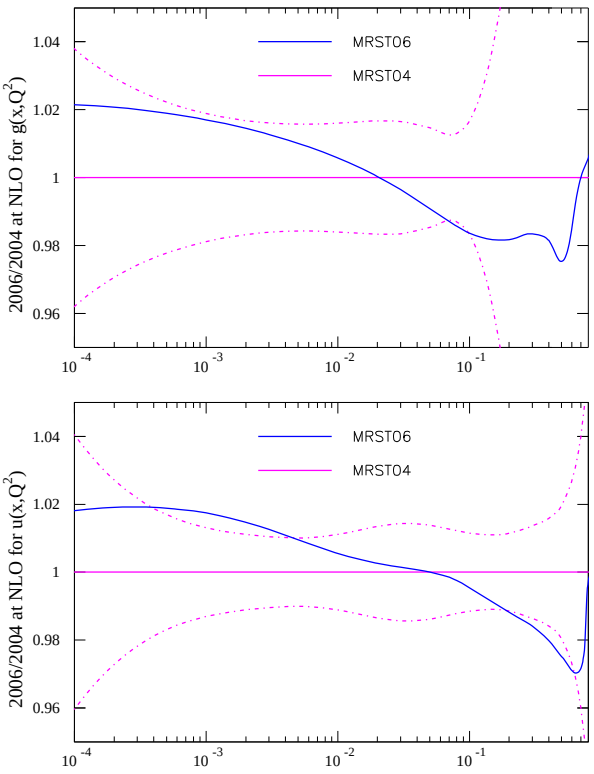

Fig. 1: A comparison of the unpublished "MRST2006 NLO" parton distributions to the MRST2004 NLO distributions. In order to illustrate the significance of the size of the differences, the uncertainty on the MRST2001 distributions is used for the 2004 distributions.

a maximum of a 2% change. Also, the value of the coupling constant increases by 0.001 from the 2004 value of $\alpha_S(M_Z^2) = 0.120$. From momentum conservation there must be a fixed point and this is at $x \sim 0.05$. Hence, W, Z and lighter particle production could be affected by up to $2 - 3\%$, and very high mass states by a similar amount, but final states similar in invariant mass to $t\bar{t}$ will be largely unaffected. Hence, we can conclude that the change in our choice of the heavy-flavour coefficient function alone leads to changes in the distributions of up to 2%, and since the change is simply a freedom we have in making a definition, this is a theoretical uncertainty on the partons, much like the frequently invoked scale uncertainty. Like the latter, it should decrease as we go to higher orders.

1.3.6 Comparisons

We have tried to make clear that both the CTEQ and the MRST/MSTW approaches are consistent with the PQCD formalism with non-zero heavy quark masses $\{m_H\}$. In this sense, they are both "valid". In addition, they both adopt certain sensible practises, such as the numerically significant rescaling-variable approach to correctly treat final-state kinematics (ACOT-χ), and the calculationally simplifying SACOT prescription for the quark-parton initiated subprocesses. These common features ensure broad agreement in their predictions. This is borne out by the fact that global QCD analyses carried out by both groups show very good agreement with all available hard scattering data, including the high-precision DIS total inclusive cross sections and semi-inclusive heavy flavor production cross sections; and that the predictions for higher energy cross sections at LHC for the important W/Z production process agree rather well in the most recent versions of these analyses [2, 3].[9] Comparisons of experiment for the abundant data on total inclusive cross sections (and the associated structure functions) with theory are well documented in the CTEQ and MRST/MSTW papers. Here we only show the comparison of the recent H1 data sets on cross sections for charm and bottom production [31] to the latest CTEQ and MSTW calculations. This figure illustrates the general close agreement between the two calculations. (Also, see below.)

Because the main source of the differences between the two implementations arise from the different conventions adopted for organizing the perturbative calculation, it is impossible to make a direct (or clear-cut) comparison between the two calculations. By staying with the conventional order-by-order formulation, the CTEQ approach has all the simplicities of the minimal GM VFNS. With the alternative LO/NLO/NNLO organization, the MRST/MSTW approach includes specifically chosen higher-order terms at each stage of the calculation for different physical quantities (e.g. $F_2^{\rm tot}, F_L^{\rm tot}, F_2^{\rm H}$, in Secs. 1.3.5) with their associated Wilson coefficients (e.g. Eqs. 15,16). The choices are a matter of taste because, with the same Wilson coefficients (with heavy quark mass) available in the literature (such as [12, 13]), both analyses can be extended to the appropriate order, and they should contain the same information. So far, MRST/MSTW has carried out their analyses to one order higher than CTEQ. In practice, we have seen one comparison of the "NLO" predictions of the two approaches in Fig. 2 that shows remarkable general agreement with each other, and with experimental data. Some expected differences at small-x, due to the higher order term included in the MRST/MSTW calculation are

[9] Some apparent worrying discrepancies in the predictions for the W/Z cross-sections at LHC between [1] and [30] have been superseded by the recent analyses.

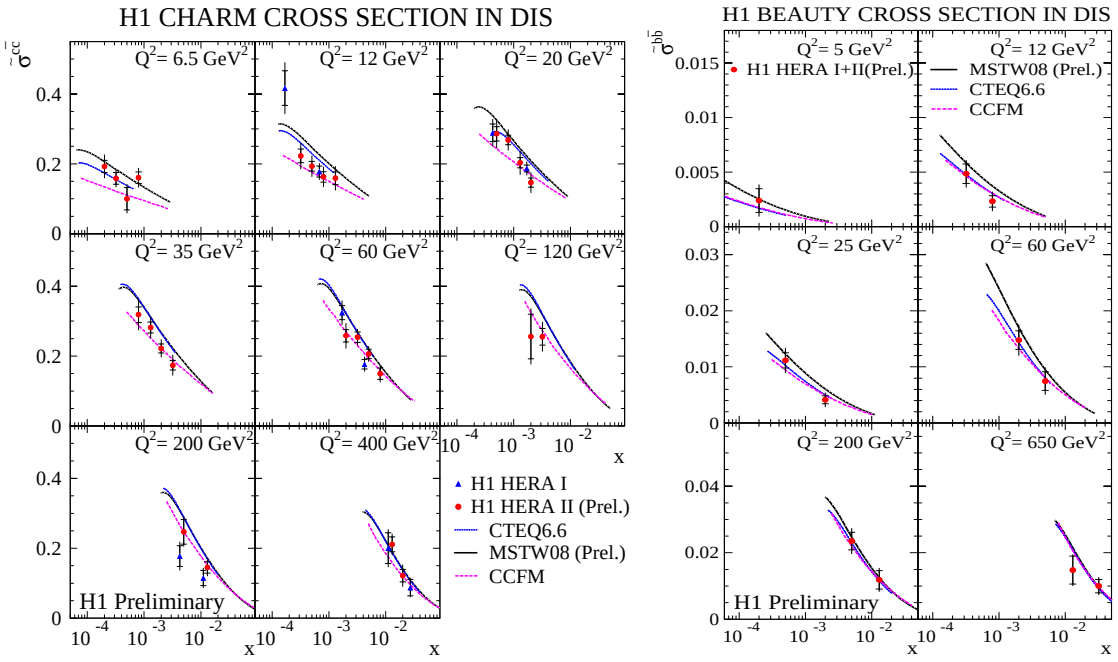

Fig. 2: Comparison of the predictions for $\tilde{\sigma}^{c\bar{c}}(x, Q^2)$ and $\tilde{\sigma}^{b\bar{b}}(x, Q^2)$ compared to preliminary data from H1.

present. Compared to experimental data, the CTEQ curves seem to give a slightly better description of data in this region of difference; but this should not be taken seriously in view of the above discussions. We intend to make a more quantitative study of the differences between the alternative formulations of a GM VFNS and ZM VFNS in a future publication.

1.4 Use of Parton Distribution Functions

Some commonly asked questions in the user community for PDFs are along the lines of: (i) Which available PDF set is most appropriate for my particular calculation? and (ii) If PDF set A was obtained using scheme A (say, ZMVFNS/GMVFNS-MSTW/GMVFNS-CTEQ) do I have to use the same scheme A for my Wilson coefficients (otherwise my calculation would be inconsistent)? Whereas it is impossible to answer all such questions at once, the following observations should provide useful guidelines toward the appropriate answers. Foremost, it is important to bear in mind that in the perturbative approach, all calculations are approximate; hence the goodness of the approximation is the most (or only) relevant consideration. Any fast, or absolute, rules or prescriptions would be misguided.

***** For applications at very high energy scales, e.g. most LHC processes, it is perfectly fine to use the ZM formulae for the hard-scattering coefficient *irrespective of the choice of PDF sets* (see below), since the ZM Wilson coefficients are good approximations to the GM ones (valid to $\mathcal{O}(M^2/Q^2)$ where M represents the typical mass in the relevant parton subprocess—heavy quarks or other produced particles), and the ZM coefficients are much simpler and *much more* readily available.

On the other hand, for applications involving physical scales $Q \sim \mathcal{O}(M)$, such as comparison to precision DIS data at HERA, it is important both to use GM Wilson coefficients, and to ensure that these are consistent with those adopted in generating the PDF set to be used in the calculation.

***** For the global analyses that yield the PDF sets, it matters whether the ZM VFNS or GM VFNS scheme is used in the calculation, since a substantial fraction of the input DIS data are in the region where Q is not very large compared to the heavy quark masses $m_{c,b}$ (the top quark does not play a significant role in these analysis). Thus, the ZM-VFNS and GM VFNS PDFs can differ in some x-range, even if they agree quite well in general (cf. [1]). For example, the widely used CTEQ6.1 (ZM-VFNS) and the most recent CTEQ6.5/CTEQ6.6 (GM VFNS) PDF sets both give excellent fits to the available data, yet the differences (mainly around $x \sim 10^{-3}$) are enough to lead to a 6% shift in the predictions for cross sections for W, Z and similar mass states at the LHC. Higher mass final states are much less affected.

The above differences arise from two sources: (i) the treatment of final-state counting (Sec. 1.2.3) and phase space (Sec. 1.2.4); and (ii) mass effects in the Wilson coefficients. The first is numerically significant for reasons explained in those sections, and it can potentially be removed to produce an improved ZM VFNS (Sec. 1.3.1).

***** The differences between PDFs obtained using different GM VFNS implementations, such as those by CTEQ and MSTW groups discussed in the main part of this review, are much smaller than those between the ZM and GM VFNS. This is because the treatments of final states are similar, and the differences in the Wilson coefficients are much reduced also. The current NLO predictions on W/Z cross sections at LHC by the CTEQ and MSTW groups, for instance, are within 2% [4].

***** What about single-flavor (say, n_f) FFNS PDFs that are commonly believed to be needed for FFNS calculations, such as for heavy flavor production processes? We would like to point out, perhaps surprisingly to many readers, that: (i) with the advent of GM VFNS PDFs, *the FFNS PDFs are not in principle needed* for consistency; and (ii) the use of n_f-flavor FFNS PDFs in a n_f-flavor calculation is much *less reliable* than using the GM VFNS (if the latter is available). The reasons for these assertions are fairly easy to see, as we now explain.

First of all, as we emphasized in Sec. 1.2.2, the GM VFNS is, by definition, a composite scheme that *is* the n_f-FFNS within the region of validity of the latter. In principle one *can* use the GM VFNS PDFs in the FFNS calculations within the region where the FFNS is reliable. (In practice this range of validity (in energy scale μ) extends up to several times m_H, cf. second to last paragraph of Sec. 1.2.2.) Secondly, since any given n_f-FFNS has only a limited range of validity (Sec. 1.2.2), the global analysis used to determine any n_f-FFNS PDF set is inherently a compromise. This compromise is likely to be a fairly bad one for two reasons. Firstly, the limited range of validity implies that only a fraction of the data used in the global analysis can be legitimately applied. If one excludes all the data outside of the region of validity of the theory (not an easily-defined region), the constraining power of the analysis would greatly suffer. If, instead, one includes all the points in the analysis anyway, the PDFs will compensate, much like the case of the fit using the basic ZM VFNS. This can result in a good comparison to data (as in the ZM VFNS [32]), but this is potentially misleading since the compensation is caused by

the wrong physics. In either of the cases, the PDFs resulting from a fit using the FFNS will be unreliable. Secondly, Wilson coefficients in the FFNS only exist for the DIS process beyond LO, hence the ZM approximation to n_f-FFNS must be used. We note, although this second point is shared by current GM VFNS analyses, the ZM VFNS approximation to GM VFNS is a much better approximation than that of ZM FFNS to n_f-FFNS. (For instance, for collider jet data sets, the ZM 3- or 4-flavor calculation would be way-off the correct one. This is not a problem for the GM VFNS case.) These inherent problems motivated an alternative approach to FFNS PDFs in [33]: rather than performing a (imperfect) FFNS global fit, one simply generates them by fixed n_f-flavor QCD evolution from a set of initial PDFs obtained in an existing (bona fide) GM VFNS global analysis! Because of the different QCD evolution, however, the PDFs will be different from the original GM VFNS ones crossing heavy flavor thresholds; and the fits to the global data will correspondingly deteriorate, particularly for the high precision HERA data sets at higher Q^2. Thus, these PDFs deviate from truth in a different way. The relative merit between this approach and the conventional FFNS global fits is difficult to gauge because there are no objective criteria for making the assessment.

Returning to the original question that started this bullet item, we can summarize the options available to match PDFs with a FFNS calculation such as HQVDIS [34] for heavy quark production: (i) conventional FFNS PDFs (CTEQ, GRV), suitably updated if necessary [35]; (ii) PDFs generated by FFNS evolution from GM VFNS PDFs at some initial scale Q_0 (MSTW [33], but also can easily be done with CTEQ); or, (iii) simply use the most up-to-date GM VFNS PDFs (MSTW, CTEQ) for all Q. For reasons discussed in the previous paragraphs, each option has its advantages and disadvantages. (i) and even (ii) are theoretically self-consistent, while (iii) is not, e.g. it opens up the akward question of how many flavours to use in the definition of α_S. However, the PDFs in (iii) are intrinsically much more accurately and precisely determined. Hence, in practical terms it is not obvious which would be most "correct".[10] The choice reduces to a matter of taste, and for some, of conviction. The differences in results, obtained using these options, should not be too large, since they are mostly of one order higher in α_s; and, in an approximate manner, they define the existing theoretical uncertainty. In principle, an approach that combines the advantages of all three, hence could work the best, would be to use PDFs obtained in the GM VFNS, but with the transition scale μ_T (Sec. 1.2.3) set at a much higher value than m_H for each heavy flavor threshold. But this option is rather cumbersome to implement (as has been hinted in Sec. 1.2.3), hence has not been done.

***** There exists another class of applications, involving multiple-scale processes, such as heavy flavor production at hadron colliders with finite transverse momentum p_T or in association with W/Z or Higgs, for which PQCD calculations are more complex than the familiar one-hard-scale case, as implicitly assumed above. Since these processes can play an important role in LHC, there has been much discussions, and controversies, in recent literature about the various approaches that may be applied [36]. Both the GM VFNS [37] and FFNS approaches have been advocated [38]. The problem is complex, generally because more than one kind of potentially large logarithms occur in these problems, and they cannot be effectively controlled all at once with some suitable choice of scheme. A detailed discussion is outside the scope of this paper,

[10] Although it is certainly better to use a current GM VFNS set of PDFs than an out-of-date FFNS set.

although our remark about the FFNS PDFs above could be helpful (and relieve some of the anxieties expressed in the literature).

All in all, for general applications, taking into account all the considerations above, the modern GM VFNS PDF sets are clearly the PDFs of choice.

1.5 Intrinsic Heavy Flavour

Throughout the above discussions we have made the assumption that all heavy quark flavour is generated from the gluon and lighter flavours through the perturbative QCD evolution, starting from the respective scale $\mu = m_H$. This is usually referred to as the *radiatively generated heavy flavor* scenario. From the theoretical point of view, this is reasonable for heavy flavors with mass scale (m_H) very much higher than the on-set of the perturbative regime, say $\sim$ 1 GeV. Thus, while this assumption is usually not questioned for bottom and top, the case for charm is less obvious. In fact, the possibility for a non-negligible *intrinsic charm* (IC) component of the nucleon at $\mu = Q \sim m_c$ was raised a long time ago [39]; and interests in this possibility have persisted over the years. Whereas the dynamical origin of such a component can be the subject of much debate, the phenomenological question of its existence can be answered by global QCD analysis: do current data support the IC idea, and if so, what is its size and shape? This problem has been studied recently by a CTEQ group [40], under two possible scenarios: IC is enhanced at high values of x (suggested by dynamical models such as [39]), or it is similar in shape to the light-flavor sea quarks (similar to, say, strange). They found that current data do not tightly constrain the charm distribution, but they *can* place meaningful bounds on its size. Thus, while the conventional radiatively generated charm is consistent with data, IC is allowed in both scenarios. For the model-inspired (large-x) case, the size of IC can be as large as ~ 3 times that of the crude model estimates, though comparison to the EMC F_2^c data [41] imply contributions somewhat smaller [42]. If such an IC component does exist, it would have significant impact on LHC phenomenology for certain beyond SM processes. For the sea-like IC case, the bound on its size is looser (because it can be easily interchanged with the other sea quarks in the global fits); its phenomenological consequences are likewise harder to pin-point.

From a theoretical point of view, intrinsic heavy flavour and GM VFNS definitions were discussed in [43]. Allowing an intrinsic heavy quark distribution actually removes the redundancy in the definition of the coefficient functions in the GM VFNS, and two different definitions of a GM VFNS will no longer be identical if formally summed to all orders, though they will only differ by contributions depending on the intrinsic flavour. Consider using identical parton distributions, including the intrinsic heavy quarks, in two different flavour schemes. The heavy-quark coefficient functions at each order are different by $\mathcal{O}(m_H^2/Q^2)$. This difference has been constructed to disappear at all orders when combining the parton distributions other than the intrinsic heavy quarks, but will persist for the intrinsic contribution. The intrinsic heavy-flavour distributions are of $\mathcal{O}(\Lambda_{QCD}^2/m_H^2)$, and when combined with the difference in coefficient functions the mass-dependence cancels leading to a difference in structure functions of $\mathcal{O}(\Lambda_{QCD}^2/Q^2)$. It has been shown [7] that for a given GM VFNS the calculation of the structure functions is limited in accuracy to $\mathcal{O}(\Lambda_{QCD}^2/Q^2)$. Hence, when including intrinsic charm, the scheme ambiguity is of the same order as the best possible accuracy one can obtain in leading twist QCD, which is admittedly better than that obtained from ignoring the intrinsic heavy flavour (if it exists) as Q^2

increases above m_H^2. It is intuitively obvious that best accuracy will be obtained from a definition of a GM VFNS where all coefficient functions respect particle kinematics. In fact, the most recent CTEQ and MSTW prescriptions would provide identical contributions to the structure functions from the same intrinsic charm parton distribution.

Acknowledgements We thank Matteo Cacciari for his unrelenting efforts to bring about this review on behalf of the Heavy Flavor Workshop of the HERALHC Workshop. We thank our collaborators in CTEQ and MRST/MSTW for collaborations which underlies much of the content of this paper. WKT would like especially to acknowledge the insight provided by John Collins on the theoretical foundation of PQCD with heavy quarks. We also thank Pavel Nadolsky, Fred Olness, Ingo Schienbein, Jack Smith and Paul Thompson for reading the manuscript and making useful comments that brought about improvements in the presentation of the paper.

The work of WKT is supported by the National Science Foundation (USA) under the grant PHY-0354838.

2 Charmed-meson fragmentation functions with finite-mass corrections

Authors: B. A. Kniehl, G. Kramer, I. Schienbein, and H. Spiesberger

A straight-forward and conventional approach to include heavy-quark mass effects in the theoretical predictions for the production of single heavy-flavor mesons consists in taking into account the non-zero quark mass m_h in a calculation where only light quarks and the gluon exist in the initial state and the heavy quark is pair-produced in the hard scattering process. Such a scheme is called a fixed-flavor-number scheme (FFNS) and can be implemented, presently, only at NLO. It is reliable in a kinematic region not far above production threshold. At high scales μ, however, the presence of logarithmic terms proportional to $\log(\mu/m_h)$ makes the predictions of a calculation in the FFNS unreliable. These logarithmic terms have to be resummed, which is conventionally done in the so-called zero-mass variable-flavor-number scheme (ZM-VFNS) where the heavy quark is treated as a parton, in addition to light quarks and the gluon. Heavy quark parton distribution functions and fragmentation functions, which are present in this scheme, can absorb the large logarithmic terms and resummation is performed with the help of the DGLAP evolution equations.

The general-mass variable-flavor-number scheme (GM-VFNS) provides a framework for the theoretical description of the inclusive production of single heavy-flavored hadrons, combining virtues of both the FFNS and the ZM-FVNS in a unified approach. It resums large logarithms by the DGLAP evolution of non-perturbative fragmentation functions, guarantees the universality of the latter as in the ZM-VFNS, and simultaneously retains the mass-dependent terms of the FFNS without additional assumptions. It was elaborated at next-to-leading order (NLO) for photo- [45] and hadroproduction [46, 47] and e^+e^- annihilation [48].

Recent progress in the implementation of the GM-VFNS at NLO allowed us to extract mass-dependent FFs for D-mesons from global fits to e^+e^- annihilation data [48]. We used experimental data from the Belle, CLEO, ALEPH, and OPAL Collaborations [44]. The fits for D^0, D^+, and D^{*+} mesons using the Bowler ansatz [49] yielded $\chi^2/\mathrm{d.o.f.} = 4.03$, 1.99, and 6.90, respectively. The result of the fit for D^+ mesons is shown in Fig. 3.

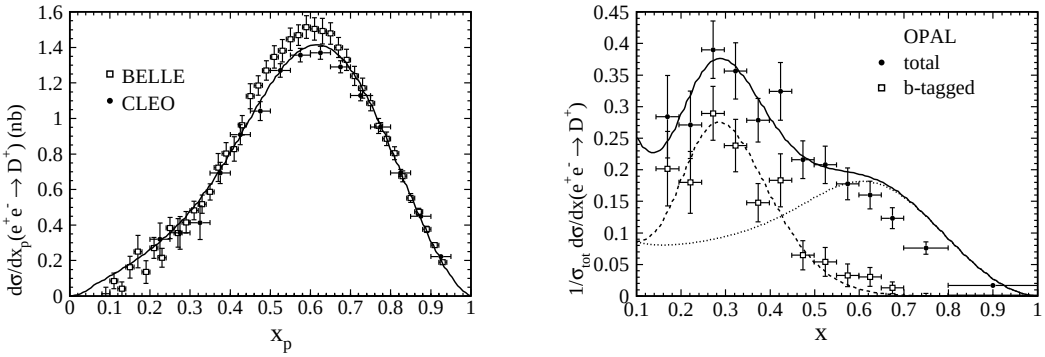

(a) (b)

Fig. 3: Comparison of (a) Belle, CLEO, and (b) OPAL data on D^+ mesons [44] with a global fit. The dotted line in panel (b) refers to the c-quark-initiated contribution.

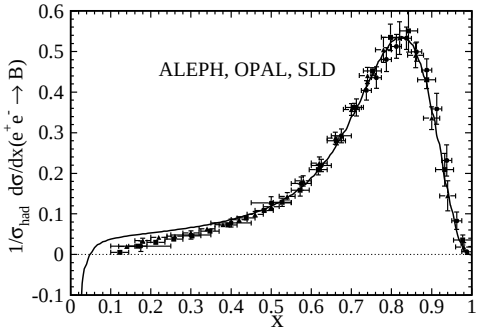

Fig. 4: Comparison of the ALEPH, OPAL, and SLD data on B meson production [50] with a fit for the $b \to B$ FF.

The significance of finite-mass effects can be assessed through a comparison with a similar analysis in the ZM-VFNS. It turned out that for the experimental conditions at Belle and CLEO, charmed-hadron mass effects on the phase space are appreciable, while charm-quark mass effects on the partonic matrix elements are less important. In Figs. 3(a) and (b), the scaled-momentum distributions from Belle and CLEO and the normalized scaled-energy distributions from OPAL for D^+ mesons are compared to the global fits. The Belle and CLEO data prefer higher values for the average x of the $c \to D$ FFs. Due to their smaller errors they dominate the global fit, and the ALEPH and OPAL data are less well described. Charmed hadrons may also originate indirectly through the fragmentation of a b quark. Our ansatz includes non-perturbative $b \to D$ FFs, but these are only weakly constrained by the Belle and CLEO data.

Previous fits of the $b \to B$ FFs in the ZM-VFNS [52] were based on e^+e^- data from ALEPH, OPAL and SLD [50] and used the Kartvelishvili-Likhoded ansatz [53]. As a recent improvement we adjusted the value of m_b and the energy scale where the DGLAP evolution starts,

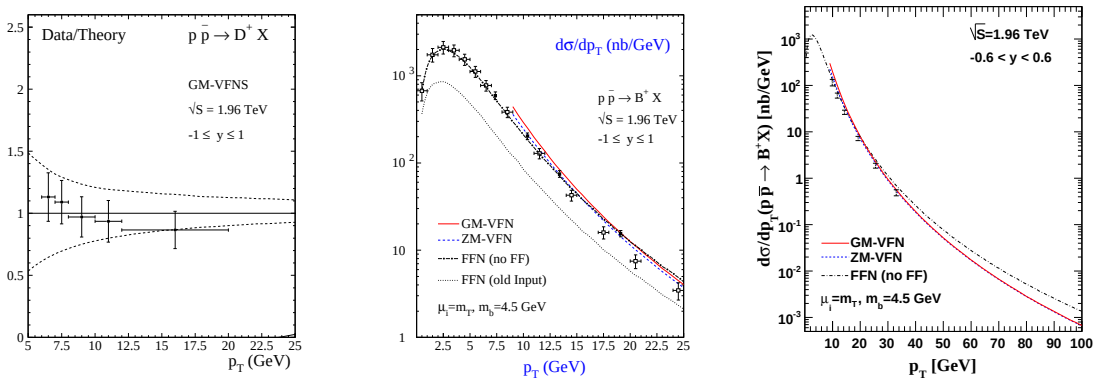

(a) (b) (c)

Fig. 5: (a) Comparison of CDF II data [51] on D^+ mesons with the global fit.

to conform with modern PDF sets. The data are well described by the fit, with a $\chi^2/\text{d.o.f.} = 1.495$. The result is shown in Fig. 4.

Usage of these new FFs leads to an improved description of the CDF data for charmed-meson production [54] from run II at the Tevatron, as may be seen by comparing Fig. 5(a) in this chapter with Fig. 2(b) of Ref. [47]. Also predictions for B-meson production agree with CDF II data [51]. Comparing massless and massive calculations, we found that finite-m_b effects moderately enhance the p_T distribution; the enhancement amounts to about 20% at $p_T = 2m_b$ and rapidly decreases with increasing values of p_T, falling below 10% at $p_T = 4m_b$ (see Fig. 5b). Such effects are thus comparable in size to the theoretical uncertainty due to the freedom of choice in the setting of the renormalization and factorization scales. At higher values of the transverse momentum, p_T, the predictions of the GM-VFNS and ZM-VFNS approach each other by construction. There, resummation of large logarithms will be important and a FFNS calculation will become inappropriate since it does not resum large logarithms. CDF data reach up to 40 GeV and preliminary data at the highest values of p_T indicate that resummation of large logarithmic terms will be necessary to obtain a reasonable description of experimental results.

3 Fragmentation of heavy quarks with an effective strong coupling constant

Authors: G. Corcella and G. Ferrera

We describe a model to include non-perturbative corrections to heavy-quark fragmentation, based on next-to-next-to-leading logarithmic threshold resummation and an effective QCD coupling constant not containing the Landau pole. Comparison with experimental data is also presented.

The hadronization of partons into hadrons cannot be calculated from first principles, but it is usually described in terms of phenomenological models, containing few parameters which need to be tuned to experimental data. In this paper we propose a different approach to describe heavy-quark (bottom and charm) fragmentation in e^+e^- processes: we use a non-perturbative model [55, 56] including power corrections via an effective strong coupling constant, which does

not exhibit the Landau pole. The interesting feature of such a model is that it does not contain any extra free parameter to be fitted to the data, besides the ones entering in the parton-level calculation. In [57, 58] such a model was also employed in the framework of B-meson decays and it was found good agreement with the experimental data. Moreover, it was even possible to extract $\alpha_S(m_Z)$ and the Cabibbo-Kobayashi-Maskawa matrix element $|V_{ub}|$ from such data [57, 58]. In the following, we shall consider heavy-quark production in e^+e^- annihilation, in particular b- and c-quark production at LEP. In [56], charm-quark fragmentation at the $\Upsilon(4S)$ resonance was also investigated.

The perturbative fragmentation approach [59], up to power corrections, factorizes the energy distribution of a heavy quark as the convolution of a process-dependent coefficient function, associated with the emission off a massless parton, and a process-independent perturbative fragmentation function, expressing the transition of the light parton into a heavy quark. The heavy-quark spectrum reads:

$$\frac{1}{\sigma}\frac{d\sigma}{dx}(x,Q,m_q) = C(x,Q,\mu_F) \otimes D(x,\mu_F,m_q) + \mathcal{O}\left((m_q/Q)\right). \tag{17}$$

where Q is the hard scale of the process, x is the heavy-quark energy fraction in the centre-of-mass frame, i.e. $x = \frac{2E_q}{Q}$, and $\mu_F \sim Q$ is the factorization scale.

The perturbative fragmentation function follows the DGLAP evolution equations. As in [55, 56], we use coefficient function and initial condition at next-to-leading order (NLO) and solve the DGLAP equations with a NLO kernel [11]. This way, one resum the large mass logarithms $\sim \ln(Q^2/m_q^2)$ in the next-to-next-to-leading logarithmic approximation [59]. Furthermore, both coefficient function and initial condition contain terms, $\sim 1/(1-x)_+$ and $\sim [\ln(1-x)/(1-x)]_+$, enhanced when x approaches 1, which corresponds to soft- or collinear-gluon radiation. One needs to resum such contributions to all orders to improve the perturbative prediction (threshold resummation) [60]. In our analysis, we implement threshold resummation in the next-to-next-to-leading logarithmic (NNLL) approximation. following the general method of [61, 62].

Let us now briefly discuss the phenomenological model which includes non-perturbative power corrections through an effective QCD coupling [55–57, 63]. We start by constructing a general analytic QCD coupling $\bar{\alpha}_S(Q^2)$ from the standard one, by means of an analyticity requirement: $\bar{\alpha}_S(Q^2)$ is defined to have the same discontinuity as the standard coupling and no other singularity [64]. The coupling constant constructed in this way exhibits no Landau pole, which is subtracted by a power correction, while it has the same discontinuity as the standard one for $Q^2 < 0$, related to gluon branching. As discussed in [55], since heavy quark fragmentation is a time-like process, we have to include the absorptive parts of the gluon polarization function into the effective coupling: that amounts to a resummation of constant terms to all orders. As detailed in [55, 56], the effective time-like coupling $\tilde{\alpha}_S(Q^2)$ is thus given by an integral over the discontinuity of the gluon propagator, with the analytic coupling $\bar{\alpha}_S(Q^2)$ entering in the integrand function. At one-loop, for example, one obtains the following effective time-like coupling constant:

$$\tilde{\alpha}_S(Q^2) = \frac{1}{\beta_0}\left[\frac{1}{2} - \frac{1}{\pi}\arctan\left(\frac{\log(Q^2/\Lambda^2)}{\pi}\right)\right]. \tag{18}$$

[11] One could go beyond such a level of accuracy and include next-to-next-to-leading order (NNLO) corrections to the coefficient function, initial condition and to the non-singlet splitting functions.

Our model simply replaces the standard $\alpha_S(Q^2)$ with the effective time-like coupling constant. As in [55, 56], $\tilde{\alpha}_S(Q^2)$ is evaluated up to NNLO, i.e. three-loop accuracy. We stress that, even if our model does not contain any free parameter to be fitted to data, we had to choose among possible different prescriptions, mostly concerning the low-energy behaviour of the effective coupling constant. The model presented in [55, 56] is the one which best describes the experimental data.

In Fig. 6 we compare the predictions of the effective-coupling model with experimental data from ALEPH [65], OPAL [66] and SLD [67] on B-hadron production at the Z^0 pole, and from ALEPH on D^{*+} production [68]. We learn from the comparison that our model, without introducing any tunable parameter, manages to give a good description of the experimental data. As discussed in [55, 56], even the moments of the B- and D-hadron cross section are reproduced quite well.

In summary, we managed to construct a simple non-perturbative model which is able to describe data from rather different processes, namely B-decays and bottom/charm fragmentation, involving pretty different hard scales. We believe that such results are highly non trivial and that our model deserves further extension to hadron-collider physics. This is in progress.

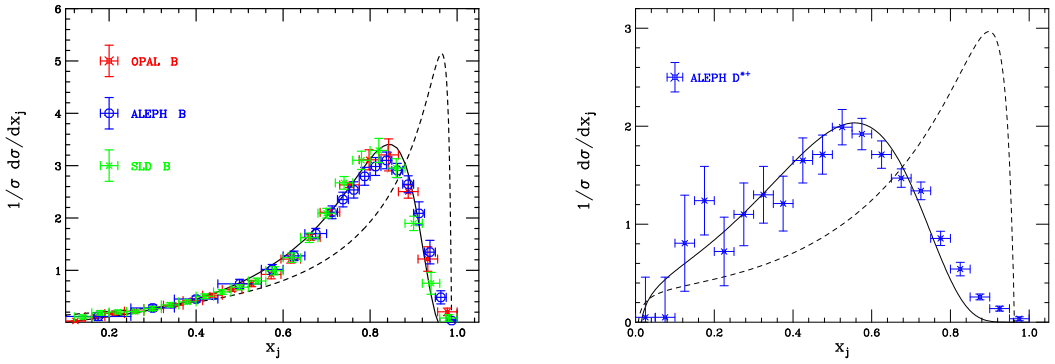

Fig. 6: Results on bottomed (left) and charmed (right) hadron production (solid line), according to the effective-coupling model, compared with the pure parton-level calculation (dashes) and with experimental data. x_j is the hadron ($j = B, D$) or quark ($j = b, c$) energy fraction at the Z^0 pole.

4 Infrared safe determination of jet flavour: theory and applications

Author: A. Banfi and G. Zanderighi

4.1 Problems in defining the flavour of a jet

Jets are so far the best-known way to map a complicated event, characterised by a high particle multiplicity, to a simpler one made up of a small number of clusters of particles, *jets*, whose energy-momentum flow is close to that of the original event. By "close to" we mean that jets have to be infrared and collinear (IRC) safe objects, that is their momenta should not change after an extremely soft particle has been added to the event or if any of the particles in the event splits into a quasi-collinear pair. With this requirement jet cross sections can be safely computed in perturbative (PT) QCD. Furthermore, given a partonic event, any IRC safe jet algorithm, in

the soft/collinear limit, does provide a unique mapping to the underlying hard event.[12] It is interesting to investigate whether jet algorithms can be extended so as to define also the flavour of a jet. More precisely, suppose we have a hard event and a new event obtained from the hard event via an arbitrary number of soft emissions and/or collinear splittings. Is it possible to cluster the new event into jets, such that not only the momenta, but also the flavour of the jets, are equal to those of the particles constituting the original hard event?

Attempts to answer this questions have been performed by different experimental groups, whose definitions of jet flavour are based either on the kinematical properties [69] or on the charge of a jet [70]. Although of considerable practical usefulness, these procedures all suffer from IRC unsafety (see [71] for a discussion on this point).

To see where IRC safety problems may arise we need first to introduce our definition of jet flavour. The flavour of a jet is defined as a n_f-dimensional vector containing in the entry f the net number of quarks (number of quarks minus number of antiquarks) of flavour f. A gluon jet will have a flavour vector in which all entries are zero. A clear source of IR unsafety is gluon splitting into a quark and an antiquark that are recombined with different jets, thus changing the underlying jet flavour. At next-to-leading order (NLO), the only singular contribution occurs when the quarks are collinear. In this case, the $q\bar{q}$ pair is always recombined in the same jet by any IRC safe jet-algorithm, and the resulting jet flavour is also IRC safe. Starting from the next perturbative order however a soft large-angle gluon splitting may produce a q and $\bar{q}$ which are both soft but may not be collinear. Therefore the two fermions can be clustered into two different jets, thereby modifying the flavour of those hard jets. In the next section we will analyse specifically the k_t algorithm, show that its standard version is not IR safe with respect to the jet flavour, and we will see how it can be modified to achieve an IR safe jet-flavour algorithm.

4.2 IR safe jet-flavour algorithms at parton level

Let us see how a jet-flavour algorithm should work in the specific case of e^+e^- annihilation into hadrons. There we consider close-to-Born events with a hard $q\bar{q}$ pair accompanied by an arbitrary number of soft/collinear partons. One of such configurations is represented in fig. 7. It contains a hard $q\bar{q}$ pair (at the bottom of each diagram) accompanied by a soft gluon and a soft $q\bar{q}$ pair originated by the splitting of a large-angle gluon. If one applies the k_t algorithm [72–74] to such a configuration, to all pairs of particles p_i, p_j one associates a distance

$$d_{ij} = 2\,(1-\cos\theta_{ij}) \times \min\{E_i^2, E_j^2\}\,, \tag{19}$$

and clusters together the pair whose d_{ij} is minimum. The resulting set of distances is represented in the picture on the left hand side of fig. 7, where a thick line represents a large distance, while small distances are represented by thin lines. The only large distance obtained with the traditional k_t algorithm is that between the hard $q\bar{q}$ pair, while all other distances are small. This is because all other pairs involve at least one soft parton and the distance in eq. (19) depends on the energy of the softest particle only. Looking in particular at the soft q and $\bar{q}$, they can be clustered in different jets thus giving either a couple of gluon jets or two multi-flavoured jets, i.e. not corresponding

[12] Beyond the soft/collinear limit, such a mapping is intrinsically ambiguous due to the presence of interference terms.

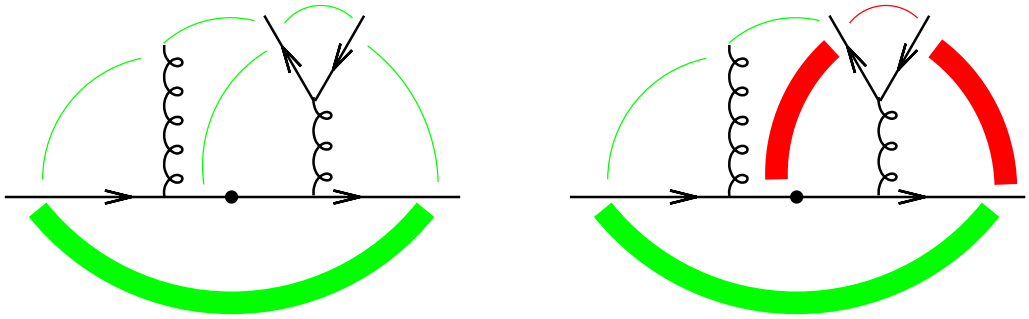

Fig. 7: Pictorial representation of recombination distances for a sample partonic final state in e^+e^- annihilation in the case of the traditional k_t algorithm (left) and a k_t-flavour algorithm (right).

to any QCD parton. The latter case can be eliminated by allowing only recombinations of $q\bar{q}$ pairs of the same flavour, but the problem of generating fake gluon jets remains. The origin of the problem is that the distance in eq. (19) is modelled so as to compensate the soft and collinear divergence in the matrix element for gluon emission. The $q\bar{q}$ splitting probability has no soft divergence, so that, without endangering the IRC safety of the algorithm, one could modify the distance in eq. (19) as follows:

$$d_{ij} = 2\,(1-\cos\theta_{ij}) \times \begin{cases} \min\{E_i^2, E_j^2\} & \text{softer of } i,j \text{ flavourless}\,, \\ \max\{E_i^2, E_j^2\} & \text{softer of } i,j \text{ flavoured}\,. \end{cases} \tag{20}$$

What happens in this case is represented in the picture on the right-hand side of fig. 7, where the new distances are highlighted in red. There, the distance between the soft $q\bar{q}$ pair is still small, what becomes large is the distance between either of the two and the hard $q\bar{q}$ pair. In this way soft $q\bar{q}$ pairs are first recombined together, and only after recombination is the resulting gluon jet recombined with other hard jets. It can be proven that with this modification the resulting flavour determination is IRC safe to all orders in perturbation theory [71].

One can generalise eq. (20) to hadron hadron collisions, defining for each pair of particles a distance parameterised by a jet radius R:

$$d_{ij} = \frac{\Delta R_{ij}^2}{R^2} \times \begin{cases} \min\{p_{t,i}^2, p_{t,j}^2\} & \text{softer of } i,j \text{ flavourless}\,, \\ \max\{p_{t,i}^2, p_{t,j}^2\} & \text{softer of } i,j \text{ flavoured}\,, \end{cases} \tag{21}$$

where ΔR_{ij}^2 is any collinear safe distance in the rapidity-azimuth y-ϕ plane, for instance $(y_i - y_j)^2 + (\phi_i - \phi_j)^2$. Furthermore, to obtain a full flavour determination, one has to add a distance between each particle and the two beams B and $\bar{B}$ at positive and negative infinite rapidity respectively. This is achieved by introducing a rapidity dependent transverse momentum for each beam $p_{t,B}(y), p_{t,\bar{B}}(y)$, and defining

$$d_{iB} = \begin{cases} \min\{p_{t,i}^2, p_{t,B}^2(y_i)\} & i \text{ flavourless}\,, \\ \max\{p_{t,i}^2, p_{t,B}^2(y_i)\} & i \text{ flavoured}\,, \end{cases} \tag{22}$$

and analogously for $d_{i\bar{B}}$. The beam hard scales $p_{t,B}(y)$ and $p_{t,\bar{B}}(y)$ have to be constructed in such a way that emissions collinear to B or $\bar{B}$ get recombined with the right beam, and that

$p_{t,B}(y)$ and $p_{t,\bar{B}}(y)$ approach the hard scale of the event for central emissions. This is achieved for instance by defining

$$\begin{aligned} p_{t,B}(y) &= \sum_i p_{ti} \left(\Theta(y_i - y) + \Theta(y - y_i)\, e^{y_i - y}\right) , \\ p_{t,\bar{B}}(y) &= \sum_i p_{ti} \left(\Theta(y_i - y) e^{y - y_i} + \Theta(y - y_i)\right) . \end{aligned} \tag{23}$$

If applied at parton level, these jet-flavour algorithms have two main applications. First of all they can be used in a NLO calculation to assign each event to an underlying Born subprocess. This is needed to correctly merge real and virtual contributions when matching NLO and resummed calculations [75]. A second application of jet-flavour algorithms is the combination of parton showers and matrix elements [76, 77]. For instance, in the CKKW approach [76], the correct Sudakov form factor to be associated to each event is decided only after having clustered the event into jets. This Sudakov form factor depends on the colour charge of the hard emitters, and is therefore correctly computed only if a flavour has been properly (i.e. in a IRC safe way) assigned to each jet.

At hadron level, in general, it is not sensible to distinguish quarks and gluons. However, there is a case in which the flavour algorithm can be successfully applied also at hadron level, that is in the case of heavy flavour production. There all hadrons containing a heavy quark (of the selected flavour) are treated as flavoured, while all other hadrons are considered flavourless. As we will see in the next section, an IRC safe jet-flavour algorithm can thus be exploited to obtain accurate QCD predictions for b-jet cross sections.

4.3 Accurate QCD predictions for b-jet cross sections

A basic measurement in b production in hadronic collisions is b-jet transverse momentum spectra. Experimentally a b-jet is defined as any jet containing at least one b-flavoured hadron [78]. It is clear that such a definition is collinear unsafe, because any jet containing a $b\bar{b}$ pair, which should be considered a gluon jet, would be classified as a quark jet. This gives rise to collinear singular contributions if the $b\bar{b}$ pair arise from a gluon collinear splitting. The resulting collinear singularity is regularised by the b-quark mass, giving rise to large logarithms at most of relative order $\alpha_s^n \ln^{2n-1}(p_t/m_b)$. These gluon splitting (GSP) processes constitute the dominant source of b-jets at the Tevatron. This is awkward since jets from GSP do not even correspond to one's physical idea of a b-jet. There are two other production channels, flavour excitation (FEX) and flavour creation (FCR). In FEX one of the constituents of a produced $b\bar{b}$ pair is collinear to the beam, while the other builds up the b-jet. This process also contains collinear singularities, which at all orders give rise to terms $\alpha_s^n \ln^n(p_t/m_b)$. FCR is the process in which a $b\bar{b}$ pair is produced directly in the hard scattering. Although, due to interference, these three processes are mixed together, they can be cleanly separated in the soft/collinear limit. All current fixed-order programs with a massive b implement only FCR at NLO [79, 80], while GSP and FEX are only LO processes. This results in K-factors (NLO/LO) and renormalisation and factorisation scale dependence that are far larger than is expected from NLO calculations, as can be seen in

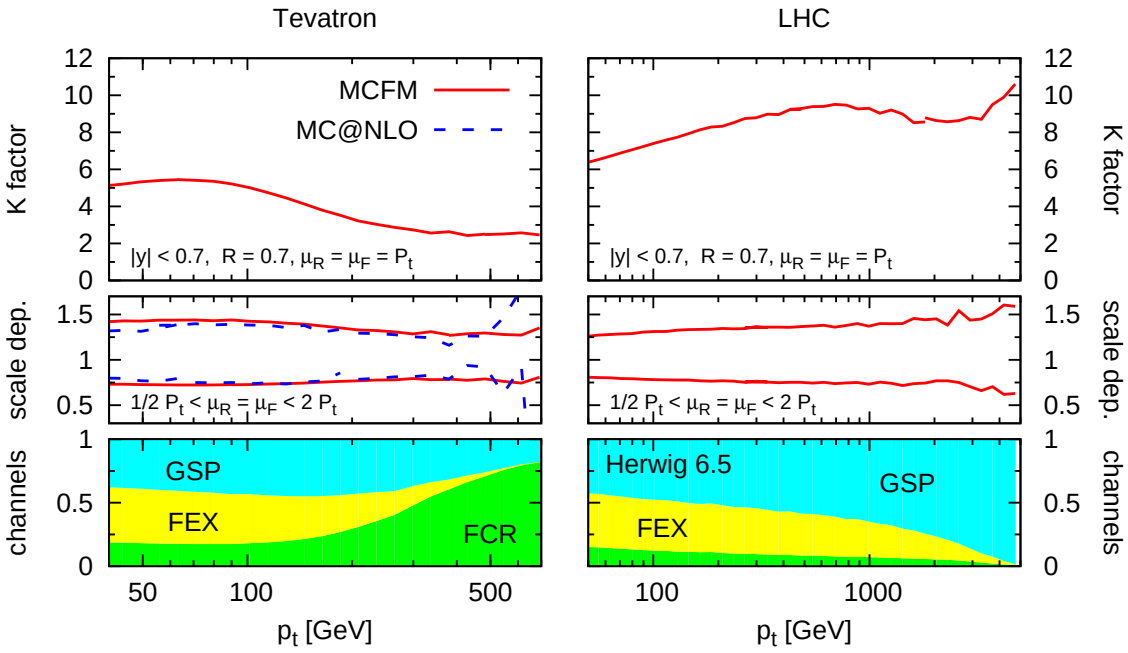

Fig. 8: Top: K-factors for inclusive b-jet spectrum as computed with MCFM, clustering particles into jets using the k_t jet-algorithm with R=0.7, and selecting jets in a central rapidity region ($|y| < 0.7$). Middle: scale dependence obtained by simultaneously varying the renormalisation and factorisation scales by a factor two around p_t, the transverse momentum of the hardest jet in the event. For the Tevatron the scale uncertainty is computed also with MC@NLO. Bottom: breakdown of the HERWIG inclusive b-jet spectrum into the three major hard underlying channels contributions (for simplicity the small $b\bar{b} \to b\bar{b}$ contribution is not shown).

fig. 8.[13] It is particularly instructive also to have a look at the bottom plots in the figure, which show the relevance of the various production channels as obtained from HERWIG [82]. Notice in particular how at the LHC GSP is the dominant process at any value of p_t. This is due to the fact that in pp collisions the process $q\bar{q} \to b\bar{b}$, the one responsible for FCR, is small also at high p_t due to the smallness of the antiquark distribution in the proton.

This situation can be significantly improved by exploiting an IRC safe definition of jet-flavour, such as the one outlined in the previous section. To overcome the experimental difficulty of discriminating b from $\bar{b}$, one can define a b-jet as a jet containing an odd number of b-hadrons without any risk for the IRC safety of the jet flavour [83]. In this case, the GSP contribution to b-jet production disappears immediately, because all jets with two b's will be classified as gluon jets, and therefore will not contribute at all to b-jet cross sections. FEX contributions give rise to jets with a single b, so they cannot be eliminated by a jet-flavour algorithm. However, the FEX collinear logarithms are precisely those resummed in the b parton density, one of the ingredients of any PT calculation with massless b's. Therefore one can compare experimental data for b-jet p_t-spectra obtained with the IRC definition of sec. 4.2 with PT predictions with massless b's, which are available at NLO accuracy [84, 85]. Since all collinear singularities have

[13] Note that the addition of a parton shower as done in MC@NLO [81] does not solve the problem. This is because the underlying hard configurations remain the same as NLO, and have therefore the same collinear singularities.

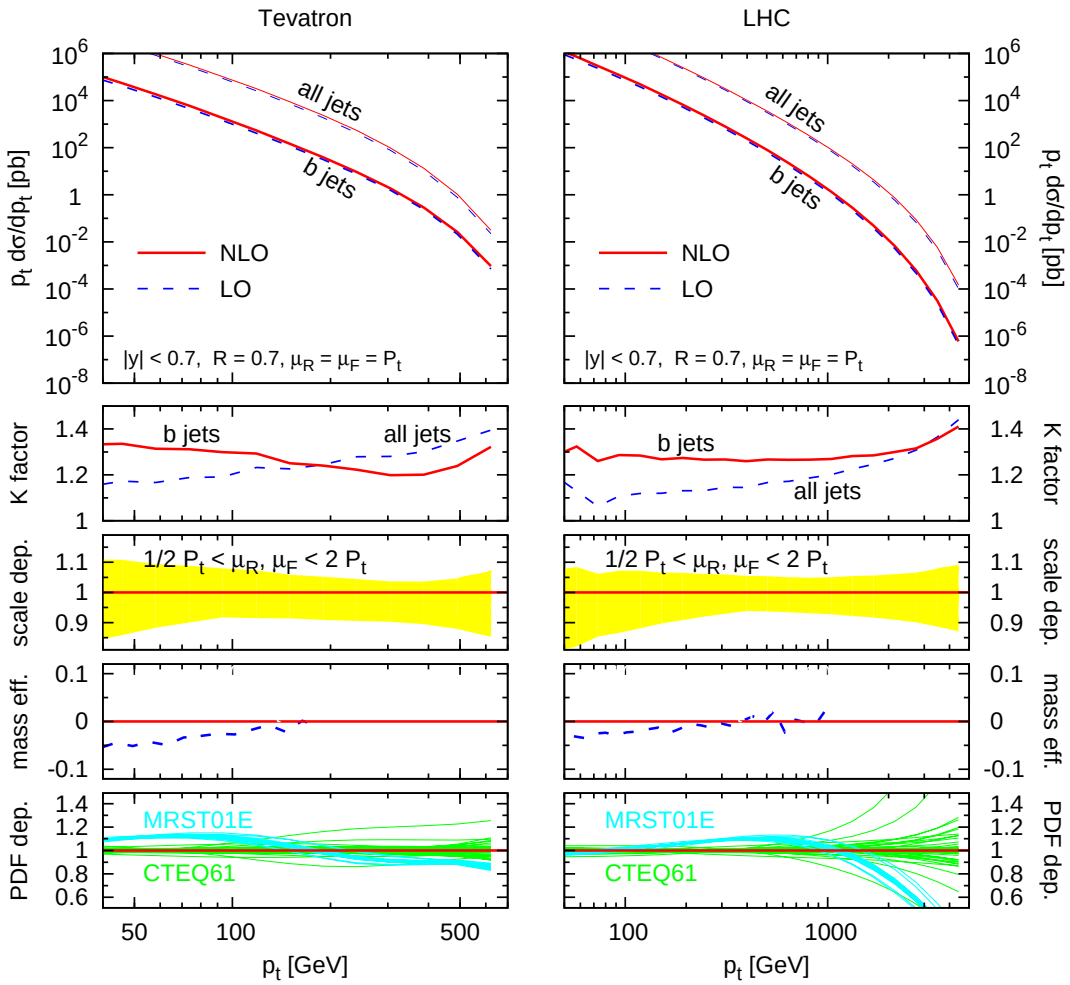

Fig. 9: The p_t spectrum for b-jets at the Tevatron (left) and at the LHC (right) obtained with NLO program NLOJET++. Below one can see, in order, K-factors for b-jets and all-flavoured inclusive jets, scale uncertainties obtained by varying *independently* renormalisation and factorisation scales by a factor of two, mass effects and PDF uncertainties.

been either eliminated or resummed, the difference between the massless and massive calculation should only involve powers of m_b^2/p_t^2 (potentially enhanced by logarithms). The resulting NLO p_t spectra at the Tevatron and at the LHC are shown in fig. 9. There one can see that now the K-factors for b-jets are comparable to those for unflavoured jets, and moderate, indicating that the PT expansion is under control. Furthermore, scale uncertainties are at most 10%, and adding PDF uncertainties the overall theoretical error does not exceed 20%, except at very high p_t values at the LHC, where PDF's are less constrained. Note that mass effects are less that 5%, therefore not contributing significantly to the total uncertainty.

A technical difficulty to perform such a calculation is that no NLO program contains information on the flavour of produced partons. One is then forced to extract this information from one's favourite NLO code (in our case NLOJET++ [85]). This procedure, although not straightforward, is nevertheless far easier than writing and testing a new code from scratch. Due to the

relevance that jet-flavour algorithms can have for precision calculations we strongly encourage the authors of NLO codes to provide flavour information by default.

We remark that very similar results are obtained for charmed jet spectra. An interesting issue there is that predictions are very sensitive to possible intrinsic charm components of the proton [86], so that these observables can be exploited to set constraints on such intrinsic components.

A last remark concerns the feasibility of the experimental measurement of heavy flavour jets defined with our flavour algorithm. For a successful comparison between theory and experiment it is crucial to identify cases in which both heavy-flavoured particles are in the same jet, so as to label this jet as a gluon jet and eliminate the contribution of these configurations from the heavy-quark jet cross sections. Experimental techniques for double b-tagging in the same jet already exist [87] and steady progress is to be expected in the near future [88–90]. However one has always a limited efficiency for single b tagging, and even more for double b-tagging in the same jet. On the other hand preliminary studies indicate that one does not necessarily need high efficiencies, but what is more crucial is that one dominates the error on those efficiencies [83]. We look forward to further investigation in this direction.

Acknowledgements. This work has been done in collaboration with Gavin Salam.

5 Towards NNLO predictions for top quark production

Author: M. Czakon

Although discovered quite some time ago, the top quark has not been studied sufficiently to not deserve a special place in the LHC physics programme. This contribution to the workshop proceedings addresses part of the latter related to the top quark pair production cross section. While ideas of applications seem to have cristalized, there has also been progress in the evaluation of the next-to-next-to-leading order corrections. Here, I give some details of the methods.

The top quark has enjoyed a sustained attention for more than a decade since its discovery. Only this year, several theoretical studies have been published on its properties in view of the LHC. The interested reader is directed to [91]. A quantity of particular importance is the total production cross section. Without entering into a detailed discussion it is sufficient to say that one may expect a precision of measurement at the level of about 5% after a few years of LHC running, a number which on the one hand constitutes a challenge to the theory, and on the other opens the door for a few applications, of which only two will be mentioned here.

The first of the applications is indirect mass determination. Clearly, the total cross section is a decreasing function of the mass due mostly to the phase space dependence on the final states. A convenient representation of the connection between the error on the top quark mass, m_t, and the error on the total cross section, $\sigma_{t\bar{t}}$, is given by

$$\frac{\Delta\sigma_{t\bar{t}}}{\sigma_{t\bar{t}}} \approx 5\frac{\Delta m_t}{m_t}, \tag{24}$$

which is valid in a broad range around the current top quark mass. Clearly, this formula points at the possibility of determining m_t with an accuracy at the one percent level, as long as the

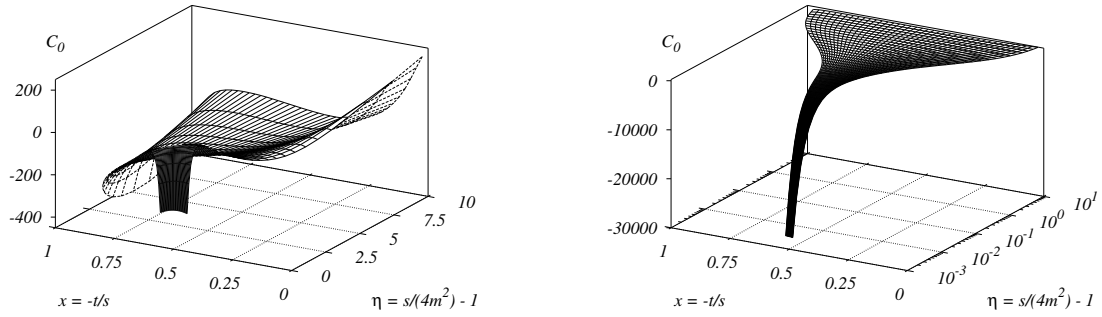

Fig. 10: Finite parts of the bosonic contributions to the two-loop amplitude in quark annihilation (most subleading color coefficient).

theory prediction of $\sigma_{t\bar{t}}$ is not a limiting factor. This is competitive with the best results from the Tevatron, but less precise than the ambitious goals of the LHC. The question remains, therefore, of the relevance of this method. A look at the way m_t is measured at present, and the variations of the central value implied, should convince a skeptic that it is important to have an independent measurement, which is far less sensitive on the kinematic reconstruction of hadronic final states.

The second application is gluon luminosity determination, to a large extent synonymous of the gluon PDF determination. While the standard luminosity monitor process for hadron colliders, Drell-Yan gauge boson production is sensitive mostly to quark PDFs, many of the non-standard processes and also the Higgs production process are induced by gluon fusion. A recent study by CTEQ [92], has shown that one can exploit the strong correlation between those cross sections and the top quark pair production cross section to reduce the errors. A prerequisite for success is a precision of 5% on both the theory and the experimental side.

In view of the above, a precise theory prediction for $\sigma_{t\bar{t}}$ would be more than welcome. As far as fixed order perturbation theory is concerned, the result of [93] shows an error, judged by scale dependence, in excess of 10%. Since there is a substantial enhancement of the production rate due to soft gluon emission, one might expect that the knowledge of higher order corrections in the threshold regime would reduce the final uncertainty. This is indeed the case, as shown in various studies, of which the most recent are [94–96]. In the end, it is possible to obtain a prediction with a conservative error estimate slightly below 10%. While this number is not quite satisfactory, there is a second drawback to the approach based on threshold resummations. Namely, it does not fit a Monte-Carlo generator. With the high statistics of the LHC, MC programs are indispensable. All in all, it seems that having a fixed order result with next-to-next-leading accuracy would be a perfect solution. This statement is only strengthened by the fact, that the error from scale dependence induced would then amount to only 3% [94].

An NNLO prediction for a production process at the LHC needs four ingredients: 1) the two-loop virtual corrections, 2) the one-loop squared corrections, 3) the one-loop corrections with an additional parton radiation, 4) the tree-level corrections with two additional partons radiated. Within the last one or two years, the first three points have been completed to a large extent for

the case of $\sigma_{t\bar{t}}$ [97–102]. Clearly, point 4) is trivial as long as all the partons are distinguishable. Performing the phase space integration over the unresolved configuration in 3) and 4) is the main remaining challenge. We are not going to discuss this issue, as it is not yet solved, but rather give a few details of the solution to point 1), which is an achievement in itself.

The main problem in the determination of the two-loop virtual corrections is the integration over the virtual momenta. The method adopted in [99] is based on a numerical solution of a system of differential equations [103]. It is suitable for problems with a relatively low number of scales and relies on the fact that Feynman integrals are smooth functions when evaluated above all thresholds as is here the case. The boundaries required are obtained from a series expansion solution to the differential equations around the high energy limit of the integrals derived in [97, 98]. While the integration of the system of equations is not fast enough to fit into a Monte-Carlo program, the presence of only two kinematic variables allows to use interpolation on a grid of precalculated values. The result for the most complicated color coefficient (most subleading term) in quark annihilation is shown in Fig. 10. The appropriate color decomposition is

$$\mathcal{A}^{(0,2)} = 2\mathrm{Re}\,\langle \mathcal{M}^{(0)} | \mathcal{M}^{(2)} \rangle = 2(N^2-1) \tag{25}$$
$$\times \left(N^2 A + B + \frac{1}{N^2} C + N n_l D_l + N n_h D_h + \frac{n_l}{N} E_l + \frac{n_h}{N} E_h + n_l^2 F_l + n_l n_h F_{lh} + n_h^2 F_h \right).$$

The result for the gluon fusion channel is underway. While there are no new complications in the method itself, the number of integrals which need boundaries and have not been determined previously is about three times larger.

6 2- and 3-loop heavy flavor contributions to $F_2(x,Q^2)$, $F_L(x,Q^2)$ and $g_{1,2}(x,Q^2)$

Authors: I. Bierenbaum, J. Blümlein and S. Klein

6.1 Introduction

In the case of single photon exchange, the deep–inelastic double differential scattering cross-section can be expressed in terms of the unpolarized structure functions $F_2(x,Q^2)$ and $F_L(x,Q^2)$, and the polarized structure functions $g_1(x,Q^2)$ and $g_2(x,Q^2)$. We are considering heavy flavor corrections to these functions. In the NLO approximation, the corrections were calculated semi–analytically in x–space for $F_2(x,Q^2)$ and $F_L(x,Q^2)$ in [104], with a fast implementation in Mellin N–space given in [105]. In the polarized case the NLO corrections are available only in the asymptotic case $Q^2 \gg m^2$ [106, 107].The $c\overline{c}$–contributions to these structure functions in the region of smaller values of Bjorken–x, are of the order of 20-40 % and exhibit different scaling violations than the contributions due to massless partons, as shown in Figure 11. For the parameterization of the parton distribution functions we used [108]. Hence, a more precise determination of the parton distribution functions and the measurement of $\Lambda_{\rm QCD}$, as reached in the non-singlet case [109], requires an extension of the heavy quark contributions to $O(a_s^3)$, as in the massless case, to perform the flavor–singlet analyzes consistently. This can be done by observing that for $Q^2 \gtrsim 10\, m_c^2$, $F_2^{c\bar{c}}(x,Q^2)$ is very well described by its asymptotic expression in the limit $Q^2 \gg m^2$, [110], where one can calculate the heavy flavor Wilson coefficients, the perturbative

part of the structure functions, analytically. More precisely, the heavy flavor Wilson coefficients in the limit $Q^2 \gg m^2$ are obtained as a convolution of the light–flavor Wilson coefficients with the corresponding massive operator matrix elements (OMEs) of flavor decomposed quarkonic and gluonic operators between massless parton states, which are obtained from the light–cone expansion. Here, we consider the level of twist–2 operators. The light Wilson coefficients are known up to three loops [111] and carry all the process dependence, whereas the OMEs, the objects to be calculated here, are universal and process–independent. Using this approximation, the heavy flavor Wilson coefficients are calculated for $F_{2,L}^{c\bar{c}}(x,Q^2)$ to 2–loop order in [110, 112, 113] and for $F_L^{c\bar{c}}(x,Q^2)$ to 3–loop order in [114]. First steps towards the asymptotic 3–loop corrections for $F_2^{c\bar{c}}(x,Q^2)$ are made by the present authors by calculating the O(ε) terms of the 2–loop heavy operator matrix elements, [26, 115], contributing to the 3–loop heavy flavor Wilson coefficients via renormalization. The logarithmic contributions in (m^2/μ^2) of the OMEs, as well as all pole terms in $1/\varepsilon$, are completely determined by renormalization, in this providing a check on the calculation, and containing in the single pole terms the respective contributions of the 3-loop anomalous dimensions. Furthermore, first steps towards a full 3–loop calculation of moments of the heavy flavor Wilson coefficients were undertaken. Here, the moments $N = 2...12$ of the NNLO non-singlet (NS) and pure-singlet (PS) contributions of the OMEs were calculated. In addition, one obtains the corresponding contributions to the three–loop anomalous dimensions given in [116, 117], cf. also [118], which are confirmed in an independent calculation.

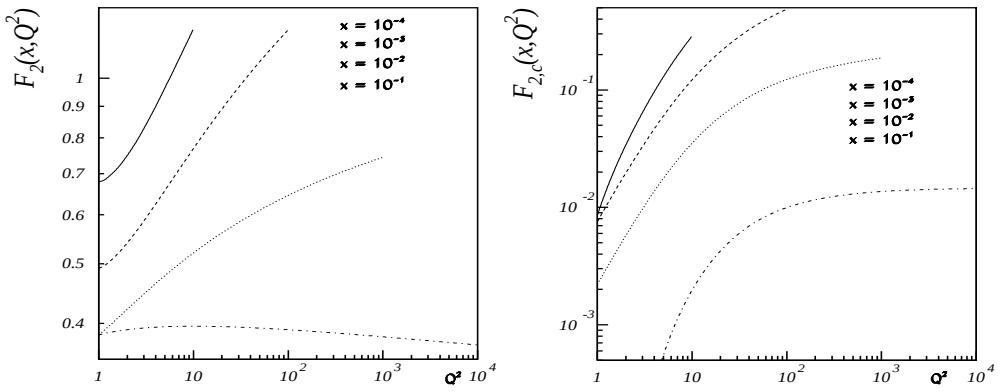

Fig. 11: The scaling violations of the light– and heavy–flavor contributions to the structure functions $F_2^{\rm light}$ and $F_{2,c}$ at leading order.

6.2 Renormalization

Our calculation is done in Mellin space. The diagrams are of the self energy type with an additional operator insertion, which widely determines the dynamics and introduces the dependence on the Mellin variable N. The external particle is massless and on–shell. The scale is set by the mass of the heavy quark. After calculating the bare heavy flavor OMEs in $D = 4 + \varepsilon$ dimensions and by using the Feynman–gauge, the renormalization is performed in four steps: We use the on–shell scheme [119] for mass renormalization and the $\overline{\rm MS}$–scheme for the charge renor-

malization.[14] The remaining two types of divergences, the UV and collinear singularities, are renormalized via the operator Z–factors and by mass factorization through the transition functions Γ. Denoting the completely unrenormalized OMEs by a double–hat, $\hat{\hat{A}}$, and those for which mass and coupling renormalization have already been performed by a single hat, the operator renormalization and mass factorization proceeds via

$$\mathbf{A} = \mathbf{Z}^{-1} \hat{\mathbf{A}} \mathbf{\Gamma}^{-1} \,, \tag{26}$$

which constitutes a matrix equation in the singlet case. This equation allows us to predict the pole-structure of the OMEs under consideration. The Z–factors read

$$\begin{aligned} Z_{ij}(N, a_s, \varepsilon) &= \delta_{i,j} + a_s S_\varepsilon \frac{\gamma_{ij,0}}{\varepsilon} + a_s^2 S_\varepsilon^2 \left\{ \frac{1}{\varepsilon^2} \left[\frac{1}{2} \gamma_{im,0} \gamma_{mj,0} + \beta_0 \gamma_{ij,0} \right] + \frac{1}{2\varepsilon} \gamma_{ij,1} \right\} \\ &+ a_s^3 S_\varepsilon^3 \left\{ \frac{1}{\varepsilon^3} \left[\frac{1}{6} \gamma_{in,0} \gamma_{nm,0} \gamma_{mj,0} + \beta_0 \gamma_{im,0} \gamma_{mj,0} + \frac{4}{3} \beta_0^2 \gamma_{ij,0} \right] \right. \\ &\left. + \frac{1}{\varepsilon^2} \left[\frac{1}{6} \left(\gamma_{im,1} \gamma_{mj,0} + 2 \gamma_{im,0} \gamma_{mj,1} \right) + \frac{2}{3} \left(\beta_0 \gamma_{ij,1} + \beta_1 \gamma_{ij,0} \right) \right] + \frac{\gamma_{ij,2}}{3\varepsilon} \right\} \end{aligned} \tag{27}$$

They are related to the anomalous dimensions of the twist–2 operators via $\gamma = \mu \partial \ln \mathbf{Z}(\mu)/\partial \mu$, allowing to express them in terms of the anomalous dimensions up to an arbitrary order in the strong coupling constant $a_s := \alpha_s/(4\pi)$ (cf. [115] up to $O(a_s^3)$). Additionally, we would have $\mathbf{\Gamma} = \mathbf{Z}^{-1}$, if all quark lines were massless, which, however, has to be modified here since we always have at least one heavy quark line. From these equations, one can infer that for operator renormalization and mass factorization at $O(a_s^3)$, the anomalous dimensions up to NNLO, [116, 117], together with the 1–loop heavy OMEs up to $O(\varepsilon^2)$ and the 2–loop heavy OMEs up to $O(\varepsilon)$ are needed. The last two quantities enter since they multiply $Z-$ and Γ–factors containing poles in ε (cf. [115]).

To see this in more detail, let us consider as an example the term $A_{gq,Q}$, which emerges for the first time at $O(a_s^2)$. By applying Eq. (26), one obtains at $O(a_s^2)$ the renormalized OME

$$A_{gq,Q}^{(2)} = \hat{A}_{gq}^{(2)} + Z_{gq}^{-1,(2)} + \left(Z_{gg}^{-1,(1)} + \hat{A}_{gg,Q}^{(1)} \right) \Gamma_{gq}^{-1,(1)}.$$

Here, the term $\hat{A}_{gg,Q}^{(1)}$, cf. [120], enters through mixing. Note that since we consider only terms involving at least one heavy quark, we adopt the definition $\hat{\gamma} := \gamma(n_f + 1) - \gamma(n_f)$ for the anomalous dimensions in order to obtain the correct color projection. Now we can predict the structure of the unrenormalized result to be

$$\hat{A}_{gq,Q}^{(2)} = \left(\frac{m^2}{\mu^2} \right)^\varepsilon \left[\frac{2\beta_{0,Q}}{\varepsilon^2} \gamma_{gq}^{(0)} + \frac{\hat{\gamma}_{gq}^{(1)}}{2\varepsilon} + a_{gq,Q}^{(2)} + \varepsilon \overline{a}_{gq,Q}^{(2)} \right] , \tag{28}$$

where we see the LO and NLO anomalous dimensions and $\beta_{0,Q} = -(4/3)T_F$ occurring in the pole terms. The terms which are in general not predictable are the constant and O(ε)–terms,

[14] For the latter we make the requirement that the heavy quark loop contributions to the gluon self–energy, $\Pi(p^2, m^2)$, are renormalized in such a way that $\Pi(0, m^2) = 0$, cf. [110, 112, 113, 115].

which, however, enter the pole and constant terms of a 3–loop OME, as mentioned above. In this particular case here, the calculation in Mellin–space in terms of Feynman–parameters is straightforward, cf. [112, 113], and a representation in Euler–Γ functions can be obtained even to all orders in ε, where we reproduced the pole terms of Eq. (28), [121]. As a last remark, note that we consider charm quark contributions here, while for heavier quarks decoupling [122] has to be applied.

6.3 O(ε) at 2–loops

The appearance of the constant and O(ε) terms in the renormalization process of the OMEs has been worked out in some detail in Ref. [115], [123], where we presented the $O(\varepsilon)$ terms $\overline{a}^{(2)}_{Qg}$, $\overline{a}^{(2),\mathsf{NS}}_{qq,Q}$ and $\overline{a}^{(2)\mathsf{PS}}_{Qq}$ in the unpolarized case. The term $\overline{a}^{(2)}_{gg,Q}$ was given in [26]. The last missing 2–loop $O(\varepsilon)$ term corresponds to the heavy OME $A^{(2)}_{gq,Q}$, [107, 121]. The corresponding constant contribution was calculated before in Ref. [120]. It contributes through operator mixing to the T_F^2–term of $A^{(3),\mathsf{PS}}_{Qq}$, which we consider in this paper.
Since we perform our calculation in Mellin space, all results are given in terms of harmonic sums, [124, 125], the argument of which we have set equal to N. Thus, the results of the constant and O(ε)–terms of the above–mentioned $A^{(2)}_{gq,Q}$, for example, are given by:

$$\begin{aligned}
a^{(2)}_{gq,Q} &= T_F C_F \left\{ \frac{4}{3} \frac{N^2+N+2}{(N-1)N(N+1)} \Big(S_2 + S_1^2 + 2\zeta_2 \Big) - \frac{8}{9} \frac{8N^3+13N^2+27N+16}{(N-1)N(N+1)^2} S_1 \right. \\
&\left. + \frac{8}{27} \frac{P_1}{(N-1)N(N+1)^3} \right\}, \qquad (29) \\
\overline{a}^{(2)}_{gq,Q} &= T_F C_F \left\{ \frac{2}{9} \frac{N^2+N+2}{(N-1)N(N+1)} \Big(-2S_3 - 3S_2 S_1 - S_1^3 + 4\zeta_3 - 6\zeta_2 S_1 \Big) \right. \\
&+ \frac{2}{9} \frac{8N^3+13N^2+27N+16}{(N-1)N(N+1)^2} \Big(2\zeta_2 + S_2 + S_1^2 \Big) - \frac{4 P_1 S_1}{27(N-1)N(N+1)^3} \\
&\left. + \frac{4 P_2}{81(N-1)N(N+1)^4} \right\}, \qquad (30) \\
P_1 &= 43N^4 + 105N^3 + 224N^2 + 230N + 86 \,. \\
P_2 &= 248N^5 + 863N^4 + 1927N^3 + 2582N^2 + 1820N + 496 \,.
\end{aligned}$$

The representation in Mellin–space allowed us to use various analytic and algebraic relations between harmonic sums, [126–128], to obtain a more compact result. Together with the result of Eq. (30), all 2–loop $O(\varepsilon)$ terms of the heavy OMEs in the unpolarized case are known by now. A corresponding calculation has been performed for the polarized case up to $O(\varepsilon)$ [107] extending the results of Ref. [106]. The contributions to the structure function $g_2(x, Q^2)$ can be obtained using Wandzura-Wilczek relations, cf. [129, 130]. For the respective formulae we refer to the original paper.

6.4 Fixed moments at 3–loops

We start by calculating the diagrams for fixed even values of Mellin N. At this order, new operator vertices appear with three and four gluonic lines, for which the Feynman–rules had not yet been derived before. The necessary 3–loop diagrams are generated using QGRAF [131] and are genuinely given as tensor integrals due to the operators contracted with the light–cone vector Δ, $\Delta^2 = 0$. The calculation proceeds in the following steps: first, the contraction with the light–cone vector is made undone, which leaves tensor integrals for each diagram. For each value of Mellin N under consideration, one then constructs a projector, which, applied to the tensor integrals, projects onto the desired N. We consider $N = 2, ..., 12$. The color factors of the diagrams are calculated using [132]. A generalization to higher moments is straightforward, however, the computing time increases rapidly. The diagrams are then translated into a form, which is suitable for the program MATAD [133], doing the expansion in ε for the corresponding massive three–loop tadpole–type diagrams. We have implemented all these steps into a FORM–program, cf. [134], and tested it against various two–loop results, including the result for $\hat{A}^{(2)}_{gq,Q}$, Eq. (28), and found agreement.

The first 3–loop objects we are investigating are the OMEs $A^{\sf NS}_{qq,Q}$, cf. [121], and $A^{\sf PS}_{Qq}$. All diagrams contain two inner quark loops, where the quark to which the operator insertion couples is heavy and the other one may be heavy or light. The latter two cases can be distinguished by a factor n_f, denoting the number of light flavors, in the result. From Eq. (26), we can obtain the pole structure of the the T_F^2 terms of the completely unrenormalized PS OME:

$$\hat{A}^{(3),\sf PS}_{Qq}\Big|_{T_F^2} = \Big(\frac{m^2}{\mu^2}\Big)^{3\varepsilon/2}\Bigg\{2\frac{n_f+4}{3\varepsilon^3}\beta_{0,Q}\hat{\gamma}^{(0)}_{qg}\gamma^{(0)}_{gq} + \frac{1}{\varepsilon^2}\Big(\frac{2-n_f}{6}\hat{\gamma}^{(0)}_{qg}\hat{\gamma}^{(1)}_{gq} - (n_f+1)\frac{4}{3}\beta_{0,Q}\hat{\gamma}^{(1)}_{\sf PS}\Big)$$
$$+\frac{1}{\varepsilon}\Big(\frac{n_f+1}{3}\hat{\bar{\gamma}}^{(2)}_{\sf PS} - 4(n_f+1)\beta_{0,Q}a^{(2),\sf PS}_{Qq} - n_f\frac{\zeta_2\beta_{0,Q}}{4}\hat{\gamma}^{(0)}_{qg}\gamma^{(0)}_{gq} + \hat{\gamma}^{(0)}_{qg}a^{(2)}_{gq,Q}\Big) + a^{(3),\sf PS}_{Qq}\Big|_{T_F^2}\Bigg\} \quad (31)$$

The n_f dependence is written explicitly and $\hat{\bar{\gamma}}^{(2)}_{\sf PS}$ is the term $\propto n_f^2$ of the NNLO anomalous dimension $\gamma^{(2)}_{\sf PS}$. It is not possible to factor out (n_f+1), not even in the triple pole term. This is due to the interplay of the prescription for coupling constant renormalization we have adopted and the fact that the transition functions Γ apply to sub–graphs containing massless lines only. We have calculated the above term using MATAD for $N = 2, ..., 12$ and all pole terms agree with Eq. (31). Detailed Tables of these results can be found in [121] and a further upcoming paper. Using Eqs. (29,31), one can obtain moments for the 3–loop anomalous dimension $\gamma^{(2)}_{\sf PS}|_{T_F^2}$, see also [121] and a corresponding paper in preparation. These latter results agree with the results from [117]. Here one has to make the replacement $n_f \to n_f(2T_F)$, with $T_F = 1/2$, and to multiply by 2, to account for the different convention for the Z–factors we adopted. As an example consider the renormalized result for the second moment. Applying Eq. (26), we obtain

$$A^{(3),\sf PS}_{Qq}\Big|_{N=2,T_F^2} = C_F T_F^2\Bigg\{-\frac{128}{81}\ln^3\Big(\frac{m^2}{\mu^2}\Big) - \frac{32}{27}\ln^2\Big(\frac{m^2}{\mu^2}\Big) - \frac{5344}{243}\ln\Big(\frac{m^2}{\mu^2}\Big) + \frac{53144}{2187}$$
$$-\frac{3584}{81}\zeta_3 + n_f\Bigg(-\frac{128}{81}\ln^3\Big(\frac{m^2}{\mu^2}\Big) + \frac{32}{27}\ln^2\Big(\frac{m^2}{\mu^2}\Big) - \frac{5104}{243}\ln\Big(\frac{m^2}{\mu^2}\Big) - \frac{34312}{2187} + \frac{1024}{81}\zeta_3\Bigg)\Bigg\} \quad (32)$$

As in Eq. (32), we observe for all moments in the NS and PS case that the terms $\propto \zeta_2$ disappear after renormalization, since the corresponding terms in the light flavor Wilson coefficients do not contain even ζ-values. This provides us with a further check on our calculation, since it is a general observation made in many $D = 4$ calculations.

For the T_F^2–terms of the heavy OME $A_{qq,Q}^{(3),\mathsf{NS}}$, a formula similar to Eq. (31) can be derived, cf. [121]. Using again MATAD, we have calculated the first 6 non-vanishing moments of the completely unrenormalized expression. The pole terms we obtain agree with what one expects from Eq. (26) and after renormalization, we again observe that there are no ζ_2's left anymore. Additionally, the values for the moments of the terms $\propto T_F$ in $\gamma_{\mathsf{NS}}^{(2)}$ agree with those in Refs. [116–118].

6.5 Conclusions and outlook

All O(ε) contributions to the unpolarized and most of the polarized heavy quark OMEs for general Mellin variable N at $O(a_s^2)$ were calculated which are needed for the renormalization at $O(a_s^3)$. This part of the calculation makes significant use of the representation of Feynman–integrals in terms of generalized hypergeometric and related functions, omitting the integration-by-parts method. The solution of the sums beyond those which could be performed by summer [125], required new techniques and were solved using SIGMA [135]. Concerning the structure of the result, we find the *universal* pattern as observed in case of the massless 2-loop Wilson coefficients and related quantities in terms of harmonic sums [126, 127, 136–138]. Furthermore, we installed a program chain to calculate the corresponding 3–loop diagrams to $O(a_s^3)$ using MATAD. As a first step, we obtained the moments of the heavy OMEs $\hat{A}_{qq,Q}^{(3),\mathsf{NS}}$ and $\hat{A}_{Qq}^{(3),\mathsf{PS}}$, for which we found agreement with the general pole structure expected from renormalization. This provides us with a good check on the method we apply for our calculation. For the calculation of high moments we will apply TFORM, [139], in the future. In the same way all other contributions to the heavy quark OMEs will be calculated.

Acknowledgments. We would like to thank M. Steinhauser and J. Vermaseren for useful discussions and M. Steinhauser for a FORM 3.0 compatible form of the code MATAD.

7 Heavy quark and quarkonium production in the Regge limit of QCD

Author: V. Saleev

We study production of hadrons containing charm and beauty quarks at HERA and Tevatron Colliders in the framework of the quasi-multi-Regge-kinematics approach at leading order in the strong-coupling constant α_s. To describe heavy quark hadronization we use the fragmentation approach in case of $D-$ and $B-$meson production, or the factorization formalism of nonrelativistic QCD at leading order in the relative velocity v of heavy quarks in quarkonia in case of heavy quarkonium production.

7.1 Theoretical basis

Heavy quark and quarkonium production at high energies has provided a useful laboratory for testing the perturbative quantum chromodynamics (pQCD) as well as the interplay of perturbative and nonperturbative phenomena in QCD. Also these studies are our potential for the observation of a new dynamical regime, namely the high-energy Regge limit, which is characterized by the following condition $\sqrt{S} \gg \mu \gg \Lambda_{QCD}$, where $\sqrt{S}$ is the total collision energy in the center of mass reference frame, Λ_{QCD} is the asymptotic scale parameter of QCD, μ is the typical energy scale of a hard interaction.

The phenomenology of strong interactions at high energies exhibits a dominant role of gluon interactions in heavy quark and quarkonium production. In the conventional parton model [140], the initial-state gluon dynamics is controlled by the Dokshitzer-Gribov-Lipatov-Altarelli-Parisi (DGLAP) evolution equations [141], in which it is assumed that $S > \mu^2 \gg \Lambda^2_{\rm QCD}$. Thus, the DGLAP evolution equation takes into account only one large logarithm, namely $\ln(\mu/\Lambda_{QCD})$ and the collinear approximation is used, in which the transverse momenta of the initial gluons (k_T) are neglected.

In the Regge limit the summation of large logarithms $\ln(\sqrt{S}/\mu)$ in the evolution equation can then be more important than the one of the $\ln(\mu/\Lambda_{QCD})$ terms. In this case, the non-collinear gluon dynamics is described by the Balitsky-Fadin-Kuraev-Lipatov (BFKL) evolution equation [142]. In the region under consideration, the transverse momenta of the incoming gluons and their off-shell properties can no longer be neglected, and we deal with *Reggeized* gluons. As the theoretical framework for this kind of high-energy phenomenology, the quasi-multi-Regge-kinematics (QMRK) approach [143], which is based on the effective quantum field theory implemented with the non-abelian gauge-invariant action [144], can be used. The *Reggeization* of particles or amplitudes is the well-known effect for electrons in high-energy quantum electrodynamics (QED) [145] and for gluons and quarks in QCD [142, 146]. Roughly speaking, the *Reggeization* is a trick, which gives an opportunity to take into account efficiently large radiative corrections to the processes under Regge limit condition beyond the collinear approximation. The main ingredients of the QMRK approach are the effective vertices of Reggeon-Reggeon-Particle (RRP) or Reggeon-Particle-Particle (RPP) interactions, which can be obtained from the effective action [144].

The factorization formalism of nonrelativistic QCD (NRQCD) [147] is a theoretical framework for the description of heavy-quarkonium production and decay. The factorization hypothesis of NRQCD assumes the separation of the effects of long and short distances in heavy-quarkonium production. NRQCD is organized as a perturbative expansion in two small parameters, the strong-coupling constant α_s and the relative velocity v of heavy quarks in quarkonium.

The studies of the open heavy-flavour production at high energies show that in calculations the precise implementation of the effect of heavy quark fragmentation is needed to describe data [45–47, 148]. The approach used here applies the universal fragmentation functions (FFs) [45–47], which satisfy DGLAP evolution equations and are fitted to e^+e^- annihilation data for the open heavy-flavour production from CERN LEP1.

Both models, the NRQCD and the fragmentation approach, don't depend on the choice of high-energy factorization scheme and they can be used in calculations both in the conventional

collinear parton model and in the QMRK approach.

7.2 Charmonium production at Tevatron and HERA

During the last decade, the CDF Collaboration at the Tevatron [149, 150] collected data on charmonium production at the energies $\sqrt{S} = 1.8$ TeV (run I) and $\sqrt{S} = 1.96$ TeV (run II) in the central region of pseudorapidity $|\eta| < 0.6$. In contrast to previous analysis in the collinear parton model [151] or the k_T-factorization approach [152–154], we perform a joint fit to the run-I and run-II CDF data [149, 150] to obtain the color-octet nonperturbative matrix elements (NMEs) for J/ψ, χ_{cJ}, and ψ' mesons. The run-II data include region of small J/ψ transverse momentum, which can't be described principally in the collinear parton model, but this region is important for fit procedure. Our calculations [155, 156] are based on exact analytical expressions for the relevant *Reggeized* amplitudes, which were previously unknown in the literature ($R + R \to H$, $R + R \to H + g$, and $R + P \to H$, where H is $q\bar{q}-$pair in the fixed quantum state, R is the *Reggeized* gluon). Our fits include five experimental data sets, which come as p_T distributions of J/ψ mesons from direct production, prompt production, χ_{cJ} decays, and ψ' decays in run I, and from prompt production in run II. In the Table I of Ref. [155, 156], we present out fit results for the relevant color-octet NMEs for three different choices of unintegrated gluon distribution function, namely JB [157], JS [158], and KMR [159]. Our fits to the Tevatron data turned out to be satisfactory, except for the one to the χ_{cJ} sample based on the JB gluon density in the proton, where the fit result significantly exceeded the measured cross section in the small-p_T region, as it is shown in Figs. 4-5 of Ref. [155, 156]. We see also that color-octet contribution in case of χ_{cJ} production is being quite unimportant. Considering the color-octet NMEs relevant for the J/ψ, ψ' and χ_{cJ} production mechanisms, we can formulate the following heuristic rule for favored transitions from color-octet to color-singlet states: $\Delta L \simeq 0$ and $\Delta S \simeq 0$; *i.e.*, these transitions are doubly chromoelectric and preserve the orbital angular momentum and the spin of the heavy-quark bound state.

At HERA, the cross section of prompt J/ψ production was measured in a wide range of the kinematic variables both in photoproduction [160], at small values of photon virtuality Q^2, and deep-inelastic scattering (DIS) [161], at large values of Q^2. In the Figs. 6-9 of Ref. [155,156], our NRQCD predictions in the high-energy factorization approach, evaluated with the NMEs from Table 1 of Ref. [155, 156], are compared with the HERA data [160, 161]. In this regime, where the contribution of $2 \to 1$ subprocesses is suppressed, the LO NRQCD predictions in the QMRK approach are mainly due to the color-singlet channels and are therefore fairly independent of the color-octet NMEs. Thus, our results agree well with the data and with the previous calculations in the color singlet model (CSM) [162], up to minor differences in the choice of the color-singlet NMEs and the c-quark mass. Let us note that first theoretical prediction for J/ψ photoproduction in the CSM and the k_T-factorization scheme has been done 15 yeas ago in Ref. [163].

7.3 Bottomonium production at the Tevatron

The CDF Collaboration measured the p_T distributions of $\Upsilon(1S)$, $\Upsilon(2S)$, and $\Upsilon(3S)$ mesons in the central region of rapidity (y), $|y| < 0.4$, at $\sqrt{S} = 1.8$ TeV (run I) [164] and that of the $\Upsilon(1S)$ meson in the rapidity regions $|y| < 0.6$, $0.6 < |y| < 1.2$, and $1.2 < |y| < 1.8$ at $\sqrt{S} = 1.96$ TeV (run II) [165]. In both cases, the S-wave bottomonia were produced promptly, *i.e.*, directly or

via non-forbidden decays of higher-lying S- and P-wave bottomonium states, including cascade transitions such as $\Upsilon(3S) \to \chi_{b1}(2P) \to \Upsilon(1S)$.

In contrast to previous analysis in the collinear parton model [166], we perform a joint fit to the CDF data from run I [164] and run II [165] for all p_T values, including the small-p_T region. Comparing the color-singlet and color-octet contributions, we observe that the latter is dominant in the $\Upsilon(3S)$ case and in the $\Upsilon(2S)$ case for $p_T \geq 13$ GeV, while it is of minor importance in the $\Upsilon(1S)$ case in the whole p_T range considered. The fits based on the KMR, JB, and JS gluons turned out to be excellent, fair, and poor, respectively. They yielded small to vanishing values for the color-octet NMEs, see Table II of Ref. [167], especially when the estimated feed-down contributions from the as-yet unobserved $\chi_{bJ}(3P)$ states were included. The presented analysis in Ref. [167], together with the investigation of charmonium production [155, 156], suggest that the color-octet NMEs of bottomonium are more strongly suppressed than those of charmonium as expected from the velocity scaling rules of NRQCD.

Using obtained NMEs for bottomonium and charmonium states we have done predictions for the LHC Collider at the energy $\sqrt{S} = 14$ TeV, which are presented in Figs. 14-17 of Ref. [168].

7.4 Open heavy-flavour production at HERA and Tevatron

At HERA $D-$meson production has been studied both in the photo-production processes and in the deep inelastic scattering (DIS) processes. The data are presented by H1 and ZEUS Collaborations for different spectra, see Refs. [169, 170]. The lowest order in α_s processes of heavy quark photoproduction or electroproduction in the QMRK approach in the massive $c-$quark scheme are the following: $\gamma(\gamma^\star) + R \to c + \bar{c}$ – direct production and $R_\gamma + R \to c + \bar{c}$ – resolved production, where R is the *Reggeized* gluon from a proton or R_γ is the one from a photon.

We find approximate agreement of our results with data from HERA for p_T spectra of $D^\star-$meson production, the pseudo-rapidity spectra are described well only at the large $p_T \geq 6$ GeV, see Figs. 3-6 in Ref. [171]. These conclusions are true both for photoproduction and for $D^\star$ production in DIS.

Recently the CDF Collaboration measured the differential cross sections $d\sigma/dp_T$ for the inclusive production of D^0, D^+, $D^{\star+}$, and D_s^+ mesons [172] in $p\bar{p}$ collisions at the Fermilab Tevatron (run I and run II) as functions of transverse momentum (p_T) in the central rapidity (y) region. At the LO QMRK approach the parton subprocesses for heavy quark production in hadron collisions are: $R + R \to c + \bar{c}$ and $Q + \bar{Q} \to c + \bar{c}$, where Q is the *Reggeized* quark in a proton. The squared matrix elements of all above mentioned processes, excluding last one with *Reggeized* initial quarks, are known in the literature [143, 173, 174]. The contribution of the subprocess $Q + \bar{Q} \to c + \bar{c}$ is studied for the first time [175].

In the paper [176], we explored the usefulness of the quark-Reggeization hypothesis in the framework of the QMRK approach by studying several observables of inclusive charm production at LO, namely the charm structure function $F_{2,c}$ of the proton measured at HERA as well as the one-particle-inclusive cross sections of $D^{*\pm}$ and $D_s^\pm$ photoproduction in ep collisions at HERA and of D^0, $D^\pm$, $D^{*\pm}$, and $D_s^\pm$ hadroproduction in $p\overline{p}$ collisions at the Tevatron Collider. In all three cases, we found satisfactory agreement between our default predictions and the ex-

perimental data, which is quite encouraging in view of the simplicity of our LO expressions for the partonic cross sections. By contrast, in the collinear parton model of QCD, the inclusion of NLO corrections is necessary to achieve such a degree of agreement. We thus recover the notion that the QMRK approach is a powerful tool for the theoretical description of QCD processes in the high-energy limit and automatically accommodates an important class of corrections that lie beyond the reach of the collinear parton model at LO.

The first theoretical prediction for the beauty production at Tevatron [177] based on high-energy factorization scheme and Reggeon-Reggeon effective vertices [143] for the process $R + R \to b + \bar{b}$ has been done in Ref. [178]. It was shown that both p_T-spectra and total cross section of $B-$mesons can be described well with KMS unintegrated gluon distribution function [179]. We performed these calculations with KMR [159] unintegrated distribution functions and Peterson $b-$quark fragmentation function [180], and have found good agreement with data too. Thus, in case of $b-$quark production, contrary to $c-$quark production, theoretical description of data both for $B-$mesons and for bottomonia looks well grounded and more simple. The $c-$quark mass is not large enough and nonperturbative effects in the hadronization of $c-$quarks need more careful description.

7.5 Conclusions

Our results show that the QMRK approach is a very powerful tool in the high-energy phenomenology of heavy quark and quarkonium production. Of course, there is a number of non-solved problems yet, such as the correct description of J/ψ polarization [181] and an estimation of NLO corrections for relevant processes. At the LHC Collider the conditions of application of the QMRK approach for heavy quark production will be satisfied with higher accuracy, therefore we see many future applications of this approach in a new kinematic regime.

The author thanks B. Kniehl, D. Vasin and A. Shipilova for cooperation in study of presented results. We thank also L. Lipatov, M. Ryskin, G. Kramer, H. Spiesberger and O. Teryaev for useful discussions.

8 Upsilonium polarization as a touchstone in understanding the parton dynamics in QCD

Authors: S. Baranov and N. Zotov

Nowadays, the production of heavy quarkonium states at high energies is under intense theoretical and experimental study [182, 183]. The production mechanism involves the physics of both short and long distances, and so, appeals to both perturbative and nonperturbative methods of QCD. This feature gives rise to two competing theoretical approaches known in the literature as the color-singlet and color-octet models. According to the color-singlet approach, the formation of a colorless final state takes place already at the level of the hard partonic subprocess (which includes the emission of hard gluons when necessary). In the color-octet model, also known as nonrelativistic QCD (NRQCD), the formation of a meson starts from a color-octet $Q\bar{Q}$ pair and proceeds via the emission of soft nonperturbative gluons.

Originally, the color-octet model was introduced to overcome the discrepancy between the large J/ψ production cross section measured in pp interactions at the Tevatron and the results of theoretical calculations based on the standard perturbative QCD. The problem was apparently

solved by attributing the discrepancy to the hypothetical contributions from the intermediate color-octet states, which must obey certain hierarchy in powers of the relative velicity of the quarks in a bound system. However, the numerical estimates of these contributions extracted from the analysis of Tevatron data are at odds with the HERA data, especially as far as the inelasticity parameter $z = E_\psi/E_\gamma$ is concerned [184]. In the k_t-factorization approach, the values of the color-octet contributions obtained as fits of the Tevatron data appear to be substantially smaller than the ones in the collinear scheme, or even can be neglected at all [153, 155, 185, 186].

The first attempts to solve the quarkonium polarization problem within the k_t-factorization approach were made in the pioneering work [187] (see also [188]) for ep collisions and in Refs. [154, 185] for pp collisions. It was emphasised that the off-shellness of the initial gluons, the intrinsic feature of the k_t-factorization approach, has an immediate consequence in the longitudinal polarization of the final state J/ψ mesons.

The goal of this paper is to derive theoretical predictions on the polarization of Υ mesons produced at the Fermilab Tevatron and CERN LHC. In the k_t-factorization approach, the cross section of a physical process is calculated as a convolution of the partonic cross section $\hat{\sigma}$ and the unintegrated parton distribustion $\mathcal{F}_g(x, k_T^2, \mu^2)$, which depend on both the longitudinal momentum fraction x and transverse momentum k_T:

$$\sigma_{pp} = \int \mathcal{F}_g(x_1, k_{1T}^2, \mu^2)\, \mathcal{F}_g(x_2, k_{2T}^2, \mu^2)\, \hat{\sigma}_{gg}(x_1, x_2, k_{1T}^2, k_{2T}^2, ...)\, dx_1\, dx_2\, dk_{1T}^2\, dk_{2T}^2. \quad (33)$$

In accordance with [173, 189–191], the off-shell gluon spin density matrix is taken in the form

$$\overline{\epsilon_g^\mu \epsilon_g^{*\nu}} = p_p^\mu p_p^\nu x_g^2/|k_T|^2 = k_T^\mu k_T^\nu/|k_T|^2. \quad (34)$$

In all other respects, our calculations follow the standard Feynman rules.

In order to estimate the degree of theoretical uncertainty connected with the choice of unintegrated gluon density, we use two different parametrizations, which are known to show the largest difference with each other, namely, the ones proposed in Refs. [189, 191] and [192]. In the first case [189], the unintegrated gluon density is derived from the ordinary (collinear) density $G(x, \mu^2)$ by differentiating it with respect to μ^2 and setting $\mu^2 = k_T^2$. Here we use the LO GRV set [193] as the input colinear density. In the following, this will be referred to as dGRV parametrisation. The other unintegrated gluon density [192] is obtained as a solution of leading order BFKL equation [191] in the double-logarithm approximation. Technically, it is calculated as the convolution of the ordinary gluon density with some universal weight factor. This will be referred to as JB parametrisation.

The production of Υ mesons in pp collisions can proceed via either direct gluon-gluon fusion or the production of P-wave states χ_b followed by their radiative decays $\chi_b \to \Upsilon + \gamma$. The direct mechanism corresponds to the partonic subprocess $g + g \to \Upsilon + g$ which includes the emission of an additional hard gluon in the final state. The production of P-wave mesons is given by $g + g \to \chi_b$, and there is no emission of any additional gluons. All the other parameters are the same as in our previous paper [194].

The polarization state of a vector meson is characterized by the spin alignment parameter α which is defined as a function of any kinematic variable as $\alpha(\mathcal{P}) = (d\sigma/d\mathcal{P} - 3d\sigma_L/d\mathcal{P})/(d\sigma/d\mathcal{P} +$

$d\sigma_L/d\mathcal{P}$), where σ is the reaction cross section and σ_L is the part of cross section corresponding to mesons with longitudinal polarization (zero helicity state). The limiting values $\alpha = 1$ and $\alpha = -1$ refer to the totally transverse and totally longitudinal polarizations. We will be interested in the behavior of α as a function of the Υ transverse momentum: $\mathcal{P} \equiv |\mathbf{p}_T|$. The experimental definition of α is based on measuring the angular distributions of the decay leptons $d\Gamma(\Upsilon \to \mu^+\mu^-)/d\cos\theta \sim 1 + \alpha\cos^2\theta$, where θ is the polar angle of the final state muon measured in the decaying meson rest frame.

The results of our calculations for the kinematic conditions of the Tevatron and LHC are displayed in Fig. 12. In both cases, the integration limits over rapidity were adjusted to the experimental acceptances of CDF ($|y_\Upsilon| < 0.6$) at the Tevatron and ATLAS ($|y_\Upsilon| < 2.5$) at the LHC. The upper panels show the predicted transverse momentum distributions. Separately shown are the contributions from the direct (dashed lines) and P-wave decay (dotted lines) mechanisms.

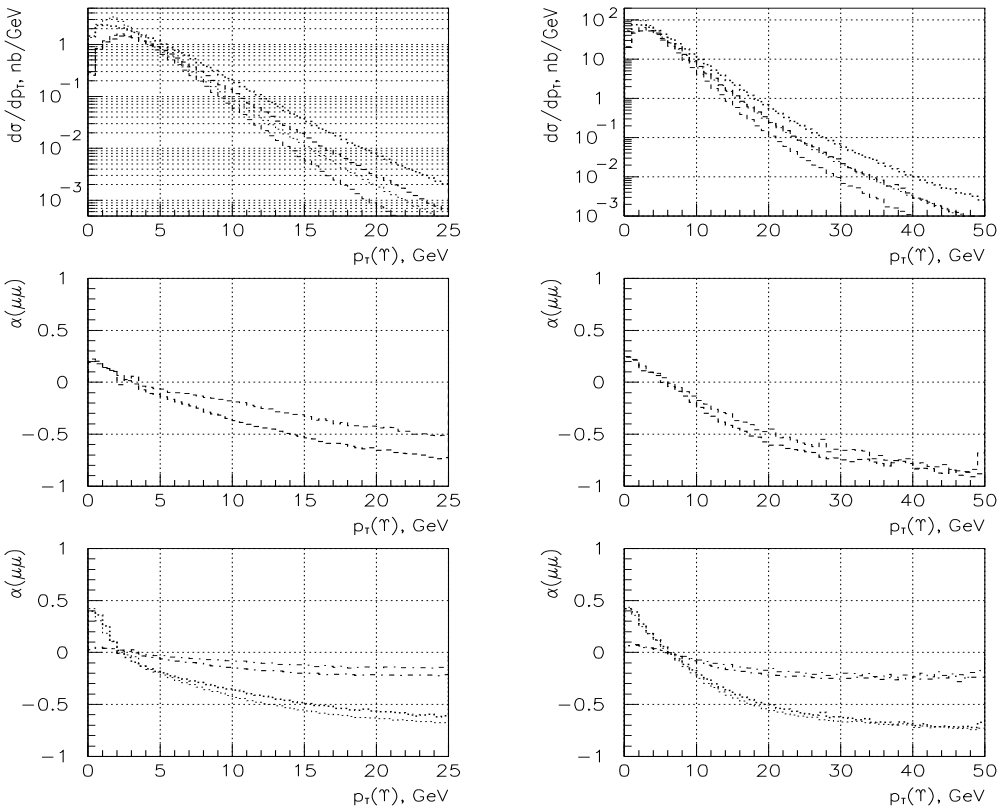

Fig. 12: Predictions on the production of Υ mesons at the Tevatron (left panel) and LHC (right panel). Thick lines, JB parametrization; thin lines, dGRV parametrization. **(a)** Transverse momentum distribution. **(b)** Spin alignment parameter α for the direct contribution. **(c)** Spin alignment parameter α with feed-down from χ_b decays taken into account. Dotted lines, the quark spin conservation hypothesis; dash-dotted lines, the full depolarization hypothesis.

As far as the decays of P-wave states are concerned, nothing is known on the polarisation

properties of these decays. If we assume that the quark spin is conserved in radiative transitions, and the emission of a photon only changes the quark orbital momentum (as it is known to be true in the electric dipole transitions in atomic physics, $\Delta S = 0$, $\Delta L = \pm 1$), then the predictions on α appear to be similar to those made for the direct channel (lower panels in Fig. 12, dotted curves). If, on the contrary, we assume that the the transition $\chi_b \to \Upsilon + \gamma$ leads to complete depolarization, then we arrive at a more moderate behavior of the parameter α (dash-dotted curves in Fig. 12).

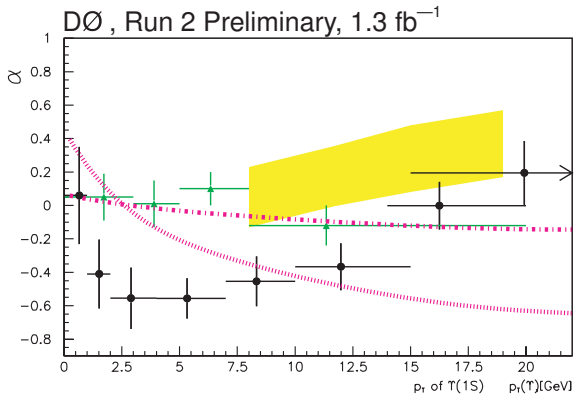

Fig. 13: Spin alignment parameter α at the Tevatron. Solid curve, quark spin conservation hypothesis; dash-dotted curves, full depolarization hypothesis; yellow band, NRQCD predictions. Green and black points, D0 Run 1 and Run 2 experimental data.

The preliminary results on the J/ψ polarization at the Tevatron obtained by the collaborations E537 [195] and CDF [196] point to logitudinal polarization with the average value of spin alignment parameter $\alpha \approx -0.2$ over the whole range of J/ψ transverse momentum p_T. In Fig. 13 our results [194] are compared with the preliminary data on the spin alignment of Υ mesons obtained by the D0 collaboration [197].

A state with purely direct production mechanism in the bottomonium family is the $\Upsilon(3S)$ meson. The calculations presented here are also valid for this state, except the lower total cross section (by an approximate factor of 1/3) because of the correspondingly lower value of the wave function

At the LHC energies, the theoretical predictions possess less sensitivity to the choice of unintegrated gluon distributions. The purest probe is provided by the polarization of $\Upsilon(3S)$ mesons.

9 B_c and double heavy baryon production and decays

Author: A. Likhoded

B_c-meson is the heaviest of the stable under strong interaction mesons. Because of its unique properties the study of its production and decay processes can be used to check current models of quark dynamics.

There are 16 narrow $(\bar{b}c)$ states below the threshold of $\bar{B}D$-pair production. In contrast to

$(c\bar{c})$ and $\left(b\bar{b}\right)$ systems there are no strong annihilation chanel for $(b\bar{c})$-mesons, so excited states can decay only to the ground states with the emission of photons and π-mesons.

Experimental value for ground state mass is $M_{B_c} = 6276.6 \pm 4 \pm 2.7$ MeV/c^2 was measured recently by CDF collaboration in exclusive decay $B_c \to J/\psi\pi$ [198]. It is in good agreement with theoretical predictions [199] within experimental and theoretical errors. Semileptonic decay mode was used recently by D0 and CDF collaborations to measure B_c-meson lifetime [200]

$$\tau_{B_c} \quad = \quad 0.448^{+0.123}_{-0.096} \pm 0.121\,\text{ps}.$$

This value is in good agreement with theoretical calculations based on operator product expansion (OPE), potential models and QCD sum rules [201]. This lifetime is caused mainly by decays of c-quark (70%), while contribution of b-quark decays and weak annihilation are 20% and 10%, respectively. It should be noted, that observed by D0 and CDF collaboration decay modes are connected with b-quark decays.

Since both constituent quarks in B_c are heavy, one can use perturbative QCD for calculation of B_c production cross section. The only nonperturbative parameter on this cross section, the value of B_c wave function at the origin, can be obtained using potential models. In this point B_c-meson production differs dramatically from production of B- and D-mesons.

In e^+e^- annihilation theory predicts usual pattern of b-quark fragmentation $b \to B_c + X$, with calculable fragmentation functions. In $\gamma\gamma \to B_c + X$, $\gamma g \to B_c + X$ and $gg \to B_c + X$ processes, on the other hand, there is strong violation of fragmentation picture for large enough transverse momentum. The factorization formula

$$\frac{d\sigma}{dp_T} \quad = \quad \int \left.\frac{d\hat{\sigma}\left(\mu, gg \to b\bar{b}\right)}{dk_T}\right|_{k_T = p_T/x} D^{b\to B_c+X}(x,\mu)\frac{dx}{x}$$

is valid only for very large values ($p_T \gtrsim 40$ GeV). As a result, to describe experimentally interesting values of B_c transverse momentum in these processes one needs to calculate total amplitude sets: 20 amplitudes for $\gamma\gamma$-, 24 for γg- and 36 for gg-subprocesses [202].

A rough estimate of total contribution to B_c production cross section (including feed-down from excited states) gives the value of order 10^{-3} of the cross section of B-meson production. CDF and D0 collaborations give their results on B_c production cross section (σ_{B_c}) in the form of the ratio over the cross section of B-meson production (σ_B):

$$R_e \quad = \quad \frac{\sigma_{B_c}\text{Br}\left(B_c \to J/\psi e^+\nu_e\right)}{\sigma_B \text{Br}\left(B_c \to J/\psi K^\pm\right)} = 0.282 \pm 0.0038 \pm 0.074$$

in the kinematical region $m_T(B) > 4.0$ GeV and $|y(B)| < 1.0$. Similar result for $B_c \to J/\psi\mu^\pm\nu_\mu$ decay is

$$R_\mu \quad = \quad 0.249 \pm 0.045^{+0.107}_{-0.076}.$$

We believe that these results contradict theoretical estimates. Using known branching fractions $Br\left(B \to J/\psi K^\pm\right) \simeq 1 \cdot 10^{-3}$ and $Br\left(B_c \to J/\psi e^\pm\nu_e\right) \simeq 2 \cdot 10^{-3}$ one can see, that

Mode	BR, %	Mode	BR, %	Mode	BR, %
$B_c^+ \to \eta_c e^+ \nu$	0.75	$B_c^+ \to J/\psi K^+$	0.011	$B_c^+ \to B_s^0 K^+$	1.06
$B_c^+ \to \eta_c \tau^+ \nu$	0.23	$B_c \to J/\psi K^{*+}$	0.022	$B_c^+ \to B_s^{*0} K^+$	0.37
$B_c^+ \to \eta_c' e^+ \nu$	0.041	$B_c^+ \to D^+ \bar{D}^0$	0.0053	$B_c^+ \to B_s^0 K^{*+}$	–
$B_c^+ \to \eta_c' \tau^+ \nu$	0.0034	$B_c^+ \to D^+ \bar{D}^{*0}$	0.0075	$B_c^+ \to B_s^{*0} K^{*+}$	–
$B_c^+ \to J/\psi e^+ \nu$	1.9	$B_c^+ \to D^{*+} \bar{D}^0$	0.0049	$B_c^+ \to B^0 \pi^+$	1.06
$B_c^+ \to J/\psi \tau^+ \nu$	0.48	$B_c^+ \to D^{*+} \bar{D}^{*0}$	0.033	$B_c^+ \to B^0 \rho^+$	0.96
$B_c^+ \to \psi' e^+ \nu$	0.132	$B_c^+ \to D_s^+ \bar{D}^0$	0.00048	$B_c^+ \to B^{*0} \pi^+$	0.95
$B_c^+ \to \psi' \tau^+ \nu$	0.011	$B_c^+ \to D_s^+ \bar{D}^{*0}$	0.00071	$B_c^+ \to B^{*0} \rho^+$	2.57
$B_c^+ \to D^0 e^+ \nu$	0.004	$B_c^+ \to D_s^{*+} \bar{D}^0$	0.00045	$B_c^+ \to B^0 K^+$	0.07
$B_c^+ \to D^0 \tau^+ \nu$	0.002	$B_c^+ \to D_s^{*+} \bar{D}^{*0}$	0.0026	$B_c^+ \to B^0 K^{*+}$	0.015
$B_c^+ \to D^{*0} e^+ \nu$	0.018	$B_c^+ \to \eta_c D_s^+$	0.86	$B_c^+ \to B^{*0} K^+$	0.055
$B_c^+ \to D^{*0} \tau^+ \nu$	0.008	$B_c^+ \to \eta_c D_s^{*+}$	0.26	$B_c^+ \to B^{*0} K^{*+}$	0.058
$B_c^+ \to B_s^0 e^+ \nu$	4.03	$B_c^+ \to J/\psi D_s^+$	0.17	$B_c^+ \to B^+ \overline{K^0}$	1.98
$B_c^+ \to B_s^{*0} e^+ \nu$	5.06	$B_c^+ \to J/\psi D_s^{*+}$	1.97	$B_c^+ \to B^+ \overline{K^{*0}}$	0.43
$B_c^+ \to B^0 e^+ \nu$	0.34	$B_c^+ \to \eta_c D^+$	0.032	$B_c^+ \to B^{*+} \overline{K^0}$	1.60
$B_c^+ \to B^{*0} e^+ \nu$	0.58	$B_c^+ \to \eta_c D^{*+}$	0.010	$B_c^+ \to B^{*+} \overline{K^{*0}}$	1.67
$B_c^+ \to \eta_c \pi^+$	0.20	$B_c^+ \to J/\psi D^+$	0.009	$B_c^+ \to B^+ \pi^0$	0.037
$B_c^+ \to \eta_c \rho^+$	0.42	$B_c^+ \to J/\psi D^{*+}$	0.074	$B_c^+ \to B^+ \rho^0$	0.034
$B_c^+ \to J/\psi \pi^+$	0.13	$B_c^+ \to B_s^0 \pi^+$	16.4	$B_c^+ \to B^{*+} \pi^0$	0.033
$B_c^+ \to J/\psi \rho^+$	0.40	$B_c^+ \to B_s^0 \rho^+$	7.2	$B_c^+ \to B^{*+} \rho^0$	0.09
$B_c^+ \to \eta_c K^+$	0.013	$B_c^+ \to B_s^{*0} \pi^+$	6.5	$B_c^+ \to \tau^+ \nu_\tau$	1.6
$B_c^+ \to \eta_c K^{*+}$	0.020	$B_c^+ \to B_s^{*0} \rho^+$	20.2	$B_c^+ \to c\bar{s}$	4.9

Table 1: Branching fractions of exclusive B_c decay modes [203]

in this kinematical region the ratio

$$\frac{\sigma(B_c)}{\sigma(B)} \quad = \quad R_e \frac{\text{Br}(B \to J/\psi K^{\pm}) \text{Br}(b \to B^{\pm})}{\text{Br}(B_c \to J/\psi e^{\pm} \nu_e)} = \frac{0.282 \cdot 10^{-3} \cdot 0.5}{2 \cdot 10^{-2}} = 0.7 \cdot 10^{-2},$$

that is about an order of magnitude higher than theoretical estimates.

Using CTEQ5L gluon distribution functions and perturbative calculation of $gg \to B_c + X$, we obtained about 0.8 μb for B_c-meson production cross section at LHC. It includes contributions from $1S_0$ (0.19 μb), $1S_1$ (0.47 μb), $2S_0$ (0.05 μb) and $2S_1$ (0.11 μb) states. After summing over all spin states we can see, that the whole contribution of P-wave levels is equal to 7% of S-state cross section.

At LHC with luminocity $\mathcal{L} = 10^{34} cm^2 s^{-1}$ and $\sqrt{s} = 14$ TeV one can expect $4.5 \cdot 10^{10}$ B_c^+ events per year. As it is clear from Table 1, branching fractions of main semileptonic and hadronic decay modes are large enough for reliable observation of B_c meson.

10 Testing time-reversal and CP symmetry with Λ_b decays

Author: Z. J. Ajaltouni

10.1 Introduction

Time-reversal (TR) is a fundamental symmetry in many branches of Physics, principally nuclear and particle Physics. Testing its validity or, conversely, searching for its violation, is an important task similar to CP symmetry violation. Few years ago, important experimental results showing clear evidence for TR violaton in $K^0 - \bar{K^0}$ oscillations have been claimed both by CP-LEAR and K-TeV experiments [204]. Then, this research has been extended to the $B-$meson system by BaBar and Belle collaborations.

Another source of TR violation could be looked for in particular decays of *hyperons*, as suggested by R. Gatto after the discovery of parity violation in β decay [205]. If we replace the s-quark belonging to an hyperon by a b-quark, analogous tests can be performed with *beauty baryons*, like Λ_b, Σ_b, etc. With the advent of the LHC, it is expected that 10% of the $b\bar{b}$ pairs produced in proton-proton collisions at $\sqrt{s} = 14$ TeV will hadronize into beauty baryons $\mathcal{B}_b$, and approximately 90% of the $\mathcal{B}_b$ will be dominated by Λ_b or $\bar{\Lambda}_b$. In the framework of the LHCb experiment whose average luminosity will be $\mathcal{L} = 2 \times 10^{32} cm^{-2} s^{-1}$, roughly 10^{11} beauty baryons will be produced each year.

10.2 Features of Time-Reversal

TR operator changes the sign of momentum $\vec{p}$ and spin $\vec{s}$ of any particle and leaves its coordinates $\vec{r}$ invariant. Any triple product $(\vec{v}_i \times \vec{v}_j) \cdot \vec{v}_k$ with $\vec{v}_{i,j,k} = \vec{p}$ or $\vec{s}$ will be *odd* under TR; a non-vanishing value of this observable being a sign of TR violation (TRV). However, an inevitable physical process as strong Final State Interactions (FSI) appears when examining hadronic decays. FSI modify particle wave-functions and generate an additional phase-shift, δ_S, to the decay amplitude; the existence of the phase δ_S could simulate a T-odd effect. Being aware of this issue, we developed a phenomenological model describing the decay $\Lambda_b \to \Lambda V(1^-)$ and used it in our search for TRV supposing that FSI are negligible. Thus a non-vanishing T-odd observable will be considered as a serious sign of TRV. In the following, emphasis will be put on TR processes and, because of the delicate problem of CP study in $\Lambda_b - \bar{\Lambda}_b$ system, only a recent reference will be mentioned [206].

10.3 Kinematics and Dynamics of $\Lambda_b \to \Lambda V(1^-)$ Decays

Different observables can be constructed in order to test TR; the main one being the polarization-vectors of the intermediate resonances coming from Λ_b decays like $\Lambda(1/2^+)$ and $V = \rho^0, \omega, J/\psi$, the vector-meson V being mainly the J/ψ decaying into $\mu^-\mu^+$. A rigorous study of these decays requires the *helicity formalism* of Jacob-Wick-Jackson which includes the Λ_b initial polarization expressed by its polarization density-matrix (PDM) [207]. Full calculations permit to deduce the Λ angular distributions in an appropriate Λ_b rest-frame. It is given by: $\frac{d\sigma}{d\Omega} = 1 + \alpha_{As}^{\Lambda_b} \vec{\mathcal{P}}^{\Lambda_b} \cdot \hat{p}$, where $\alpha_{As}^{\Lambda_b}$ is the decay asymmetry parameter of the Λ_b resonance, $\vec{\mathcal{P}}^{\Lambda_b}$ is its polarization-vector and $\hat{p}$ is the unit-vector parallel to Λ momentum.

A special dynamical model has been performed in order to compute the decay amplitude [208]. It is divided into two main parts : (i) In the framework of the *factorization hypothesis*, the Operator Product Expansion (OPE) techniques are used in order to evaluate both the *soft* (non-perturbative) contributions and the *hard* (perturbative) ones to the hadronic matrix element; the color number

N_c is left *free*. (ii) The form-factors arising in the matrix element are computed by means of the Heavy Quark Effective Theory (HQET) and corrections of order $\mathcal{O}(1/m_b)$ are performed. Finally, both tree and penguin diagrams have been taken into account in our model.

10.4 Main Physical Results

• In order to test the model, the branching ratio $BR(\Lambda_b \to \Lambda J/\psi)$ and other ones are computed according to the effective color number, N_c^{eff}, and compared to the experimental data.

N_c^{eff}	2	2.5	3	3.5
$\Lambda J/\psi$	8.95×10^{-4}	2.79×10^{-4}	0.62×10^{-4}	0.03×10^{-4}
$\Lambda\rho^0$	1.62×10^{-7}	1.89×10^{-7}	2.2×10^{-7}	2.4×10^{-7}
$\Lambda\omega$	22.3×10^{-7}	4.75×10^{-7}	0.2×10^{-7}	0.64×10^{-7}

Table 2: Branching ratio, $\mathcal{BR}$, for $\Lambda_b \to \Lambda J/\Psi$, $\Lambda_b \to \Lambda\rho^0$ and $\Lambda_b \to \Lambda\omega$.

The experimental value, $BR(\Lambda_b \to \Lambda J/\psi) = (4.7 \pm 2.1 \pm 1.9) \times 10^{-4}$ (PDG 2006), favours the range of values $2.0 \leq N_c^{eff} \leq 3.0$.

• Other essential parameters like Λ_b asymmetry, Λ polarization and its non-diagonal matrix element, and the probability of longitudinal polarization for each vector meson can also be obtained :

Parameter	$\Lambda\rho^0 - \omega$	$\Lambda J/\psi$
$\alpha_{AS}^{\Lambda_b}$	0.194	0.490
$\mathcal{P}^{\Lambda}$	-0.21	-0.17
ρ_{+-}^{Λ}	0.31	0.25
ρ_{00}^{V}	0.79	0.66

10.5 Direct Test of Time-Reversal

Special Angles :

We define $\vec{n}_\Lambda$ and $\vec{n}_V$ respectively as the unit normal vetors to Λ and V decay planes in the Λ_b rest-frame, $\vec{e}_Z$ being the quantization axis.

$$\vec{n}_\Lambda = \frac{\vec{p}_p \times \vec{p}_\pi}{|\vec{p}_p \times \vec{p}_\pi|}\ ,\ \ \vec{n}_V = \frac{\vec{p}_{l^+} \times \vec{p}_{l^-}}{|\vec{p}_{l^+} \times \vec{p}_{l^-}|}\ ,\ \text{ or }\ \vec{n}_V = \frac{\vec{p}_{h^+} \times \vec{p}_{h^-}}{|\vec{p}_{h^+} \times \vec{p}_{h^-}|}$$

Those vectors are **even** under TR. But the cosine and the sine of their azimutal angles defined by :

$$\vec{u}_i = \frac{\vec{e}_Z \times \vec{n}_i}{|\vec{e_Z} \times \vec{n}_i|}\ ,\ \ \cos\phi_{(n_i)} = \vec{e}_Y \cdot \vec{u}_i\ ,\ \ \sin\phi_{(n_i)} = \vec{e}_Z \cdot (\vec{e}_Y \times \vec{u}_i)\ ,$$

with $\phi_{(n_i)} = \phi_{\vec{n}_\Lambda}$, $\phi_{\vec{n}_V}$ are both **odd** under TR. Their distributions exhibit asymmetries which depend directly on the Λ azimuthal angle distribution whose analytical expression is given by:

$$d\sigma/d\phi \propto 1 + \frac{\pi}{2}\alpha_{As}^{\Lambda}\Big(\Re e(\rho_{+-}^{\Lambda_b})\cos\phi - \Im m(\rho_{+-}^{\Lambda_b})\sin\phi\Big) .$$

The initial Λ_b PDM being unknown, we make the following hypothesis in our simulations : $\mathcal{P}^{\Lambda_b} = 100\%$ and $\Re e(\rho_{+-}^{\Lambda_b}) = -\Im m(\rho_{+-}^{\Lambda_b}) = \sqrt{2}/2$. The following asymmetries are obtained [206] :

Asymmetries	$\Lambda\rho^0 - \omega$	$\Lambda J/\psi$
$AS(\cos\phi_{\vec{n}_\Lambda})$	$(2.4 \pm 0.3)\%$	$(5.2 \pm 0.3)\%$
$AS(\sin\phi_{\vec{n}_\Lambda})$	$-(2.7 \pm 0.3)\%$	$-(5.0 \pm 0.3)\%$

Vector-Polarizations

In a second step, vector-polarizations have been carefully examined, mainly by considering a new frame related to each resonance R_i and defined as follows:

$$\vec{e}_L = \frac{\vec{p}}{p} , \ \vec{e}_T = \frac{\vec{e}_Z \times \vec{e}_L}{|\vec{e}_Z \times \vec{e}_L|} , \ \vec{e}_N = \vec{e}_T \times \vec{e}_L .$$

Each vector-polarization $\vec{\mathcal{P}}^{(i)}$ can be expanded on the new basis by writing: $\vec{\mathcal{P}}^{(i)} = P_L^{(i)}\vec{e}_L + P_N^{(i)}\vec{e}_N + P_T^{(i)}\vec{e}_T$, with $P_j^{(i)} = \vec{\mathcal{P}}^{(i)} \cdot \vec{e}_j$ and $j = L, N, T$. These components as well as the basis vectors $\vec{e}_L, \vec{e}_T$ and $\vec{e}_N$, are studied under parity and time-reversal operations. The results are straightforward: P_L and P_T are both $Parity-$odd and $T-$even , while P_N is $Parity-$even but $T-$**odd**.

So, if the normal component P_N is not equal to zero, it would be a signal of TR violation.

10.6 Conclusion

The process $\Lambda_b \to \Lambda J/\psi$ is a promising channel to look for the validity of TR symmetry at LHC energies. Complete kinematical calculations have been performed by stressing the importance of the resonance polarizations. Our dynamics model is very realistic, because it is based on the OPE formalism and completed by HQET for the computation of the form-factors. An extension of these calculations is under study in order to perform rigorous tests of both CP and TR symmetries among beauty baryons in a model-independent way [209].

11 Production and detection of massive exotic hadrons

Authors: D. Milstead and O. Piskounova

Exotic stable massive particles are proposed in many models of physics beyond the Standard Model. Understanding their interactions in matter is critical for any search. This paper outlines a model for the scattering of stable massive hadrons which is based on Regge phenomenology and the quark gluon string model.

11.1 Introduction

Searches for exotic stable[15] massive particles (SMPs) are performed at colliders as a matter of routine whenever a new collision energy is reached [210]. An additional motivation to make such searches at the LHC arises from the hierarchy problem, proposed solutions to which suggest that new physics processes may be manifest at TeV energies; indeed SMPs are predicted in a number of exotic physics models, such as supersymmetry [210]. Prior to data taking it is important to establish that LHC experiments are able both to detect and extract the quantum numbers of any SMP which may be observed. To do this, an understanding of the interactions of SMPs in matter is needed. As part of this workshop a model [211] has been developed for the scattering of hadronic SMPs (termed H-hadrons) which uses Regge phenomenology [212] and the quark gluon string model (QGSM) [213]. This work has clear implications for future searches using HERA data and the interpretation of earlier searches.

11.2 Interactions of H-Hadrons in Matter

A qualitative picture of the scattering process can be built up [214]. The heavy exotic quark will be a spectator, and the low energy light quark system is involved in the interaction. Regge phenomenology and the QGSM are thus appropriate tools with which the interactions of exotic hadrons in matter can be explored. Fig. 14 shows the predicted cross section for the interaction of a H-meson with a stationary nucleon in a nucleus comprising equal amounts of protons and neutrons as a function of the Lorentz factor γ of the H-meson. Reggeon and pomeron contributions are shown separately.

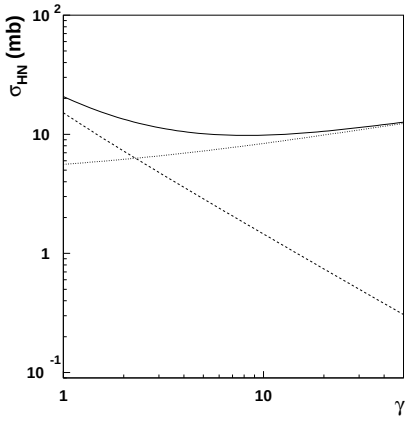

Fig. 14: Pomeron (dotted) and reggeon (dashed) contributions to the exotic-meson-nucleon cross section. The sum of the two processes is shown as a solid line.

Exotic hadrons which contain a light constituent anti-quark, eg $H_{Q\bar{q}}$ or a $H_{\bar{Q}\bar{q}\bar{q}}$ can undergo pomeron and reggeon exchanges. Conversely, hadrons containing a light constituent quark ($H_{\bar{Q}q}$, H_{Qqq}) can only undergo pomeron exchange. Anti-baryons and baryons may undergo both

[15]The term stable implies a particle will not decay as it traverses a detector.

reggeon and pomeron exchange, and pomeron exchange only processes, respectively. The overall cross sections for interactions involving baryons and anti-baryons is estimated by doubling the pomeron contribution to the meson cross sections shown in Fig. 14 to take into account the extra light quark contribution. The reggeon contribution to anti-baryon interactions is set to twice the value for meson scattering together with an additional contribution from processes in which exotic anti-baryons can annihilate to exotic mesons and ordinary mesons. This latter contribution is suppressed.

11.3 Energy Loss

The PYTHIA [215] program was used to produce samples of stable fourth generation quark pair production events. For reasons of detector acceptance, the β value of the H-hadrons was restricted to be greater than 0.7 and the pseudorapidity to $|\eta| < 2.5$ [216]. Using a Monte Carlo method, the H-hadrons were transported through iron corresponding to the material distribution of the ATLAS detector sub-systems enclosed within the muon detector system. Using a triple regge ansatz [211] H-hadron energy loss can be estimated. Fig. 15 shows the total energy loss of H-hadrons after they pass through the detector material. Distributions are presented for H-hadrons formed from different types of exotic quarks and anti-quarks with masses 200 and 1000 GeV. The distributions are normalised to the total number N of a given type of H-hadron satisfying the β and η requirements. There is little difference between them, with a peak around 5 GeV. H-hadrons containing up-like quarks typically lose more energy than those with down-like quarks owing to the greater fraction of neutral H-hadrons with down-like quarks.

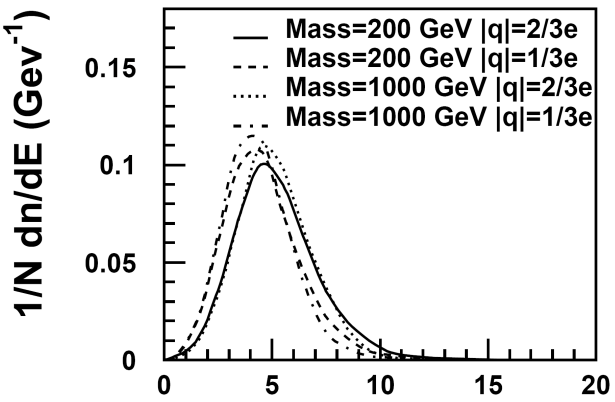

Fig. 15: Total energy loss for H-hadrons of different types and masses.

11.4 Acknowledgements

D. Milstead is a Royal Swedish Academy Research Fellow supported by a grant from the Knut and Alice Wallenberg Foundation.

References

[1] W. K. Tung *et al.,* JHEP **02**, 053 (2007). hep-ph/0611254.

[2] A. D. Martin, W. J. Stirling, R. S. Thorne, and G. Watt, Phys. Lett. **B652**, 292 (2007). 0706.0459.

[3] P. M. Nadolsky *et al.,* Phys. Rev. **D78**, 013004 (2008). 0802.0007.

[4] G. Watt, A. D. Martin, W. J. Stirling, and R. S. Thorne, *Recent Progress in Global PDF Analysis.* Preprint 0806.4890, 2008.

[5] A. D. Martin, W. J. Stirling, R. S. Thorne, and G. Watt (2009). 0901.0002.

[6] J. C. Collins and W.-K. Tung, Nucl. Phys. **B278**, 934 (1986).

[7] J. C. Collins, Phys. Rev. **D58**, 094002 (1998). hep-ph/9806259.

[8] E. L. M. P. Laenen, S. Riemersma, J. Smith, and W. L. van Neerven, Nucl. Phys. **B392**, 162 (1993).

[9] M. A. G. Aivazis, J. C. Collins, F. I. Olness, and W.-K. Tung, Phys. Rev. **D50**, 3102 (1994). hep-ph/9312319.

[10] J. C. Collins, F. Wilczek, and A. Zee, Phys. Rev. **D18**, 242 (1978).

[11] M. Gluck, E. Reya, and A. Vogt, Eur. Phys. J. **C5**, 461 (1998). hep-ph/9806404.

[12] M. Buza, Y. Matiounine, J. Smith, R. Migneron, and W. L. van Neerven, Nucl. Phys. **B472**, 611 (1996). hep-ph/9601302.

[13] M. Buza, Y. Matiounine, J. Smith, and W. L. van Neerven, Eur. Phys. J. **C1**, 301 (1998). hep-ph/9612398.

[14] R. S. Thorne and R. G. Roberts, Phys. Lett. **B421**, 303 (1998). hep-ph/9711223.

[15] R. S. Thorne and R. G. Roberts, Phys. Rev. **D57**, 6871 (1998). hep-ph/9709442.

[16] M. Dittmar *et al., Parton distributions: Summary report for the HERA - LHC workshop*. Preprint hep-ph/0511119, 2005.

[17] R. M. Barnett, Phys. Rev. Lett. **36**, 1163 (1976).

[18] W. K. Tung, S. Kretzer, and C. Schmidt, J. Phys. **G28**, 983 (2002). hep-ph/0110247.

[19] S. Kretzer, H. L. Lai, F. I. Olness, and W. K. Tung, Phys. Rev. **D69**, 114005 (2004). hep-ph/0307022.

[20] R. S. Thorne, Phys. Rev. **D73**, 054019 (2006). hep-ph/0601245.

[21] A. Chuvakin, J. Smith, and W. L. van Neerven, Phys. Rev. **D61**, 096004 (2000). hep-ph/9910250.

[22] M. Kramer, F. I. Olness, and D. E. Soper, Phys. Rev. **D62**, 096007 (2000). hep-ph/0003035.

[23] S. Kretzer and I. Schienbein, Phys. Rev. **D58**, 094035 (1998). hep-ph/9805233.

[24] E. L. M. P. Laenen and S. O. Moch, Phys. Rev. **D59**, 034027 (1999). hep-ph/9809550.

[25] S. Catani, M. Ciafaloni, and F. Hautmann, Nucl. Phys. **B366**, 135 (1991).

[26] I. Bierenbaum, J. Blümlein, and S. Klein, Acta Phys. Pol. **B39** (2008) 1531 (2008). 0806.0451.

[27] M. Buza and W. L. van Neerven, Nucl. Phys. **B500**, 301 (1997). hep-ph/9702242.

[28] A. D. Martin, W. J. Stirling, R. S. Thorne, and G. Watt, *Parton distributions for the LHC*. Preprint in preparation, 2008.

[29] A. D. Martin, R. G. Roberts, W. J. Stirling, and R. S. Thorne, Phys. Lett. **B531**, 216 (2002). hep-ph/0201127.

[30] A. D. Martin, R. G. Roberts, W. J. Stirling, and R. S. Thorne, Phys. Lett. **B604**, 61 (2004). hep-ph/0410230.

[31] H. collaboration:, *Measurement of $F_2^{c\bar{c}}$ and $F_2^{b\bar{b}}$ using the H1 vertex detector at HERA*. 34th International Conference on High Energy Physics Philadelphia, 30th July - 5th August, 2008.

[32] S. Alekhin, Phys. Rev. **D68**, 014002 (2003). hep-ph/0211096.

[33] A. D. Martin, W. J. Stirling, and R. S. Thorne, Phys. Lett. **B636**, 259 (2006). hep-ph/0603143.

[34] B. W. Harris and J. Smith, Nucl. Phys. **B452**, 109 (1995). hep-ph/9503484.

[35] P. Jimenez-Delgado and E. Reya, *Dynamical NNLO parton distributions*. Preprint 0810.4274, 2008.

[36] J. M. Campbell, *Overview of the theory of W/Z + jets and heavy flavor*. Preprint 0808.3517, 2008.

[37] B. A. Kniehl, *Inclusive production of heavy-flavored hadrons at NLO in the GM-VFNS*. Preprint 0807.2215, 2008.

[38] C. Buttar *et al.* (2006). hep-ph/0604120.

[39] S. J. Brodsky, P. Hoyer, C. Peterson, and N. Sakai, Phys. Lett. **B93**, 451 (1980).

[40] J. Pumplin, H. L. Lai, and W. K. Tung, Phys. Rev. **D75**, 054029 (2007). hep-ph/0701220.

[41] European Muon Collaboration, J. J. Aubert *et al.*, Nucl. Phys. **B213**, 31 (1983).

[42] A. D. Martin, R. G. Roberts, W. J. Stirling, and R. S. Thorne, Eur. Phys. J. **C4**, 463 (1998). hep-ph/9803445.

[43] R. S. Thorne, J. Phys. **G25**, 1307 (1999). hep-ph/9902299.

[44] OPAL Collaboration, G. Alexander *et al.*, Z. Phys. **C72**, 1 (1996);
OPAL Collaboration, K. Ackerstaff *et al.*, Eur. Phys. J. **C1**, 439 (1998);
ALEPH Collaboration, R. Barate *et al.*, Eur. Phys. J. **C16**, 597 (200);
CLEO Collaboration, M. Artuso *et al.*, Phys. Rev. **D70**, 112001 (2004);
Belle Collaboration, R. Seuster *et al.*, Phys. Rev. **D73**, 032002 (2006).

[45] G. Kramer and H. Spiesberger, Eur. Phys. J. **C22**, 289 (2001);
G. Kramer and H. Spiesberger, Eur. Phys. J. **C28**, 495 (2003);
G. Kramer and H. Spiesberger, Eur. Phys. J. **C38**, 309 (2004).

[46] B. A. Kniehl, G. Kramer, I. Schienbein, and H. Spiesberger, Phys. Rev. **D71**, 014018 (2005);
B. A. Kniehl, G. Kramer, I. Schienbein, and H. Spiesberger, Eur. Phys. J. **C41**, 199 (2005).

[47] B. A. Kniehl, G. Kramer, I. Schienbein, and H. Spiesberger, Phys. Rev. Lett. **96**, 012001 (2006).

[48] T. Kneesch, B. A. Kniehl, G. Kramer, and I. Schienbein, Nucl. Phys. **B799**, 34 (2008).

[49] M. G. Bowler, Z. Phys. **C11**, 169 (1981).

[50] SLD Collaboration, K. Abe *et al.*, Phys. Rev. Lett. **84**, 4300 (2000);
SLD Collaboration, K. Abe *et al.*, Phys. Rev. **D65**, 092006 (2002);
SLD Collaboration, K. Abe *et al.*, Phys. Rev. **D66**, 079905(E) (2002);
ALEPH Collaboration, A. Heister *et al.*, Phys. Lett. **B512**, 30 (2001);
OPAL Collaboration, G. Abbiendi *et al.*, Eur. Phys. J. **C29**, 463 (2003).

[51] CDF Collaboration, D. Acosta *et al.*, Phys. Rev. **D71**, 021001 (2005);
CDF Collaboration, A. Abulencia *et al.*, Phys. Rev. **D75**, 012010 (2007).

[52] J. Binnewies, B. A. Kniehl, and G. Kramer, Phys. Rev. **D58**, 034016 (1998).

[53] V. G. Kartvelishvili and A. K. Likhoded, Sov. J. Nucl. Phys. **42**, 823 (1985). [Yad. Fiz. **42**, 1306 (1985)].

[54] CDF Collaboration, D. Acosta *et al.*, Phys. Rev. Lett. **91**, 241804 (2003).

[55] U. Aglietti, G. Corcella, and G. Ferrera, Nucl. Phys. **B775**, 162 (2007).

[56] G. Corcella and G. Ferrera, J. High Energy Phys. **12**, 029 (2007).

[57] U. Aglietti, G. Ferrera, and G. Ricciardi, Nucl. Phys. **B768**, 85 (2007).

[58] U. Aglietti, F. Di Lodovico, G. Ferrera, and G. Ricciardi, arXiv:0711.0860. 0711.0860.

[59] B. Mele and P. Nason, Nucl. Phys. **B617**, 626 (1991).

[60] M. Cacciari and S. Catani, Nucl. Phys. **B617**, 253 (2001).

[61] G. Sterman, Nucl. Phys. **B281**, 310 (1987).

[62] S. Catani and L. Trentadue, Nucl. Phys. **B327**, 323 (1989).

[63] U. Aglietti and G. Ricciardi, Phys. Rev. **D70**, 114008 (2004).

[64] D. Shirkov, Nucl. Phys. Proc. Suppl. **152**, 51 (2006).

[65] ALEPH Collaboration, A. Heister *et al.*, Phys. Lett. **B512**, 30 (2001).

[66] OPAL Collaboration, G. Abbiendi *et al.*, Eur. Phys. J. **C29**, 463 (2003).

[67] SLD Collaboration, K. Abe *et al.*, Phys. Rev. Lett. **84**, 4300 (2000).

[68] ALEPH Collaboration, R. Barate *et al.*, Eur. Phys. J. **C16**, 597 (2000).

[69] ZEUS Collaboration, S. Chekanov *et al.*, Nucl. Phys. **B700**, 3 (2004). hep-ex/0405065.

[70] CDF Collaboration, F. Abe *et al.*, Phys. Rev. **D60**, 072003 (1999). hep-ex/9903011.

[71] A. Banfi, G. P. Salam, and G. Zanderighi, Eur. Phys. J. **C47**, 113 (2006). hep-ph/0601139.

[72] S. Catani, Y. L. Dokshitzer, M. Olsson, G. Turnock, and B. R. Webber, Phys. Lett. **B269**, 432 (1991).

[73] S. Catani, Y. L. Dokshitzer, M. H. Seymour, and B. R. Webber, Nucl. Phys. **B406**, 187 (1993).

[74] S. D. Ellis and D. E. Soper, Phys. Rev. **D48**, 3160 (1993). hep-ph/9305266.

[75] A. Banfi, G. P. Salam, and G. Zanderighi, JHEP **08**, 062 (2004). hep-ph/0407287.

[76] S. Catani, F. Krauss, R. Kuhn, and B. R. Webber, JHEP **11**, 063 (2001). hep-ph/0109231.

[77] M. L. Mangano, M. Moretti, and R. Pittau, Nucl. Phys. **B632**, 343 (2002). hep-ph/0108069.

[78] *Measurement of the inclusive b-jet cross section in $p\bar{p}$ collisions at $\sqrt{s} = 1.96\mathrm{TeV}$* (unpublished). Note 8418.

[79] J. M. Campbell and R. K. Ellis, Phys. Rev. **D62**, 114012 (2000). hep-ph/0006304.

[80] M. L. Mangano, P. Nason, and G. Ridolfi, Nucl. Phys. **B373**, 295 (1992).

[81] S. Frixione, P. Nason, and B. R. Webber, JHEP **08**, 007 (2003). hep-ph/0305252.

[82] G. Corcella *et al.*, JHEP **01**, 010 (2001). hep-ph/0011363.

[83] A. Banfi, G. P. Salam, and G. Zanderighi, JHEP **07**, 026 (2007). 0704.2999.

[84] W. T. Giele, E. W. N. Glover, and D. A. Kosower, Nucl. Phys. **B403**, 633 (1993). hep-ph/9302225.

[85] Z. Nagy, Phys. Rev. Lett. **88**, 122003 (2002). hep-ph/0110315.

[86] J. Pumplin, H. L. Lai, and W. K. Tung, Phys. Rev. **D75**, 054029 (2007). hep-ph/0701220.

[87] CDF Collaboration, D. E. Acosta *et al.*, Phys. Rev. **D71**, 092001 (2005). hep-ex/0412006.

[88] C. Weiser, *A combined secondary vertex based b-tagging algorithm in CMS* (unpublished). CMS NOTE-2006/014.

[89] M. Sapinski, *Expected performance of ATLAS for measurements of jets, b-jets, tau-jets, and* $E_{T,\mathrm{mis}}$ (unpublished). SN-ATLAS-2002-012, ATL-COM-CONF-2001-006.

[90] J. Bastos, physics/0702041 (2007). physics/0702041.

[91] W. Bernreuther, J. Phys. **G35**, 083001 (2008). 0805.1333.

[92] P. M. Nadolsky *et al.*, Phys. Rev. **D78**, 013004 (2008). 0802.0007.

[93] P. Nason, S. Dawson, and R. K. Ellis, Nucl. Phys. **B303**, 607 (1988).

[94] S. Moch and P. Uwer, Phys. Rev. **D78**, 034003 (2008). 0804.1476.

[95] M. Cacciari, S. Frixione, M. M. Mangano, P. Nason, and G. Ridolfi (2008). 0804.2800.

[96] N. Kidonakis and R. Vogt, arXiv:0805.3844 (2008). 0805.3844.

[97] M. Czakon, A. Mitov, and S. Moch, Phys. Lett. **B651**, 147 (2007). 0705.1975.

[98] M. Czakon, A. Mitov, and S. Moch, Nucl. Phys. **B798**, 210 (2008). 0707.4139.

[99] M. Czakon, Phys. Lett. **B664**, 307 (2008). 0803.1400.

[100] J. G. Körner, Z. Merebashvili, and M. Rogal, Phys. Rev. **D73**, 034030 (2006). hep-ph/0511264.

[101] J. G. Körner, Z. Merebashvili, and M. Rogal, Phys. Rev. **D77**, 094011 (2008). 0802.0106.

[102] S. Dittmaier, P. Uwer, and S. Weinzierl, Phys. Rev. Lett. **98**, 262002 (2007). hep-ph/0703120.

[103] M. Caffo, H. Czyz, S. Laporta, and E. Remiddi, Nuovo Cim. **A111**, 365 (1998). hep-th/9805118.

[104] E. Laenen, S. Riemersma, J. Smith, and W. L. van Neerven, Nucl. Phys. **B392**, 162 (1993);
S. Riemersma, J. Smith, and W. L. van Neerven, Phys. Lett. **B347**, 143 (1995). hep-ph/9411431.

[105] S. Alekhin and J. Blümlein, Phys. Lett. **B594**, 299 (2004). hep-ph/0404034.

[106] M. Buza, Y. Matiounine, J. Smith, and W. L. van Neerven, Nucl. Phys. **B485**, 420 (1997). hep-ph/9608342.

[107] I. Bierenbaum, J. Blümlein, and S. Klein, in preparation.

[108] S. Alekhin, K. Melnikov, and F. Petriello, Phys. Rev. **D74**, 054033 (2006). hep-ph/0606237.

[109] Blümlein, H. J., Böttcher, and A. Guffanti, Nucl. Phys. **B774**, 182 (2007). hep-ph/0607200.

[110] M. Buza, Y. Matiounine, J. Smith, R. Migneron, and W. L. van Neerven, Nucl. Phys. **B472**, 611 (1996). hep-ph/9601302.

[111] J. A. M. Vermaseren, A. Vogt, and S. Moch, Nucl. Phys. **B724**, 3 (2005). hep-ph/0504242.

[112] I. Bierenbaum, J. Blümlein, and S. Klein, Nucl. Phys. **B780**, 40 (2007). hep-ph/0703285.

[113] I. Bierenbaum, J. Blümlein, and S. Klein, Phys. Lett. **B648**, 195 (2007). hep-ph/0702265.

[114] J. Blümlein, A. De Freitas, W. L. van Neerven, and S. Klein, Nucl. Phys. **B755**, 272 (2006). hep-ph/0608024.

[115] I. Bierenbaum, Blümlein, S. J., Klein, and C. Schneider, Nucl. Phys. **B803**, 1 (2008). 0803.0273.

[116] S. A. Larin, T. van Ritbergen, and J. A. M. Vermaseren, Nucl. Phys. **B427**, 41 (1994);
S. A. Larin, P. Nogueira, T. van Ritbergen, and J. A. M. Vermaseren, Nucl. Phys. **B492**, 338 (1997). hep-ph/9605317;
A. Retey and J. A. M. Vermaseren, Nucl. Phys. **B604**, 281 (2001). hep-ph/0007294;
J. Blümlein and J. A. M. Vermaseren, Phys. Lett. **B606**, 130 (2005). hep-ph/0411111;
S. Moch, J. A. M. Vermaseren, and A. Vogt, Nucl. Phys. **B688**, 101 (2004). hep-ph/0403192.

[117] A. Vogt, S. Moch, and J. A. M. Vermaseren, Nucl. Phys. **B691**, 129 (2004). hep-ph/0404111.

[118] J. A. Gracey, Phys. Lett. **B322**, 141 (1994). hep-ph/9401214.

[119] N. Gray, D. J. Broadhurst, W. Grafe, and K. Schilcher, Z. Phys. **C48**, 673 (1990).

[120] M. Buza, Y. Matiounine, J. Smith, and W. L. van Neerven, Eur. Phys. J. **C1**, 301 (1998). hep-ph/9612398.

[121] I. Bierenbaum, J. Blümlein, and S. Klein, arxiv:0806.4613 [hep-ph] (2008). 0806.4613.

[122] B. A. Ovrut and H. J. Schnitzer, Nucl. Phys. **B179**, 381 (1981);
B. A. Ovrut and H. J. Schnitzer, Nucl. Phys. **B189**, 509 (1981);
W. Bernreuther and W. Wetzel, Nucl. Phys. **B197**, 228 (1982);
W. Bernreuther, Ann. Phys. **151**, 127 (1983).

[123] I. Bierenbaum, J. Blümlein, and S. Klein, Acta Phys. Polon. **B38**, 3543 (2007). 0710.3348.

[124] J. Blümlein and S. Kurth, Phys. Rev. **D60**, 014018 (1999). hep-ph/9810241.

[125] J. A. M. Vermaseren, Int. J. Mod. Phys. **A14**, 2037 (1999). hep-ph/9806280.

[126] J. Blümlein, Comput. Phys. Commun. **159**, 19 (2004). hep-ph/0311046.

[127] J. Blümlein and S. Klein, arxiv:0706.2426 [hep-ph] (2007). 0706.2426.

[128] J. Blümlein, arxiv:0807.0700 [math-ph] (2008). 0807.0700.

[129] J. Blümlein and N. Kochelev, Phys. Lett. **B381**, 296 (1996). hep-ph/9603397.

[130] J. Blümlein, V. Ravindran, and W. L. van Neerven, Phys. Rev. **D68**, 114004 (2003). hep-ph/0304292.

[131] P. Nogueira, J. Comput. Phys. **105**, 279 (1993).

[132] T. van Ritbergen, A. N. Schellekens, and J. A. M. Vermaseren, Int. J. Mod. Phys. **A14**, 41 (1999). hep-ph/9802376.

[133] M. Steinhauser, Comput. Phys. Commun. **134**, 335 (2001). hep-ph/0009029.

[134] J. A. M. Vermaseren, math-ph/0010025 (2000). math-ph/0010025.

[135] C. Schneider, Ann.Comb., **9** (1) (2005) 75; Proc. ISSAC'05, (2005) pp. 285 (ACM Press); Proc. FPSAC'07, (2007) 1; J. Diffr. Equations Appl., **11** (9) (2005) 799; J. Algebra Appl., **6** (3) (2007) 415; Sém. Lothar. Combin. **56** (2007) Article B56b and Habilitation Thesis, JKU Linz, (2007).

[136] J. Blümlein, DESY 08–042.

[137] J. Blümlein and V. Ravindran, Nucl. Phys. **B716**, 128 (2005). hep-ph/0501178.

[138] J. Blümlein and V. Ravindran, Nucl. Phys. **B749**, 1 (2006). hep-ph/0604019.

[139] M. Tentyukov and J. A. M. Vermaseren, hep-ph/0702279 (2007). hep-ph/0702279.

[140] CTEQ Collaboration, R. Brock *et al.*, Rev. Mod. Phys. **67**, 157 (1995).

[141] V. N. Gribov and L. N. Lipatov, Sov. J. Nucl. Phys. **15**, 438 (1972). [Yad. Fiz. **15**, 781 (1972)];
Y. L. Dokshitzer, Sov. Phys. JETP **46**, 641 (1977). [Zh. Eksp. Teor. Fiz. **73**, 1216 (1977)];
G. Altarelli and G. Parisi, Nucl. Phys. **B126**, 298 (1977).

[142] E. A. Kuraev, L. N. Lipatov, and V. S. Fadin, Sov. Phys. JETP **44**, 443 (1976). [Zh. Eksp. Teor. Fiz. **71**, 840 (1976)];
I. I. Balitsky and L. N. Lipatov, Sov. J. Nucl. Phys. **28**, 822 (1978). [Yad. Fiz. **28**, 1597 (1978)].

[143] V. S. Fadin and L. N. Lipatov, Nucl. Phys. **B477**, 767 (1996).

[144] L. N. Lipatov, Nucl. Phys. **B452**, 452 (1995);
E. N. Antonov, L. N. Lipatov, E. A. Kuraev, and I. O. Cherednikov, Nucl. Phys. **B721**, 111 (2005);
L. N. Lipatov and M. I. Vyazovsky, Nucl. Phys. **B597**, 399 (2001).

[145] M. Gell-Mann, M. L. Goldberger, F. E. Low, E. Marx, and F. Zachariasen, Phys. Rev. **133**, 145B (1964).

[146] V. S. Fadin and V. E. Sherman, JETP Lett. **23**, 548 (1976);
V. S. Fadin and V. E. Sherman, JETP **45**, 861 (1977).

[147] G. T. Bodwin, E. Braaten, and G. P. Lepage, Phys. Rev. **D51**, 1125 (1995). Phys. Rev. **D55**, 5853E (1997).

[148] M. Cacciari and P. Nason, JHEP **09**, 006 (2003).

[149] CDF Collaboration, F. Abe *et al.*, Phys. Rev. Lett. **79**, 572 (1997);
CDF Collaboration, F. Abe *et al.*, Phys. Rev. Lett. **79**, 578 (1997);
CDF Collaboration, T. Affolder *et al.*, Phys. Rev. Lett. **85**, 2886 (2000).

[150] CDF Collaboration, D. Acosta *et al.*, Phys. Rev. **D71**, 032001 (2005).

[151] G. T. Bodwin, E. Braaten, and J. Lee, Phys. Rev. **D72**, 014004 (2005).

[152] P. Hägler, R. Kirschner, A. Schäfer, L. Szymanowski, and O. V. Teryaev, Phys. Rev. **D62**, 071502 (2000);
P. Hägler, R. Kirschner, A. Schäfer, L. Szymanowski, and O. V. Teryaev, Phys. Rev. Lett. **86**, 1446 (2001).

[153] F. Yuan and K. T. Chao, Phys. Rev. **D63**, 034006 (2001).

[154] F. Yuan and K. T. Chao, Phys. Rev. Lett. **87**, 022002 (2001).

[155] B. A. Kniehl, D. V. Vasin, and V. A. Saleev, Phys. Rev. **D73**, 074022 (2006).

[156] V. A. Saleev and D. V. Vasin, Phys. Rev. **D68**, 114013 (2003);
V. A. Saleev and D. V. Vasin, Phys. Atom. Nucl. **68**, 94 (2005). [Yad. Fiz. **68**, 95 (2005)].

[157] J. Blümlein, preprint (1995). DESY 95-121.

[158] H. Jung and G. P. Salam, Eur. Phys. J. **C19**, 351 (2001).

[159] M. A. Kimber, A. D. Martin, and M. G. Ryskin, Phys. Rev. **D63**, 114027 (2001).

[160] ZEUS Collaboration, S. Chekanov *et al.*, Eur. Phys. J. **C27**, 173 (2003).

[161] H1 Collaboration, C. Adloff *et al.*, Eur. Phys. J. **C25**, 41 (2002).

[162] V. A. Saleev and D. V. Vasin, Phys. Lett. **B548**, 161 (2002);
V. A. Saleev, Phys. Rev. **D65**, 054041 (2002).

[163] V. A. Saleev and N. P. Zotov, Mod. Phys. Lett. **A9**, 151 (1994).

[164] CDF Collaboration, F. Abe *et al.*, Phys. Rev. Lett. **75**, 4358 (1995);
CDF Collaboration, D. Acosta *et al.*, Phys. Rev. Lett. **88**, 161802 (2002).

[165] CDF Collaboration, V. M. Abazov *et al.*, Phys. Rev. Lett. **94**, 232001 (2005).

[166] E. Braaten, S. Fleming, and A. K. Leibovich, Phys. Rev. **D63**, 094006 (2001).

[167] B. A. Kniehl, V. A. Saleev, and D. V. Vasin, Phys. Rev. **D74**, 014024 (2006).

[168] V. A. Saleev and D. V. Vasin, Phys. Part. Nucl. **38**, 635 (2007).

[169] H1 Collaboration, C. Adloff *et al.*, Nucl. Phys. **B545**, 21 (1999).

[170] ZEUS Collaboration, J. Breitweg *et al.*, Eur. Phys. J. **C6**, 67 (1999). Phys. Lett. **B481**, 213 (2000).

[171] V. A. Saleev and D. V. Vasin, Phys. Atom. Nucl. **68**, 95 (2005).

[172] CDF Collaboration, D. Acosta *et al.*, Phys. Rev. Lett. **91**, 241804 (2003).

[173] J. C. Collins and R. K. Ellis, Nucl. Phys. **B360**, 3 (1991).

[174] S. Catani, M. Ciafaloni, and F. Hautmann, Nucl. Phys. **B366**, 135 (1991).

[175] B. A. Kniehl, A. V. Shipilova, and V. A. Saleev, to be published.

[176] B. A. Kniehl, A. V. Shipilova, and V. A. Saleev, DESY-08-194 **2008**.
`arXiv:0812.3376[hep-ph]`.

[177] CDF Collaboration, F. Abe *et al.*, Phys. Rev. **D55**, 2546 (1997).

[178] P. Hagler *et al.,* Phys. Rev. **D62**, 071502(R) (2000).

[179] J. Kwiecinski, A. Martin, and S. A., Phys. Rev. **D56**, 3991 (1997).

[180] C. Peterson *et al.,* Phys. Rev. **D27**, 105 (1983).

[181] V. A. Saleev and D. V. Vasin. arXiv:0709.0259.

[182] M. Kramer, Prog. Part. Nucl. Phys. **47**, 141 (2001). hep-ph/0106120.

[183] Quarkonium Working Group Collaboration, N. Brambilla *et al.* (2004). hep-ph/0412158.

[184] B. A. Kniehl and L. Zwirner, Nucl. Phys. **B621**, 337 (2002). hep-ph/0112199.

[185] S. P. Baranov, Phys. Rev. **D66**, 114003 (2002).

[186] P. Hagler, R. Kirschner, A. Schafer, L. Szymanowski, and O. V. Teryaev, Phys. Rev. **D63**, 077501 (2001). hep-ph/0008316.

[187] S. P. Baranov, Phys. Lett. **B428**, 377 (1998).

[188] S. P. Baranov, A. V. Lipatov, and N. P. Zotov (2001). hep-ph/0106229.

[189] L. V. Gribov, E. M. Levin, and M. G. Ryskin, Phys. Rept. **100**, 1 (1983).

[190] S. Catani, M. Ciafaloni, and F. Hautmann, Phys. Lett. **B242**, 97 (1990).

[191] E. A. Kuraev, L. N. Lipatov, and V. S. Fadin, Sov. Phys. JETP **45**, 199 (1977).

[192] J. Blümlein, J. Phys. **G19**, 1623 (1993).

[193] M. Gluck, E. Reya, and A. Vogt, Eur. Phys. J. **C5**, 461 (1998). hep-ph/9806404.

[194] S. P. Baranov and N. P. Zotov, JETP Lett. **86**, 435 (2007). 0707.0253.

[195] C. Akerlof *et al.,* Phys. Rev. **D48**, 5067 (1993).

[196] CDF Collaboration, A. A. Affolder *et al.,* Phys. Rev. Lett. **85**, 2886 (2000). hep-ex/0004027.

[197] D0 Collaboration, V. M. Abazov *et al.* (2008). 0804.2799.

[198] V. Papadimitriou, AIP Conf. Proc. **815**, 157 (2006). [arXiv:hep-ex/0511043];
M. D. Corcoran, others (for the CDF, and D. Coll.), arXiv:hep-ex/0506061.

[199] S. S. Gershtein, V. V. Kiselev, A. K. Likhoded, and A. V. Tkabladze, Phys. Usp. **38**, 1 (1995). [Usp. Fiz. Nauk. **165** (1995) 3, arXiv:hep-ph/9504319];
V. V. Kiselev, A. K. Likhoded, and A. V. Tkabladze, Phys. Rev. **D51**, 3613 (1995);
S. N. Gupta and J. M. Johnson, Phys. Rev. **D53**, 312 (1996);
D. Ebert, R. N. Faustov, and V. O. Galkin, Phys. Rev. **D67**, 014027 (2003);

N. Brambilla, Y. Sumin, and A. Vairo, Phys. Rev. **D65**, 034001 (2002);
S. M. Ikhdair and R. Sever, Int. J. Mod. Phys. **A20**, 6509 (2005);
S. Godfrey, Phys. Rev. **D70**, 054017 (2004).

[200] CDF Collaboration, A. Abulencia *et al.*, Phys. Rev. Lett. **97**, 242003 (2006);
D0 Collaboration, V. M. Abazov *et al.*, Phys. Rev. Lett. **97**, 021802 (2006).

[201] I. P. Gouz, V. V. Kiselev, A. K. Likhoded, V. I. Romanovsky, and O. P. Yushchenko, Phys. Atom. Nucl. **67**, 1559 (2004). [Yad. Fiz. **67**, 1581 (2004), arXiv:hep-ph/0211432];
V. V. Kiselev, A. E. Kovalsky, and A. K. Likhoded, Nucl. Phys. **B585**, 353 (2000);
C. H. Chang, Int. J. Mod. Phys. **A21**, 777 (2006);
V. V. Kiselev, arXiv:hep-ph/0308214.

[202] V. V. Kiselev, A. K. Likhoded, and A. I. Onishchenko, Nucl. Phys. **B569**, 473 (2000);
A. V. Berezhnoi, V. V. Kiselev, and A. K. Likhoded, Z. Phys. **A356**, 79 (1996);
K. Kolodziej and R. Rückl, Nucl. Instrum. Meth. **A408**, 33 (1998);
C. H. Chang, Y. Q. Chen, G. P. Han, and H. T. Jiang, Phys. Lett. **B364**, 78 (1995).

[203] S. S. Gershtein and A. K. Likhoded, arXiv:0706.0963.

[204] L. Alvarez-Gaumé *et al.*, arXiv:hep-ph/9812326.

[205] R. Gatto, Nucl. Phys. **5**, 183 (1958).

[206] E. Conte, Thèse de Docteur de l'Université Blaise Pascal **PPCF T 0710** (2007).

[207] Z. J. Ajaltouni *et al.*, Phys. Lett. **B614**, 165 (2005).

[208] O. Leitner, Z. J. Ajaltouni, and E. Conte, arXiv:hep-ph/0602043;
Z. J. Ajaltouni *et al.*, Nucl. Phys. B Proc. Suppl. **174**, 169 (2007).

[209] D. S. E. *et al.*, PCCF RI 0802 (2008).

[210] M. Fairbairn *et al.*, Phys. Rept. **438**, 1 (2007). `hep-ph/0611040`.

[211] Y. R. de Boer, A. B. Kaidalov, D. A. Milstead, and O. I. Piskounova, J. Phys. **G35**, 075009 (2008). `0710.3930`.

[212] P. D. B. Collins, Phys. Rept. **1**, 103 (1971);
P. D. B. Collins. Cambridge 1977, 445p.

[213] A. B. Kaidalov, Phys. Lett. **B116**, 459 (1982);
A. B. Kaidalov and K. A. Ter-Martirosian, Phys. Lett. **B117**, 247 (1982);
A. B. Kaidalov and K. A. Ter-Martirosian, Sov. J. Nucl. Phys. **39**, 979 (1984);
A. B. Kaidalov and O. I. Piskunova, Z. Phys. **C30**, 145 (1986).

[214] M. Drees and X. Tata, Phys. Lett. **B252**, 695 (1990);
A. C. Kraan, Eur. Phys. J. **C37**, 91 (2004). `hep-ex/0404001`.

[215] T. Sjostrand, S. Mrenna, and P. Skands, JHEP **05**, 026 (2006). `hep-ph/0603175`.

[216] A. C. Kraan, J. B. Hansen, and P. Nevski, Eur. Phys. J. **C49**, 623 (2007). hep-ex/0511014.